DESIGN OF A SLOTTED WAVEGUIDE ARRAY ANTENNA AND ITS FEED SYSTEM

A THESIS SUBMITTED TO
THE GRADUATE SCHOOL OF NATURAL AND APPLIED SCIENCES
OF
MIDDLE EAST TECHNICAL UNIVERSITY

BY

CAN BARIŞ TOP

IN PARTIAL FULFILLMENT OF THE REQUIREMENTS FOR THE DEGREE
OF
MASTER OF SCIENCE
IN
ELECTRICAL AND ELECTRONICS ENGINEERING

SEPTEMBER 2006

Approval of the Graduate School of Natural and Applied Sciences

_____

Prof. Dr. Canan ÖZGEN
Director

I certify that this thesis satisfies all the requirements as a thesis for the degree of Master of Science.

_____

Prof. Dr. İsmet ERKMEN
Head of Department

This is to certify that we have read this thesis and that in our opinion it is fully adequate, in scope and quality, as a thesis for the degree of Master of Science.

_____

Prof. Dr. Altunkan HIZAL
Supervisor

Examining Committee Members

Assoc.Prof. Dr. Şimşek DEMİR (Chairman) (METU,EE) _____

Prof. Dr. Altunkan HIZAL (METU,EE) _____

Assoc. Prof. Dr. Özlem AYDIN ÇİVİ (METU,EE) _____

Asst. Prof. Dr. Lale ALATAN (METU,EE) _____

Mehmet Erim İNAL (M.S.E.E) (ASELSAN A.Ş) _____

I hereby declare that all information in this document has been obtained and presented in accordance with academic rules and ethical conduct. I also declare that, as required by these rules and conduct, I have fully cited and referenced all material and results that are not original to this work.

Name, Last name:

Signature :

ABSTRACT

DESIGN OF A SLOTTED WAVEGUIDE ARRAY ANTENNA AND ITS FEED SYSTEM

TOP, Can Barış
M.S., Department of Electrical and Electronics Engineering
Supervisor: Prof. Dr. Altunkan HIZAL
September 2006, 95 Pages

Slotted waveguide array (SWGA) antennas find application in systems which require planarity, low profile, high power handling capabilities such as radars. In this thesis, a planar, low sidelobe, phased array antenna, capable of electronically beam scanning in E-plane is designed, manufactured and measured. In the design, slot characterization is done with HFSS and by measurements, and mutual coupling between slots are calculated analytically. A MATLAB code is developed for the synthesis of the SWGA antenna. Grating lobe problem in the scanning array, which is caused by the slot positions, is solved using baffles on the array.

A high power feeding section for the planar array, having an amplitude tapering to get low sidelobes is also designed using a corrugated E-plane sectoral horn. The power divider is designed analytically, and simulated and optimized with HFSS.

Keywords: Slotted Waveguides, Single Ridged Slotted Waveguide Arrays, Second Order Beams, E-plane Sectoral Corrugated Horn

ÖZ

YARIKLI DALGA KILAVUZU DİZİ ANTENİ VE BESLEME SİSTEMİNİN TASARIMI

TOP, Can Barış
Yüksek Lisans, Elektrik ve Elektronik Mühendisliği Bölümü
Tez Yöneticisi: Prof. Dr. Altunkan HIZAL
Eylül 2006, 95 Sayfa

Yarıklı dalga kılavuzu dizi (YDKD) antenler, radarlar gibi düzlemsellik, incelik ve yüksek güç gerektiren sistemlerde sıklıkla kullanılırlar. Bu tezde, X-bantta çalışan düzlemsel, düşük yan huzmeli, E-alan düzleminde elektronik huzme taraması yapabilen bir faz dizili YDKD anten tasarlanmış ve üretilip ölçülmüştür. Tasarımda yarık modellemesi için Ansoft HFSS programı ve ölçümler, yarıklar arası karşılıklı etkileşim için analitik formüller kullanılmıştır. Dizi anten sentezi için MATLAB kodu geliştirilmiştir. Yarıkların dalga kılavuzu üzerindeki pozisyonlarından kaynaklanan yüksek yan huzme problemi antenin üzerine ızgara konularak çözülmüştür.

Düzlemsel anteni beslemek için E-düzlemli kıvrımlı yassı boynuz anten ile yüksek güçlü bir besleme yapısı oluşturulmuştur. Analitik olarak tasarlanan bu yapının HFSS ‘te benzeşimi yapılmış ve optimize edilmiştir.

Anahtar Kelimeler : Yarıklı Dalga Kılavuzları, Tek Sırtlı Yarıklı Dalga Kılavuzu Dizi Antenler, İkinci Derece Huzmeleri, Kıvrımlı E-düzlemli Yassı Horn

To my family and Özden

ACKNOWLEDGMENTS

I would like to express my sincere gratitude to my advisor, Prof. Dr. Altunkan Hızal for his guidance, support and suggestions throughout the study. I would also like to thank Asst. Prof. Dr. Lale Alatan for her valuable advises and help and also for allowing me use the MATLAB program she developed for the resonant fed slotted waveguide antennas. My special thanks go to Kenan Çağlar and Mehmet Erim İnal for their help and guidance in the design and manufacturing process. I am also grateful to Assoc. Prof. Dr. Özlem Aydın Çivi for her support and advises.

I would also like to express my sincere appreciation for Erdinç Erçil, Nizam Ayyıldız, Bülent Alıcıoğlu, Necip Şahan, Burak Alişan for their valuable friendship, support and help.

I am grateful to ASELSAN A.Ş. for the facilities provided for the completion of this thesis.

For their understanding my spending lots of time on this work, my sincere thanks go to my sister and to my parents.

Lastly, for her great support, understanding and love, I am also grateful to my fiancée, Özden.

TABLE OF CONTENTS

LIST OF TABLES

LIST OF FIGURES

CHAPTER 1

INTRODUCTION

Slotted Waveguide Array (SWGA) antennas have been widely used in applications requiring high power handling, planarity and low profile specifications, such as satellites, radars and remote sensing. Their insertion loss is very low.

SWGA antennas are formed by cutting narrow slots periodically on the wall of a waveguide. The slots are resonant at nearly a half wavelength long, and are Babinet equivalent of a dipole antenna. There are various radiating slot elements: longitudinal, transversal or inclined slots cut on the broadwall of the waveguide; inclined slots, I or C shaped slots cut on the waveguide's narrow wall. The amount of radiation from a single slot can be controlled by its mechanical parameters, and an array of slots can be designed so that the desired radiation pattern is achieved.

Waveguide-fed slots are being used since late 1940's. The first works for this kind of antennas are made by Watson, Stevenson and Booker
[1]-[3]. Stevenson was the one who formulated the electric field on the slot aperture, giving theoretical means to the Watson's experimental work. Booker solved the integral equation using waveguide Green's functions and the analogy between dipoles and slots based on Babinet's principle.

Stegen made an experimental work on the admittance and resonant length of a slot with respect to slot displacement (offset) for longitudinal broadwall slots and produced universal curves for the admittance of a slot as a function of its length normalized to its resonant length [4]. In fact this characterization should be done in the center frequency before designing the array. This can be done experimentally or numerically. Most of the work in literature concerns characterization of a single slot

by numerical methods. In this thesis, characterization is done both experimentally and with Ansoft HFSS EM simulation software.

In 1978, Elliott published a paper about designing a resonant linear slot array with the use of characterization data, including external mutual coupling between slots [5]. The mutual coupling was based on the analogy of the slots and dipoles. Thereafter, this method has been used for designing SWGA antennas. A year later, in 1979, Elliott applied this design procedure for traveling wave arrays [6].

In this thesis, a planar, low side lobe traveling wave type SWGA array operating in the X-Band is designed. Planar array is formed by stacking linear slotted waveguides. Also a feed section for the array, involving an E-plane corrugated sectoral horn is introduced. The first part (chapters 2 to 6) of the thesis is about the design of the antenna array, where in the second part (chapter 7), a different high power feed section is proposed.

In chapter 2, different types of radiating slots cut in waveguides; longitudinal broadwall slots, inclined narrow wall slots, inclined broadwall slots and compound broadwall slots, are introduced and their properties are discussed. The two types of SWGA antennas, namely resonant and traveling wave, are introduced. Also, design procedures for both the resonant and traveling wave types of linear SWGA antennas are given.

Chapter 3 is about designing the linear array. The slots are fed by a non-standard single ridged waveguide. Chapter begins with the calculations of cut-off frequency and characteristic impedance of the single ridged waveguides, and continues with slot characterization for the designed single ridged waveguide, which is done with Ansoft HFSS EM simulation software. A linear array with low sidelobes is synthesized. Its simulation and measurement results are also given in this chapter.

In chapter 4, the theory of the secondary beam problem which is presented in chapter 3 is discussed. Some of the solutions to the problem are given.

In chapter 5, design of a linear array with baffles is presented. Firstly, characterization for a single slot radiating between baffles is explained. Then, the array based on this characterization is synthesized, simulated and manufactured. Simulation and measurement results are presented. Measurements are done in the planar near-field range.

Chapter 6 is about planar array having the single ridged SWGA (SR-SWGA), which was designed in chapter 6, as the array element. The array is formed stacking 18 linear SR-SWGA antennas in elevation axis. The planar array is simulated with CST Microwave Studio EM simulation software. The radation pattern of the manufactured array is measured in a planar near-field system.

In the second part of the thesis, a power divider for feeding a planar array of 18 linear SWGA antennas is introduced.

Chapter 7 starts with an introduction for the feed system and continues with the theory of corrugated sectoral horns. Then design of the horn and design of the coupling waveguide parts are explained in separate parts. Simulation results are discussed. The power divider is actually an E-plane corrugated sectoral horn. Its return loss is below 25dB through the entire band and it possesses a maximum SLL of -30 dB. The divider can be integrated to the planar array with some additional waveguide adapter parts in order to match the divider to antenna array mechanically.

CHAPTER 2

WAVEGUIDE SLOT ELEMENT

The waveguide surface current distribution of TE_{10} mode shown in Figure 2.1, which is the dominant mode, can be expressed by

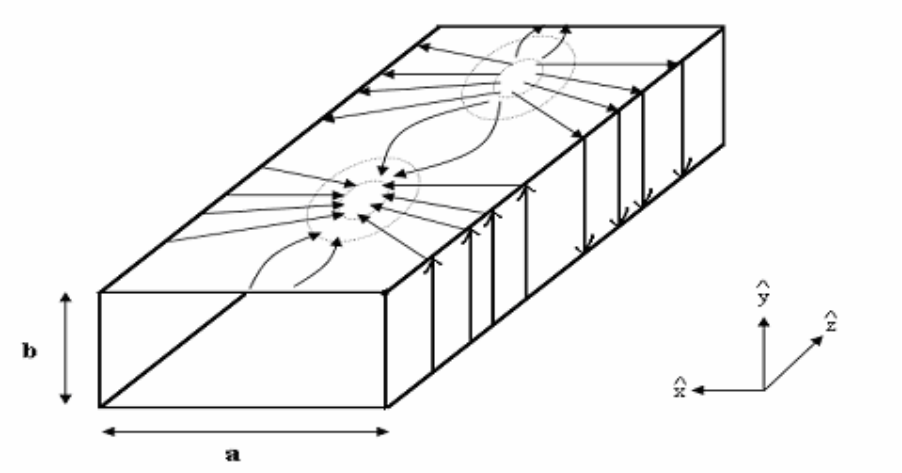

Figure 2.1 Waveguide surface currents

$$\vec{J}_s = \hat{n}x\vec{H} \qquad (2.1)$$

Where H is the magnetic field of mode TE_{10} evaluated at the surface of conductor which is given by:

$$\vec{H} = -A_{10}\frac{\beta_{10}}{\pi/a}\sin(\frac{\pi x}{a})e^{-j\beta_{10}z}\hat{x} + jA_{10}\cos(\frac{\pi x}{a})e^{-j\beta_{10}z}\hat{y} \qquad (2.2)$$

If a slot is cut disturbing this current distribution, it radiates energy to the outside. If the slot is narrow and nearly half a wave length, it is a magnetic dipole from Babinet's principle.

2.1. Types of Waveguide Fed Slots

There are four types of slots generally used as antenna elements: longitudinal broad wall slots, inclined narrow wall slots, inclined broad wall slots and compound broad wall slots.

2.1.1. Longitudinal Slot on the Broad Wall

As shown in Figure 2.2**,** this type of slot interrupts transverse currents on the broad wall. Radiated power increases as the offset (slot's distance from the center of the waveguide) is increased. Polarity is reversed when the slot is cut in the other side of the waveguide. A slot cut on the center does not radiate, because it interrupts nearly no net current and it is ideal for probing the field in the waveguide.

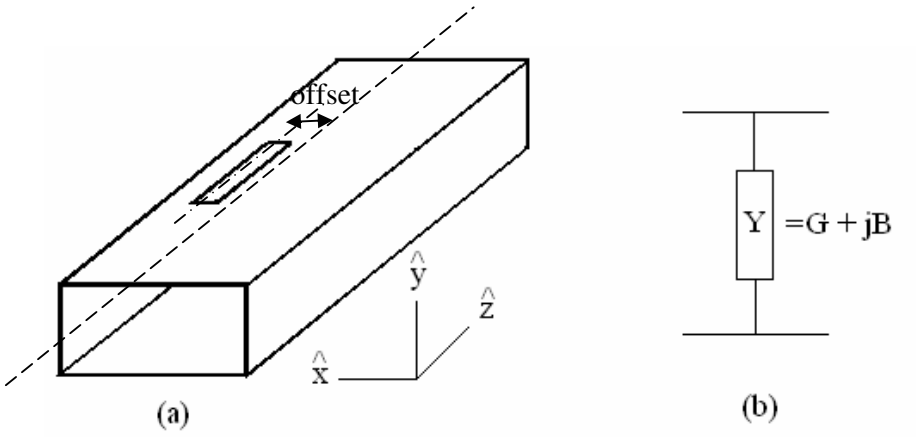

Figure 2.2 (a) Longitudinal broad wall slot. (b) Circuit representation

The internal backward and forward scattered waves due to the presence of the slot are equal [3]. Hence, these types of slots are represented by a parallel admittance (Figure 2.2).

The E-field in the slot is sinusoidal and in the x-direction mainly (Figure 2.3) for narrow slots (ie. length/width of the slot >7). Z-component E-field is very weak and can be neglected unless the slot offset is not very small. Therefore, the cross-polarization of these types of SWGA arrays is low. The polarization of the array is vertical.

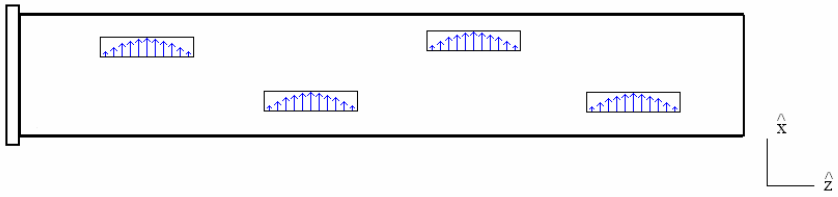

Figure 2.3 E-Field on longitudinal broad wall slots

2.1.2. Inclined Slot Cut on The Broad Wall

Mainly longitudinal currents are interrupted in this case and the induced E-field in the slot increases as the slot's tilt angle (α) - measured from the center line of the waveguide- increases. Polarity is reversed if the direction of the tilt is reversed.

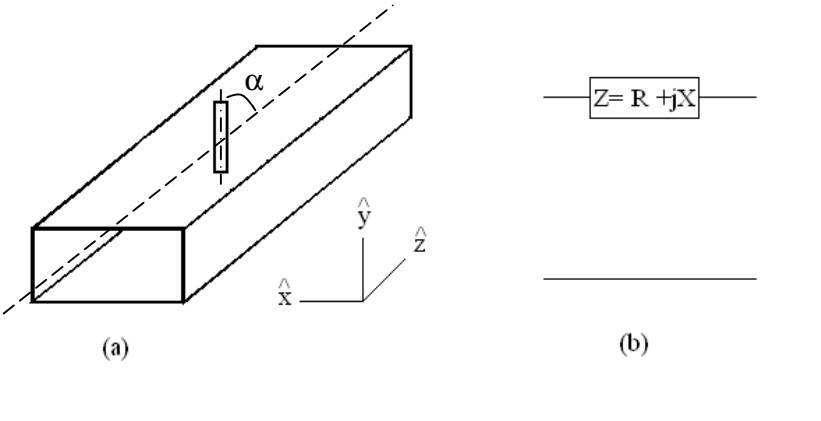

Figure 2.4 (a) Inclined Broad wall slot. (b) Circuit representation

These kinds of slots are represented with series impedance (Figure 2.4). Since E-field in the slot has x and y direction components, cross-polarization is high in arrays of these slots. Generally this type is used for feeding planar slotted waveguide arrays.

2.1.3. Inclined Slot on the Narrow Wall

This type of slot (Figure 2.5) causes interruption of the transverse current in the narrow wall. Induced E-field in the slot increases with increasing the inclination angle(α). Polarity is changed if the direction of inclination is reversed.

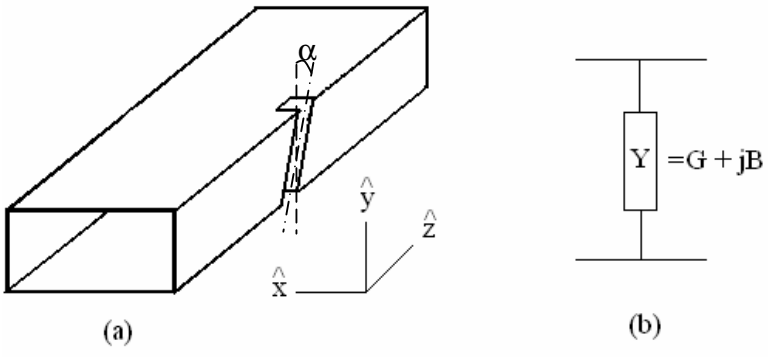

Figure 2.5 (a) Inclined broad wall slot. (b) Circuit representation

The slot extends to broad wall in order to have the resonant length. This brings difficulties in design because analysis of slot's self admittance and mutual interactions with other slots are difficult. Cross-polarization is in y-direction and also high because of the inclination. Despite these disadvantages, planar phased arrays with large scanning sector in the y - direction can easily be constructed since waveguide's narrow wall dimension permits scanning in a wide sector. When the array is formed with this kind of slots, the polarization is horizontal since the y-components of the successive slots cancel each other (the successive slots in the array will have alternating tilt angles because of the reasons explained in part 2.2). However, the angles of the successive slots in the array are not equal thus the cancellation is not perfect. The cross-polarized component is high for this reason.

2.1.4. Compound (Inclined Slots with Offset) Slots on the Broad Wall

This is a combination of longitudinal and inclined slots on the broad wall. It has both an offset and inclination on the broad wall and its amplitude and phase can be controlled independently. It interrupts both the transversal and the longitudinal components of surface current.

2.2. Types of Linear SWGA Antennas

In all types of slots, amount of radiation is adjusted by offsets or tilt angles. In a waveguide, there can be a number of slots making a linear array as shown in Figure 2.6. Sidelobe level of the array can be controlled by employing amplitude tapering (such as Binomial, Tchebychev, Taylor, etc.) along the array. Therefore, low side lobe linear antennas may be designed by adjusting slot offsets or tilt angles along the array. In the linear array, slot offsets (or tilt angles) can be alternating or non-alternating. Arrays with alternating slot offsets as shown in Figure 2.6 (or tilt angles) are generally used because of the grating lobe problem in non-alternating arrays. Besides, the cross-polarization of the inclined slotted array types will be high for non-alternating arrays, since there will be no cancellation of the cross-

polarized component. The disadvantage of the alternating slot geometry is the secondary beam problem which will be discussed in chapter 4. Stacking these waveguides side by side, planar arrays can be formed. Because of the E – field direction, cross-polarized components are high for inclined slot arrays.

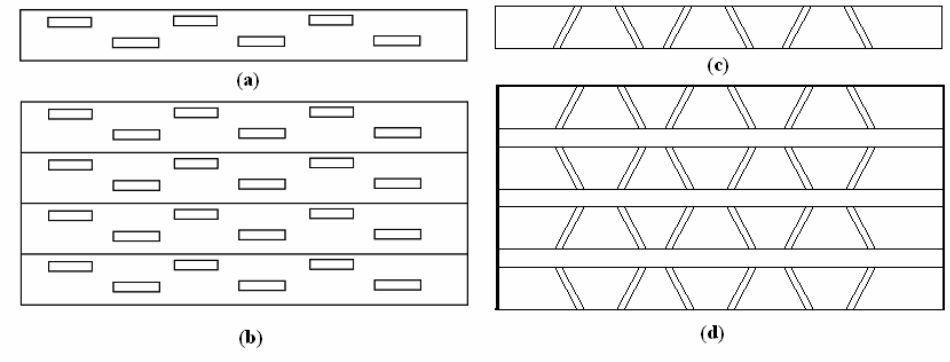

Figure 2.6 (a) Linear array of longitudinal broad wall slots (b) Planar array of longitudinal broad wall slots (c) Linear array of inclined narrow wall slots (d) Planar array of inclined narrow wall slots

A linear SWGA antenna can be constructed in two ways: resonant or traveling wave.

2.2.1. Standing Wave Fed (Resonant) Array

In this type, distance between two successive slots is a half guided wavelength (λ_g / 2) at the center frequency. If the spacing was to be λ_g, grating lobe problem would arise since the guided wavelength is always greater than free space wavelength ($\lambda_g > \lambda_o$) in a waveguide. If a slot's position is alternated with respect to the waveguide center line, its phase changes 180°. Thus, all the slots are in phase if successive slots are placed with alternating offsets with respect to waveguide center line. Waveguide is terminated with a short circuit which is λ_g / 4 away from the last slot. Since all the slots are in phase, main beam is on the broadside.

Resonant slotted waveguide arrays have narrower bandwidth (< 3-4 %) as compared to non-resonant ones. The slot conductances add in-phase at the input, and input matching is only done for the center frequency. The number of elements should be small for input matching, however large arrays can be constructed using smaller subarrays. Beam splitting occurs for frequencies out of the band. Planar arrays of this type can be fed from center or end of the waveguides.

2.2.2. Traveling Wave Fed (Non-Resonant) Array

In this case, the distance between two successive slots in the array is not $\lambda_g / 2$, but a little smaller (for backward firing) or larger (for forward firing). Main beam is squinted from the broad side because there is a certain phase difference between two successive slots in the array, and as the operating frequency change, beam squint angle changes. A matched load is required at the end of the waveguide in order to have no reflection back. Generally, 5-10 % of the input power is dissipated in the load. These types of slotted waveguides are end-fed usually. Since the slots are not in phase, the input matching is very good over the entire frequency band especially for the large arrays. Bandwidth of the array is generally smaller than or equal to 10 %, and restricted by radiation pattern of the array, if the power loss at the mathed load is not a concern.

2.3. Design of a Linear SWGA

For the design of a SWGA array, the frequency of operation must be considered and appropriate waveguide must be selected firstly. Elliott's design procedure [7] is used in this thesis. Slot admittance data for different offsets (or inclination angles) and lengths $y_{self}(x,l)$ must be known for the synthesis. This data can be calculated numerically or experimentally. Four polynomials, which are called characterization polynomials, are then extracted from these data :

g(x) : Resonant conductance vs. slot offset (or inclination),

v(x) : Resonant length vs. slot offset (inclination),

h1(y) : Normalized conductance vs. normalized length (w.r.t resonant length),

h2(y) : Normalized susceptance (w.r.t. resonant conductance) vs. normalized length.

where,

x is the slot's distance from the waveguide center (slot's offset);

y is the normalized length of the slot with respect to the resonant length for a spesific slot offset value.

It will be later shown that these four polynomials model the isolated slot admittance ($y_{self}(x,l)$) as a function of the slot offset and the length. It is generally enough to have the data of 6- 7 different offsets and 6-7 different lengths. Then other offset and lengths can be interpolated. For length, data for %95 to %105 of resonant length is adequate.

Before synthesis of the array, the array excitation coefficients for desired gain and side lobe level and the number of slot elements for the required half power beamwidth must be chosen.

2.3.1. Design Procedure for Resonant Slotted Waveguide Arrays

For a resonant array, element spacing is λ_g / 2 and array is ended with a short circuit, which is λ_g / 4 away from the last slot. In order to get the slots in phase, successive slots are placed in the opposite side of waveguide center line. If they were in the same side of the waveguide with λ_g spacing, they would be in-phase again but since $\lambda_g > \lambda_0$, unwanted grating lobe would be in visible space.

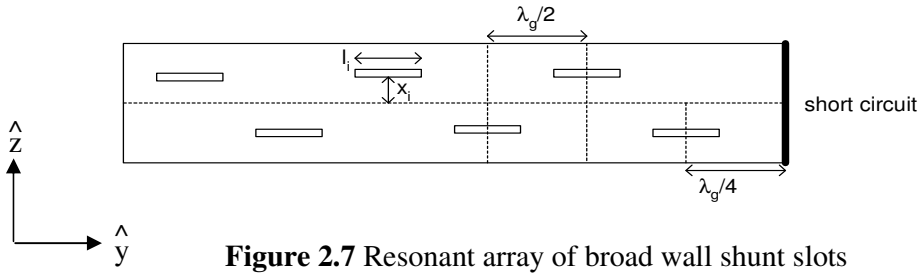

Figure 2.7 Resonant array of broad wall shunt slots

In design, mutual coupling between the slots must be taken into account. With mutual coupling considered, a slot is modelled by an active admittance which is

$$Y_n^a = Y_s + Y_{m.} \qquad (2.3)$$

The active admittance is a function of offset and length which was derived by Elliott [5];

$$Y_n^a = \frac{K.f_n(x_n, l_n).V_n^s}{V_n} \qquad (2.4)$$

where

$$f_n(x,l) = \frac{(\pi/2kl)\cos(\beta l)}{(\pi/2kl)^2 - (\beta/k)^2}\sin(\frac{\pi x}{a}) \qquad (2.5)$$

$$K = \frac{1}{j(a/\lambda)}\sqrt{\frac{2}{\eta G_0(\beta/k)(ka)(kb)}} \qquad (2.6)$$

Y_n^a : Active admittance of a slot normalized w.r.t waveguide characteristic admittance (TE_{10} wave impedance)

V_n^s : Slot Excitation Voltage

V_n : TE_{10} Mode Voltage on Y_n^a

$x = x_n$: Offset of n^{th} slot

$l = l_n$: Length of n^{th} slot

k : Free space wave number

β : Waveguide wave number for TE_{10} mode

G_0 : Waveguide characteristic admittance(TE_{10} wave admittance)

Active admittance of a slot in array can be also written in terms of slot offset, length and mutual coupling as:

$$Y_n^{\,a} = \frac{2.f_n^{\,2}(x,l)}{\dfrac{2.f_n^{\,2}(x,l)}{Y_n(x,l)} + j\dfrac{\beta}{k}(k_0 b)(\dfrac{a}{\lambda})^3 \sum_{m=1}^{N}{}' \dfrac{V_m^{\,s}}{V_n^{\,s}} g_{mn}} \qquad (2.7)$$

a, b :Waveguide broad wall and narrow wall sizes respectively

$Y_n(x,l)$:Self admittance of slot normalized w.r.t waveguide characteristic admittance

g_{mn} :Mutual coupling term given by

$$g_{mn} = \int_{-k_0 l_m}^{k_0 l_m} \cos(\frac{z_m'}{4lm/\lambda_0})\left\{\frac{1}{(4l_n/\lambda_0)}\left[\frac{e^{-jk_0R_1}}{k_0R_1}+\frac{e^{-jk_0R_2}}{k_0R_2}\right]+\left[1-\frac{1}{(4l_n/\lambda_0)^2}\right]\int_{-k_0 l_n}^{k_0 l_n}\cos(\frac{z_n'}{4l_n/\lambda_0})\frac{e^{-jk_0R}}{k_0R}dz_n'\right\}dz_m'$$

(2.8)

The formula above for the mutual coupling is actually the mutual coupling between two dipole elements for the echelon geometry given in Figure 2.8.

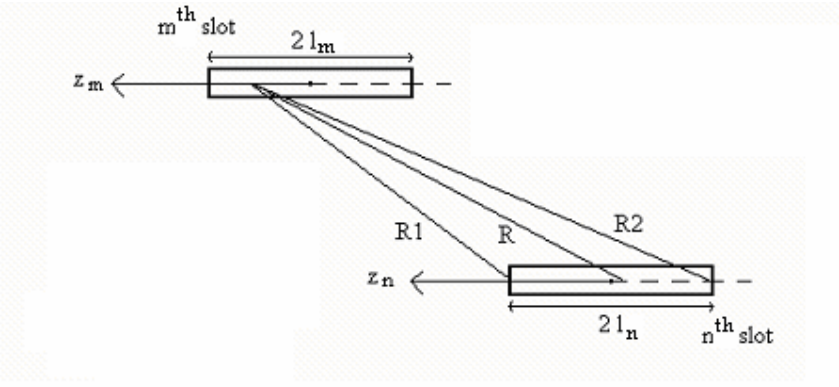

Figure 2.8 Geometry of slots for Mutual Impedance

Self admittance (isolated slot admittance) Y_n of a slot can be expressed in terms of extracted polynomials :

$$Y_n(x, y) = g(x)h(y) \qquad (2.9)$$

where

$$h(y) = h1(y) + jh2(y) \qquad (2.10)$$

and

$$y = \frac{l}{l_{res}} \qquad (2.11)$$

$$v(x) = k_0 . l_{res} \qquad (2.12)$$

- For input matching, slot admittance's must satisfy:

$$\sum_{n=1}^{N} Y_n^a(x_n, l_n) = 1 \qquad (2.13)$$

- And the conductance relations between slots are given by:

$$\frac{Y_n^a(x_n, l_n)}{Y_n^a(x_m, l_m)} = \frac{f(x_n, l_n) V_n^s V_m}{f(x_m, l_m) V_m^s V_n} \qquad (2.14)$$

Design Steps:

- make an initial guess for all slot offsets and lengths (x_n,l_n) (for example take all ofsets are zero and and all slot lengths are half wavelength initially) Calculate g_{mn} from (2.8).
- all the (x_n,l_n) pairs should satisfy the ratio for the slot voltages V_n^s (amplitude coefficients) (2.14) and the imaginary part of (2.7) should be zero. With equation (2.13) imposed on these conditions, there is a unique solution for all (x_n,l_n) pairs. However g_{mn} term is not valid since offsets and lengths are different from the initial guess.
- calculate g_{mn} for the new (x_n,l_n) pairs.

- Iterate the procedure until (x_n,l_n) pairs converge.

2.3.2. Design Procedure for Traveling-Wave Slotted Waveguide Arrays

For the traveling-wave-fed array, slot spacing is different than λ_g / 2, and waveguide is terminated by a matched load. Since spacing is not λ_g / 2, main beam is not at the broadside, and design is more complex because the slots are not in-phase and mode voltage for each slot is different.

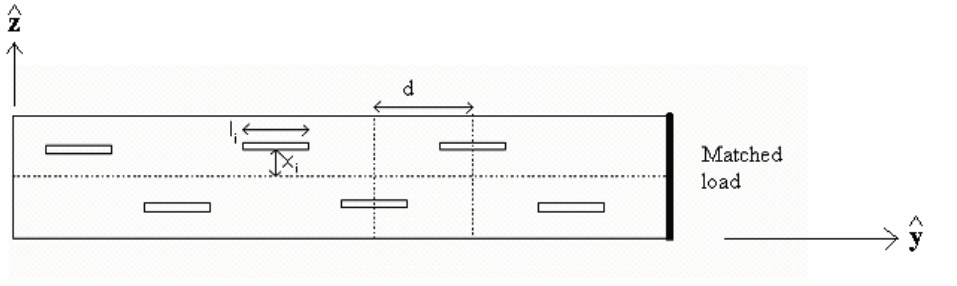

Figure 2.9 Traveling wave array of broad wall shunt slots

There are two cases of non-resonant array. Slots can be on the same side of waveguide, or can be alternating as in the case of resonant array. If they are on the same side, array factor will be

$$AF = \sum_{n=1}^{N} a_n e^{jk_0 \hat{r}.(n.d\hat{y} + x_n \hat{z}) - j\beta nd} \qquad (2.15)$$

and main beam direction is

$$\Phi_0 = \arcsin(\beta / k_0) \qquad (2.16)$$

If slots are alternating, array factor and main beam direction are given by

$$AF = \sum_{n=1}^{N} a_n e^{jk_0 \hat{r}.(n.d\hat{y} + x_n \hat{z}) - j\beta nd + jn\pi} \qquad (2.17)$$

$$\Phi_0 = \arcsin\left(\frac{\beta d - \pi}{k_0 d}\right) = \arcsin(\beta/k_0 - \lambda_0/2d) \qquad (2.18)$$

This type of slotted waveguide arrays are designed in this thesis.

Equivalent circuit for traveling wave array is shown in Figure 2.10.

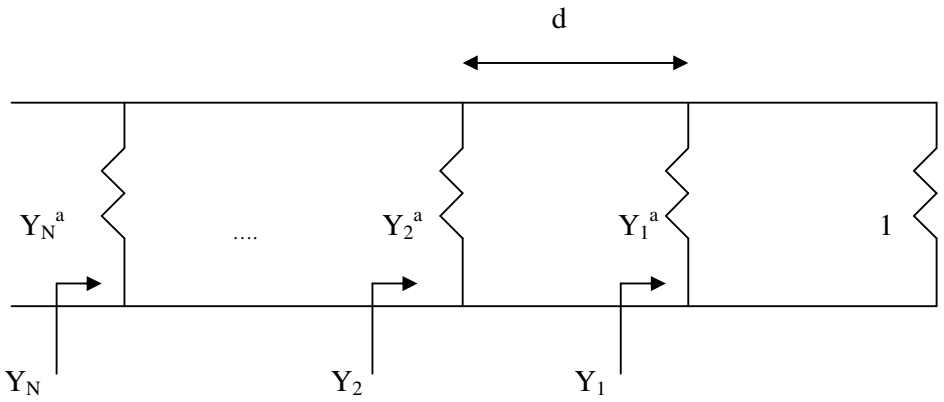

Figure 2.10 Circuit representation of traveling wave broad wall shunt slot array

Total normalized admittance seen from n^{th} junction is Y_n.

$$Y_n = Y_n^{\,a} + \frac{Y_{n-1}\cos\beta d + j\sin\beta d}{\cos\beta d + jY_{n-1}\sin\beta d} \qquad (2.19)$$

Relation between mode voltages of successive slots are given by

$$V_n = V_{n-1}\left[\cos\beta d + jY_{n-1}\sin\beta d\right] \qquad (2.20)$$

Equation (2.14) can be written for two successive slots as:

$$\frac{Y_n^{\,a}}{f_n(x,l)} = \frac{Y_{n-1}^{\,a}}{f_{n-1}(x,l)}\frac{V_n^{\,s}/V_{n-1}^{\,s}}{\cos\beta d + jY_{n-1}\sin\beta d} \qquad (2.21)$$

It must be noted that phase difference (βd) between slots must be taken into account in complex slot voltages V_n^s / V_{n-1}^s .

Design procedure for alternating traveling wave fed array is as follows:

-Spacing between slots is determined by the required main beam direction by the formula (2.16) or (2.18). Small d causes mutual coupling to increase, and large d may produce unwanted grating lobe if d = λ_0 for some frequency inside the operation band.

-For the calculation of mutual coupling between slots, initial offset and length values for all slots must be given. It is adequate to give all the slots zero offset and $\lambda_0/2$ length initially. Mutual coupling calculation (2.8) must be done for all the slots.

-Choose an initial value for the last slots offset (x_1). It is then possible to calculate values of $v(x_1)$, $g(x_1)$ and $f_n(x_1,l_{res1})$. The initial value is important because it is a starting point of the slot offsets and the whole array is designed iteratively. The power delivered to load is a function of slot admittances, thus the last slot's offset determine the power delivered to load in that manner.

-Calculated values of $f_n(x_1,l_{res1})$,$Y_n(x_1)$ and g_{mn} are placed in the equation (2.7). Then with a search algorithm, the slot length (l_1) which makes the imaginary part of the right hand side zero is found. By this way first slot's (first w.r.t matched load) offset, length and thus active admittance $Y_n^a{}_1$ is found.

-Y_1 can be found from equation (2.19). Next step is to search the couplet (x_2,l_2) for the second slot. This is done by simultaneously solving for equation (2.21) and diminishing the imaginary part of equation (2.7).

- Once (x_2,l_2) is found, the search for next slot is initiated. This process is repeated till the offset and length of the last slot (x_N,l_N) is found.

- Then mutual coupling matrix is calculated with new offsets and lengths and process is repeated. After a few iterations slot offsets and lengths converge to some value.

At this point the issues below must be checked:

- Is input admittance matched ($Y_N \approx 1$)? If not distance between the slots should be changed.

- Is maximum offset in the array in the safe limit? The slot's circuit model is no longer valid for very large offsets.

-Power delivered to load is calculated by the formulas below:

Power dissipated at n^{th} slot :

$$P_n = \frac{1}{2}\mathrm{Re}V_n V_n^{*}(\frac{Y_n^{a}}{G_0})^{*} \qquad (2.22)$$

Power delivered to load:

$$f = \frac{\frac{1}{2}V_1 V_1^{*}}{\frac{1}{2}V_1 V_1^{*} + \sum P_n} \qquad (2.23)$$

If the power dissipated in the load is greater than desired limit, first slot's offset, which was guessed initially, should be made greater. And design procedure is repeated with this value. Generally %5-10 of the power can be dissipated in the load.

In this thesis, a planar array of broad wall slotted waveguide, that will make a +/- 35 degrees phase steering in elevation is designed. The narrow wall inclined slot is not chosen because of its higher cross-polarization level and also the calculation of the mutual coupling betweeen the slots in the array is difficult for that kind of arrays. Bandwidth of the array should be %7, 3dB beam width in azimuth $\theta_{3dB,az}$ is 2° and elevation $\theta_{3dB,el}$ is 7°. Since bandwidth is relatively large, the array is chosen to be of end fed-traveling wave type. Suitable standard waveguide for operating frequency is WR90. The dimensions of WR90 is a = 22.86 mm and b = 10.16 mm and standard WR90 waveguide has a wall thickness of 1.27 mm, thus element spacing in elevation becomes 25.4 mm. This spacing is not suitable for 35° steering at the operation frequency, for which unwanted grating lobe goes in visible space. In order not to have grating lobe for 35° steering angle, broad wall dimension of the waveguide must be smaller. Formula below is used to calculate the maximum element spacing:

$$d_{\max} = \frac{\lambda}{1+\sin(35^\circ)} \qquad (2.24)$$

Waveguide broad wall dimension for this array was chosen as 18 mm including wall thickness. Wall thickness is 1 mm, and waveguide's inner broad wall dimension is 16 mm. A regular rectangular waveguide having a broad wall dimension of this length will have a cut off wavelength of $\lambda_c = 2a = 32$ mm, which falls into the operation frequency of this design. Therefore, the waveguide should be ridged waveguide for cut-off frequency to be lower, and since the top broad wall of the waveguide contains slots, the waveguide is designed to be a single ridged waveguide. Next chapter is about designing the single ridged slotted waveguide array (SR-SWGA) antenna.

CHAPTER 3

DESIGN OF A LINEAR SINGLE RIDGED WAVEGUIDE SLOTTED ARRAY ANTENNA

3.1. Single Ridged Waveguides

The geometry of a single ridged waveguide is given in Figure 3.1.

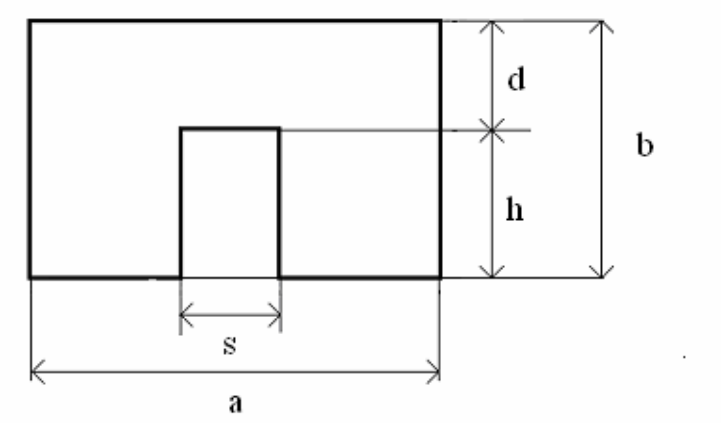

Figure 3.1 Ridge dimensions

The gap between the ridge and the top wall of the waveguide (d) form a parallel-plate waveguide, which propagates a TEM mode wave without a cut-off frequency. Narrower the gap, lower the cut-off frequency of the fundamental mode TE_{10}. Normally the bandwidth of the ridged waveguides is the band between the TE_{10} and TE_{30} mode cut offs for symmetrically excited waveguides (i.e TE_{20} is not excited). In this work, the waveguide will be used only in X-band.

3.1.1. Cut-Off Frequencies Of A Single Ridged Waveguide

The cut-off wavelengths of the odd TE_{n0} modes for a double ridged waveguide are given by [8]:

$$\frac{b}{d}\tan\theta_2 - \cot\theta_1 + \frac{B_c}{Y_{01}} = 0 \qquad (3.1)$$

and for even TE_{n0} modes,

$$\frac{b}{d}\cot\theta_2 - \cot\theta_1 + \frac{B_c}{Y_{01}} = 0 \qquad (3.2)$$

Where,

$$\theta_1 = \pi\frac{a-s}{\lambda} \qquad \theta_2 = \pi\frac{s}{\lambda} \qquad (3.3)$$

$\frac{B_C}{Y_{01}}$ is the normalized equivalent susceptance for the discontinuities in the ridge wave guide cross-section. It is given by [9]:

$$\frac{B_C}{Y_{01}} = \frac{\pi b}{\varepsilon\lambda}C_d \qquad (3.4)$$

and

$$C_d = \frac{\varepsilon}{\pi}\left[\frac{\alpha^2+1}{\alpha}\cosh^{-1}\left(\frac{1+\alpha^2}{1-\alpha^2}\right) - 2\ln\left(\frac{4\alpha}{1-\alpha^2}\right)\right] \qquad (3.5)$$

where

$\alpha = \frac{d}{b}$

Equation for odd modes can be written for a single ridged waveguide as

$$\frac{b}{d}\tan\left(\pi\frac{s/a}{\lambda/a}\right) - \cot\left[\pi\left(\frac{1-s/a}{\lambda/a}\right)\right] + 2\frac{b/a}{\lambda/a}\frac{\pi}{\varepsilon}C_d = 0 \qquad (3.6)$$

and for even modes;

$$\frac{b}{d}\cot\left(\pi\frac{s/a}{\lambda/a}\right)+\cot\left[\pi\left(\frac{1-s/a}{\lambda/a}\right)\right]-2\frac{b/a}{\lambda/a}\frac{\pi}{\varepsilon}C_d=0 \qquad (3.7)$$

for a single ridged waveguide.

A MATLAB code is written in order to solve this equation for s and d given that TE_{10} cut-off frequency = 6.25 GHz, b = 10.16mm and a = 16mm. s and d are chosen as 3 mm and 4.5mm respectively.

With these dimensions, $f_{c,10}$ = 6.275 GHz, $f_{c,20}$ = 16.681 GHz and $f_{c,30}$ = 24.914 GHz which is suitable for the purpose of operation.

3.1.2. Characteristic Impedance Of Single Ridged Waveguide

The characteristic impedance of a single ridged waveguide for TE_{10} mode at infinite frequency can be given as [8]:

$$Y_{0\infty}=2\sqrt{\frac{\varepsilon_0}{\mu_0}}\frac{\lambda_c}{2\pi l}\left[\frac{4d}{\lambda_c}\cos^2(\frac{\pi s}{\lambda_c})\ln\cos ec(\frac{\pi l}{2b})+\frac{\pi s}{2\lambda_c}+\frac{1}{4}\sin(\frac{2\pi s}{\lambda_c})+\frac{d}{b}\frac{\cos^2(\frac{\pi s}{\lambda_c})}{\sin^2(\frac{\pi(a-s)}{\lambda_c})}\left(\frac{\pi(a-s)}{2\lambda_c}-\frac{1}{4}\sin(\frac{2\pi(a-s)}{\lambda_c})\right)\right] \qquad (3.8)$$

At any frequency, characteristic impedance is:

$$Z_0(f)=\frac{1}{Y_{0\infty}\sqrt{1-\left(\frac{f_0}{f}\right)^2}} \qquad (3.9)$$

f_0: cut-off frequency of the TE_{10} mode.

Calculated Z_0 at the center frequency is 479.4 ohms.

3.2. Slot Characterization for the Single Ridged Waveguide

The first step in design is to get the admittance data of isolated slots for different slot offsets and lengths. Initially resonant length for each offset value is found with

Ansoft HFSS EM simulation software. The model for the simulation is shown in Figure 3.2. Simulations are done at slot offsets x = 1 mm, 1.5 mm, 2 mm, 2.5 mm, 3 mm and 3.5 mm. Admittance is calculated from the S-parameters by a way similar to described in [10].

A slot is cut on a waveguide part of length 4λg. The length and the offset value of the slot is input as a parametric variable in HFSS, making it possible to easily run a parametric sweep of variables. Error function of the simulations are chosen as δ = 0.003.

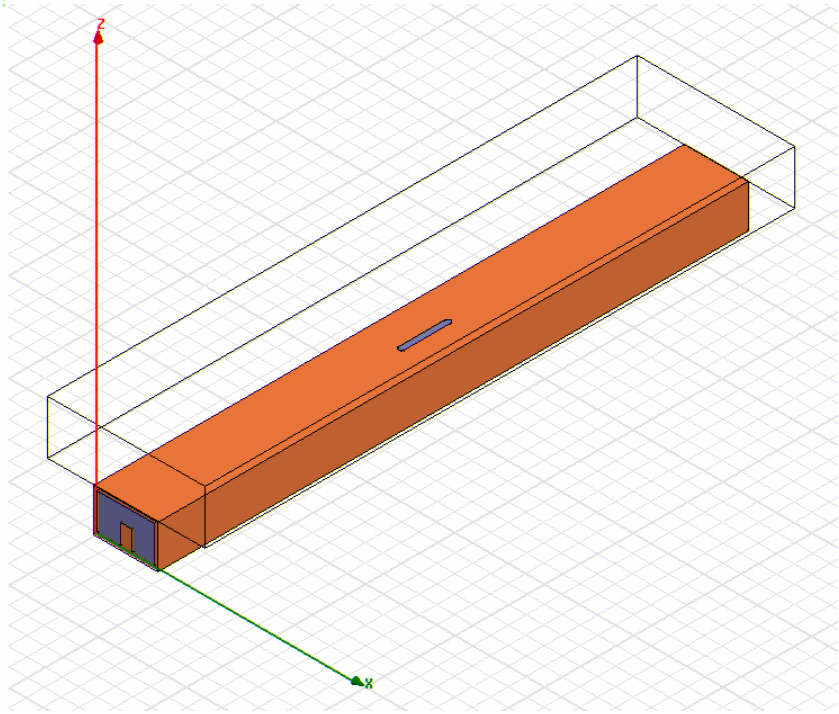

Figure 3.2 HFSS model for isolated slot characterization

For reference, a waveguide part without a slot is also simulated. The S_{21} parameter of this part is the reference for taking out the empty waveguide parts (Figure 3.3). Since the length of the waveguide part is same for on each side (slot is just in the middle), this reference can be used for all S_{11}, S_{21}, S_{12}, and S_{22} parameters.

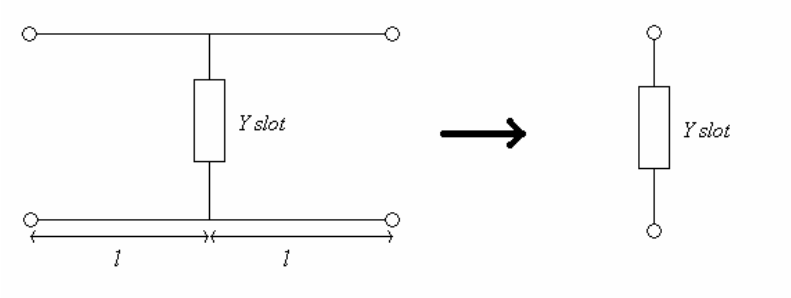

Figure 3.3 Circuit representation of modeled slot and removal of empty waveguide parts

$$S_{11,norm} = S_{11} / S_{21ref} \quad (3.10)$$

$$S_{21,norm} = S_{21} / S_{21ref} \quad (3.11)$$

$$S_{12,norm} = S_{12} / S_{12ref} \quad (3.12)$$

$$S_{22,norm} = S_{22} / S_{12ref} \quad (3.13)$$

Then Y can be deduced from S_{11} and S_{21}. Ideally S_{11} and S_{22}, S_{21} and S_{12} should be same. However, there are little differences because of the simulation error. Average of the admittance value obtained from reflection and transmission parameters is used (eqn. (3.16)).

Admittance obtained from reflection parameters:

$$Y_r = \frac{-(S_{11norm} + S_{22norm})}{1 + (S_{11norm} + S_{22norm})/2} \quad (3.14)$$

Admittance obtained from transmission parameters:

$$Y_t = \frac{2}{(S_{21\,norm} + S_{12\,norm})/2} - 2 \quad (3.15)$$

$$Y = \frac{Y_r + Y_t}{2} \qquad (3.16)$$

Characterization polynomials are then derived from these data, and plotted in Figure 3.4.

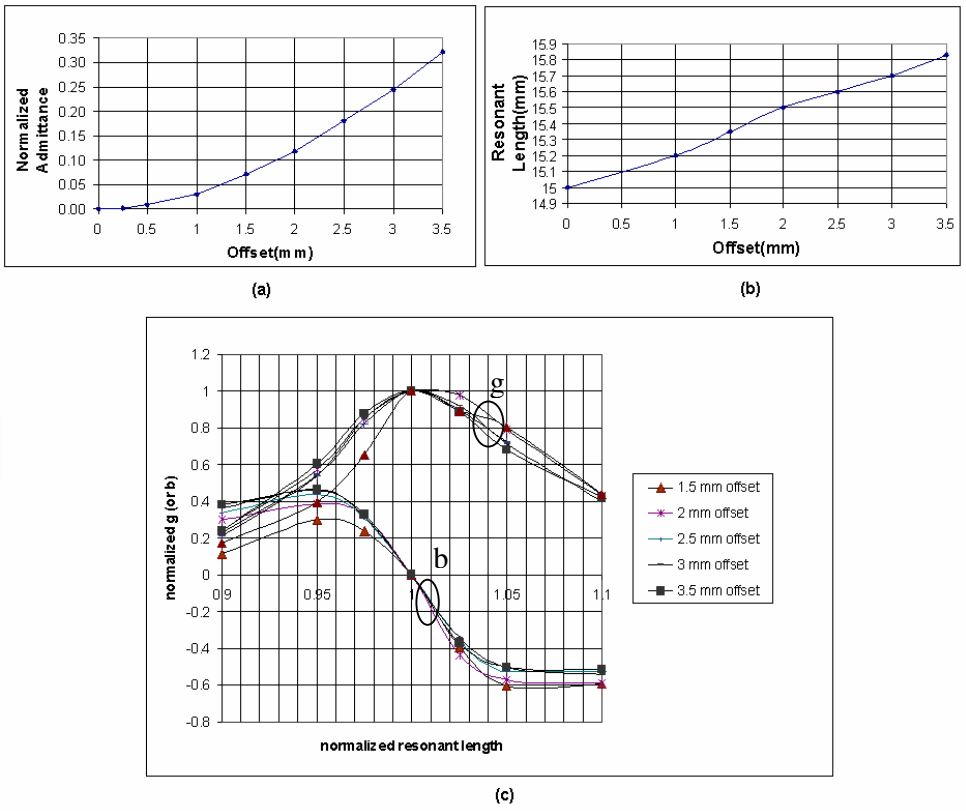

Figure 3.4 Characterization polynomials generated using simulation results: (a) Slot admittance vs. slot offset (b) Slot resonant length vs. slot offset (c) Normalized admittance vs. normalized length

3.3. Synthesis of the Array

A MATLAB code was written for synthesis of a traveling wave shunt slotted waveguide. Code runs with the algorithm described in section 2.3.2. The inputs of the code are:

- Design Frequency at which the characterization polynomials are generated.
- Number of slots and array amplitude distribution
- Distance between slots
- Offset of the last slot (nearest to matched load)

And the outputs of the synthesis program are:

- Slot offsets
- Slot lengths
- Fractional power dissipated at the matched load.
- Active admittance of the slots in the array

Design Criteria:

- Azimuth 3dB Beamwidth : 2°
- Max. Sidelobe Level : -35 dB
- Operation Band : X - Band
- Max. Return Loss : 30 dB
- Max. Power dissipated in the load: % 5 of input power

The element spacing d should be $> \lambda_g/2$ or $< \lambda_g/2$. Since mutual coupling will be less for $d > \lambda_g/2$, d is chosen to be $0.59\lambda_g$. Thus the main beam direction will be

$$\Phi_0 = \arcsin(\beta/k_0 - \lambda_0/2d) = 6.2° \qquad (3.17)$$

at the center frequency.

Array amplitude distribution is chosen to be Taylor 35 dB ñ=5. Taylor distribution has the advantage that the far sidelobes decrease compared to other distributions such as Tchebychev, binomial, etc. In order to have 2° beamwidth for this spacing,

and amplitude distribution, 42 elements are used. A linear array having 42 slot elements with spacing $0.59\lambda_g$ and Taylor 35 dB ñ=5 amplitude distribution is synthesized. The coefficients of the amplitude distribution are shown in Table 3.1.

Table 3.1 Taylor 35 dB ñ=5 amplitude distribution

Element No	Amplitude Coefficient	Element No	Amplitude Coefficient	Element No	Amplitude Coefficient
1	0.1628	15	0.8291	29	0.7778
2	0.1692	16	0.8752	30	0.7223
3	0.188	17	0.9153	31	0.6638
4	0.2182	18	0.9485	32	0.6031
5	0.2583	19	0.9739	33	0.5413
6	0.3064	20	0.9912	34	0.4795
7	0.3605	21	1	35	0.4187
8	0.4187	22	1	36	0.3605
9	0.4795	23	0.9912	37	0.3064
10	0.5413	24	0.9739	38	0.2583
11	0.6031	25	0.9485	39	0.2182
12	0.6638	26	0.9153	40	0.188
13	0.7223	27	0.8752	41	0.1692
14	0.7778	28	0.8291	42	0.1629

3.4. Simulation Results

The synthesized linear array is simulated by Ansoft HFSS EM simulation software.

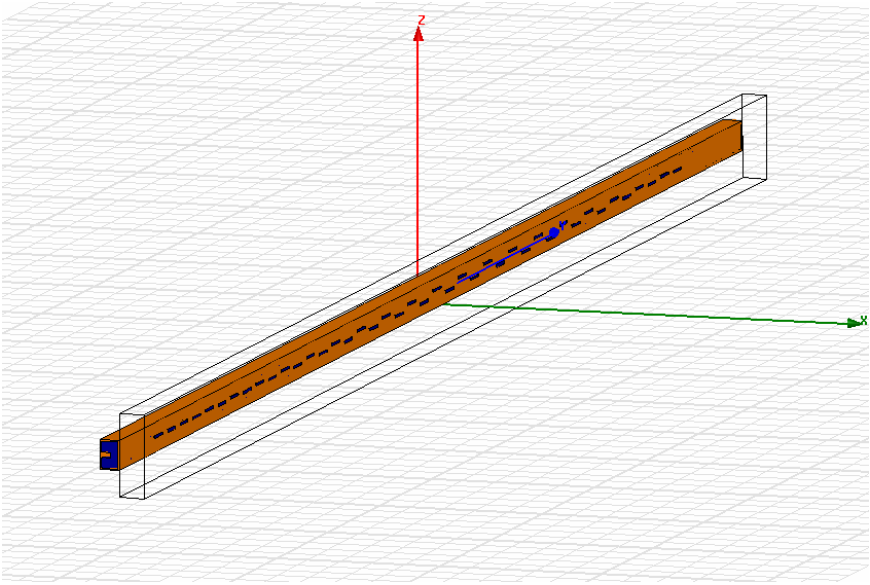

Figure 3.5 Geometry of the linear single ridged slotted waveguide array

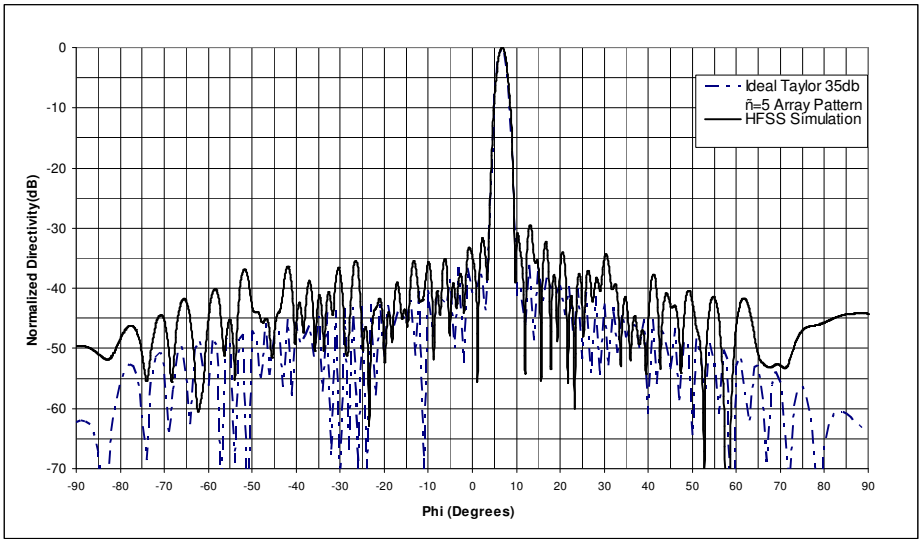

Figure 3.6 Simulated azimuth (θ = 90°) co-polarized pattern of the linear SR-SWGA antenna

In the principal plane cut (θ = 90°), sidelobes are higher in the order of 5-6dB than the array factor of Taylor 35dB ñ=5 amplitude distribution. Half power beamwidth of the array is 2.1 degrees in the azimuth cut. It is necessary to investigate the

radiation pattern in the whole space, since sidelobes should be low in the whole pattern.

HFSS analysis of the co-polarized and cross-polarized radiation pattern in the front hemisphere is shown in Figure 3.7 and Figure 3.8 respectively. In the figures, floor (the light blue grid) is 35 dB below maximum directivity. The non-linearity of the pattern is due to the fact that the array is of traveling wave type. At some specific angles, side lobes are much higher than the desired level for both co- and cross polarization. These side lobes are called; butterfly lobes (because of the shape they have), secondary lobes, or Gruenberg lobes. Gruenberg was the first one to analyze this effect [11]. The reason for these lobes is the non - collinear placement of the slots and can be deduced from the array factor. The butterfly lobes are discussed in the next chapter in detail, and the solutions for suppressing these lobes are given.

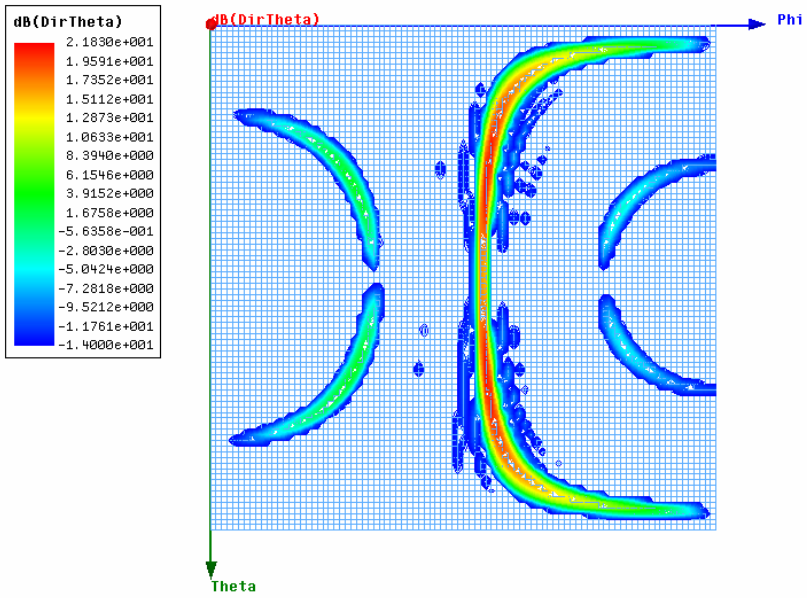

Figure 3.7 2-D simulated co-polarized radiation pattern (directivity) of the linear SR-SWGA antenna

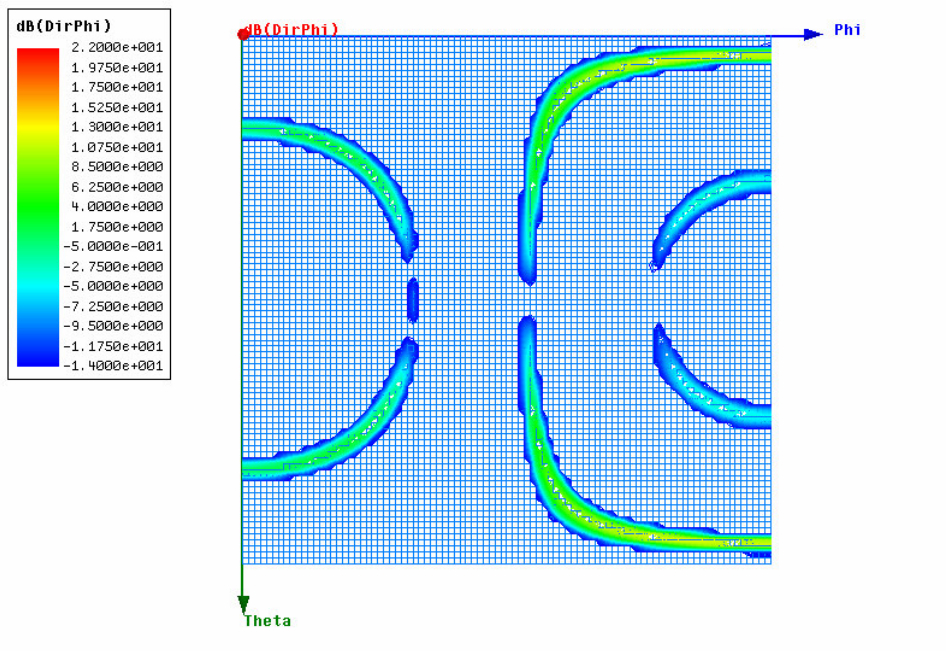

Figure 3.8 2-D simulated cross-polarized radiation pattern of the linear SR-SWGA antenna

It is deduced from Figure 3.8 that, the cross polarization level at the main beam position increases as the theta (θ) angle deviates from 90° (θ=90° is a principle plane-cut). However the cross-pol. should be low since cross-pol. component is low for a single slot. At first, the reason for this was thought to be the closeness of the ridge to the radiating slotss in the waveguide. However, a linear SWGA antenna employing standard WR-90 waveguide was also investigated from this point of view and it was found that its cross-polarized pattern is only a 2dB lower than that of SR-SWGA antenna. The reason of this is investigated by simulations made in CST Microwave Studio software. Two slots are used in simulations, and the resultant cross- and co- polarized E-fields on the slot are drawn in Figure 3.9 and Figure 3.10, respectively. It is obvious from Figure 3.9 that at the slot ends cross-polarized component is not zero. Furthermore, the direction of the cross-polarized field is reversed in the adjacent slot. This explains why the cross-polarized component in the far field radiation patern vanishes in the θ=90° principal plane cut.

This high-cross-pol. problem arises for the 2D planar array, when the beam is steered in elevation plane(φ is at the main beam position (φ=6.2°), θ_0 is steered).

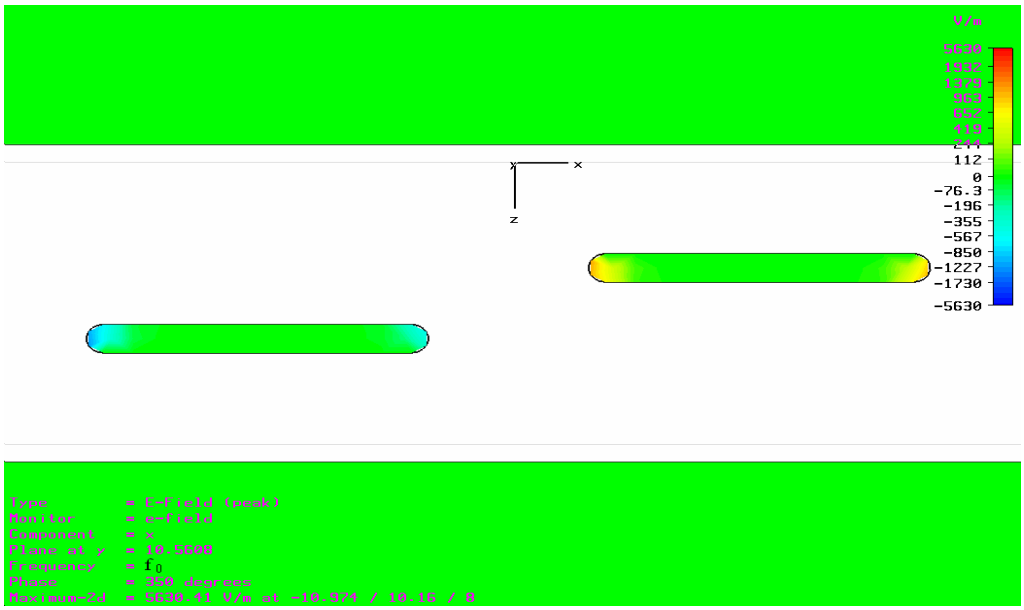

Figure 3.9 Simulated cross-polarized component of E-field on two slot geometry

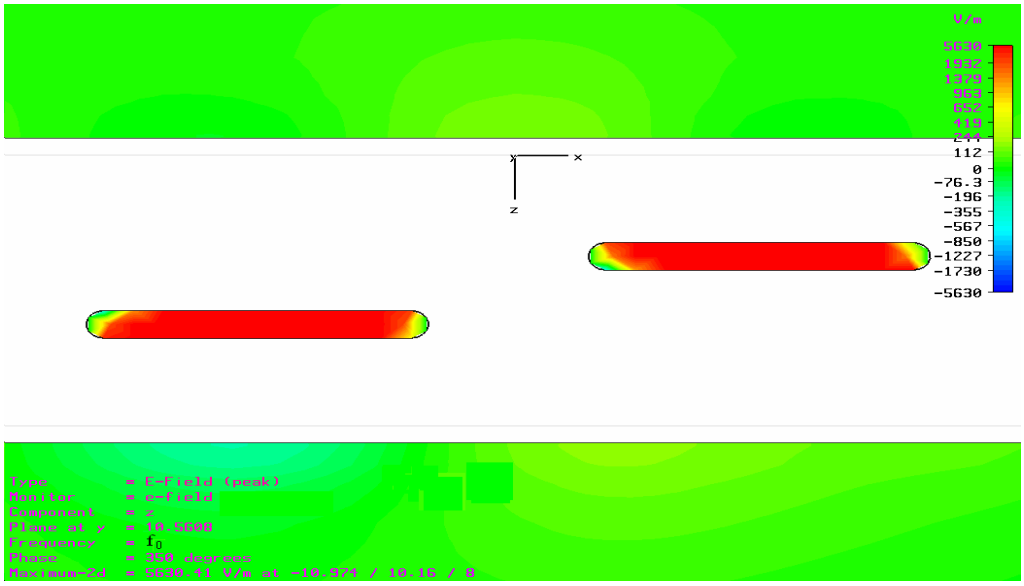

Figure 3.10 Simulated co-polarized component of E-field on two slot geometry.

In chapter 6 , planar array will be formed and in the measurement results it will be shown that the cross-pol. value will be below a certain value that can be put up with, in this particular design.

3.5. Measurements of the Linear SR-SWGA

The designed array is manufactured and the radiation pattern of the array is measured in a planar near – field antenna measurement system for 10% frequency band (Figure 3.12 **-** Figure 3.22). The slot offsets and lengths of the manufactured antenna is measured with a Coordinate Measuring Machine(CMM). The array is simulated in Ansoft HFSS again with the measured values, in center frequency. The measured and simulated radiation pattern of the antenna in principal azimuth cut is plotted in Figure 3.11. The simulated and measured patterns are consistent with eachother. If the HFSS simulation results in Figure 3.6 and Figure 3.11 are compared, it is seen that at some specific angles (-34° and +48°), there is a side lobe increase in Figure 3.11. Since this simulation is done with measured slot offsets and lengths, it is understandable that the increase is due to the manufacturing errors.

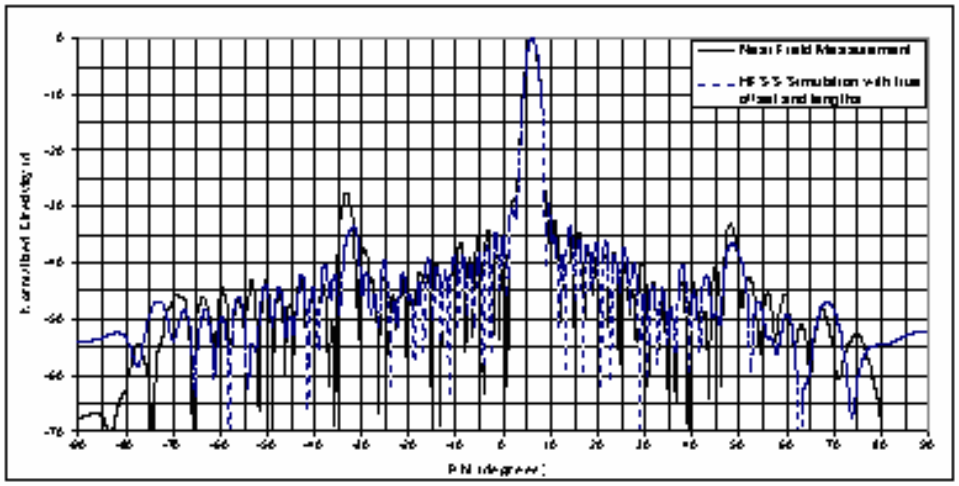

Figure 3.11 Measured azimuth (θ= 90°) co-polarized pattern of the linear SR-SWGA antennna

Azimuth cut for different frequencies are also given in this section. In addition 2-D radiation pattern for front hemisphere of the antenna is shown in Figure 3.23. The amplitude of the secondary beam is as high as -14dB relative to the beam peak. Figure 3.24 shows the power dissipated at the load.

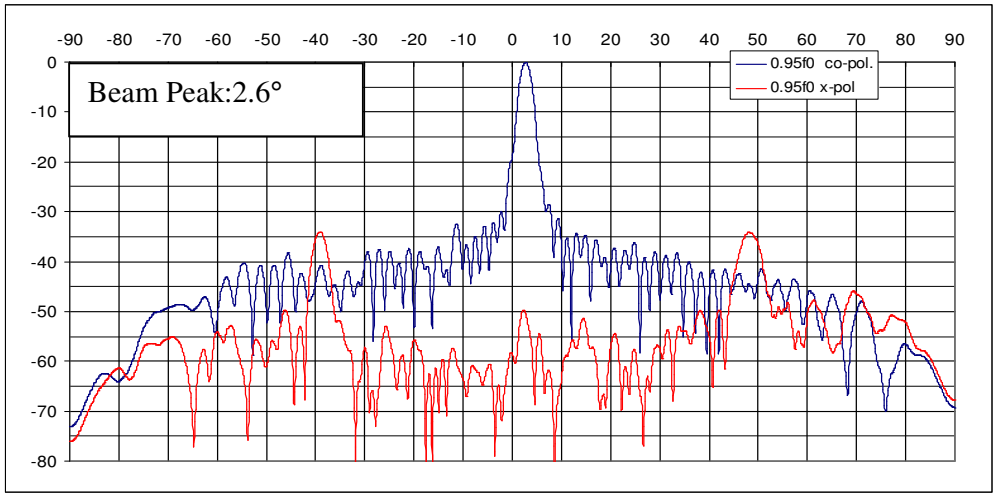

Figure 3.12 Measured azimuth (θ= 90°) co and cross - polarized patterns of the linear SR-SWGA antenna at $0.95f_0$.

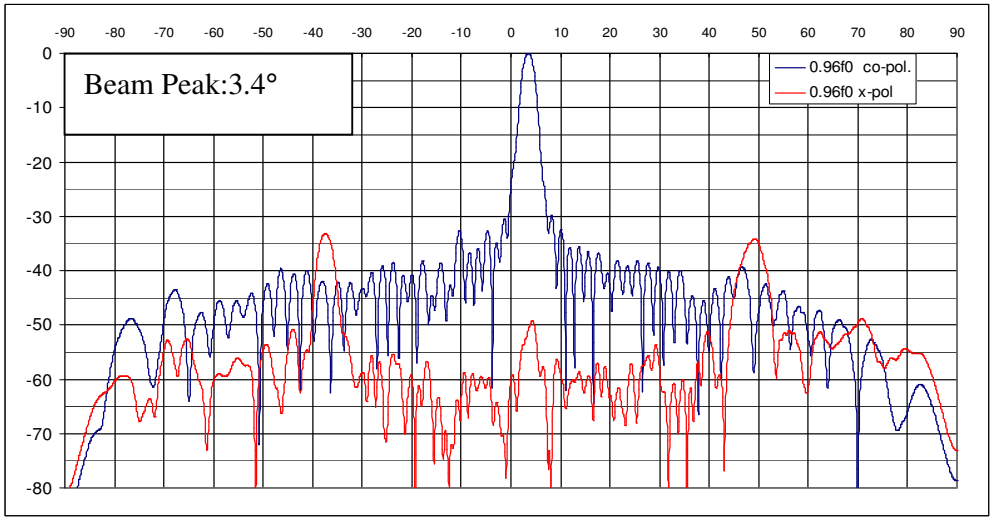

Figure 3.13 Measured azimuth (θ= 90°) co and cross - polarized patterns of the linear SR-SWGA antenna at $0.96f_0$.

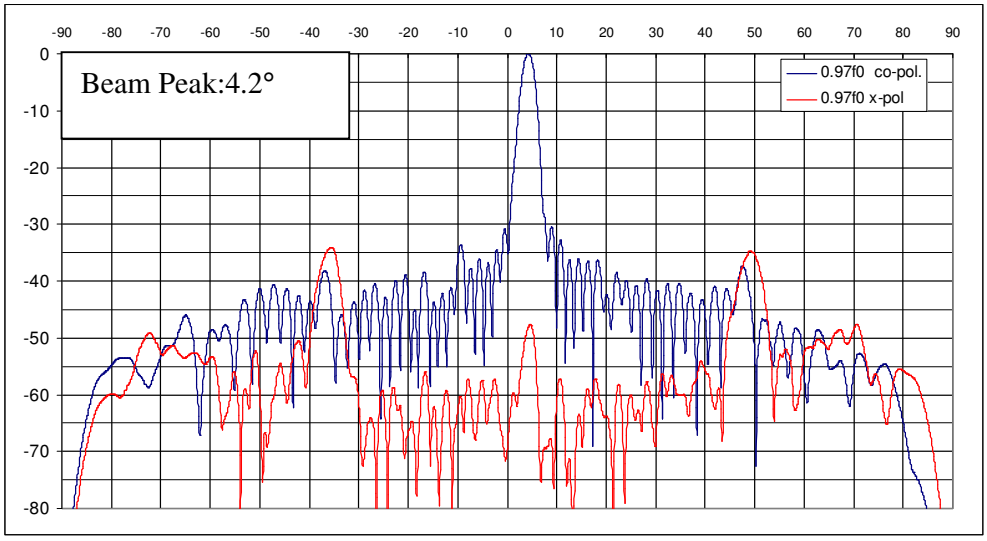

Figure 3.14 Measured azimuth (θ= 90°) co and cross - polarized patterns of the linear SR-SWGA antenna at $0.97f_0$.

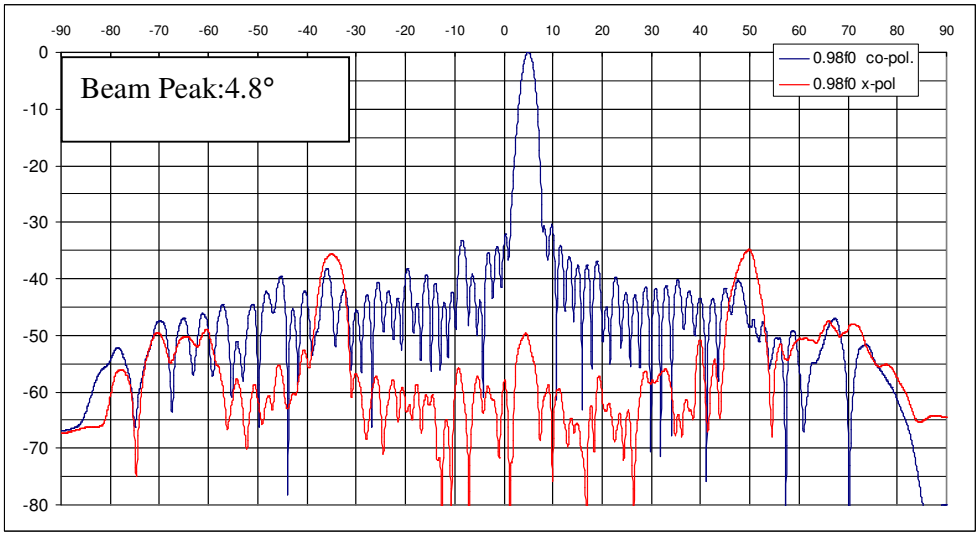

Figure 3.15 Measured azimuth (θ= 90°) co and cross - polarized patterns of the linear SR-SWGA antenna at $0.98f_0$.

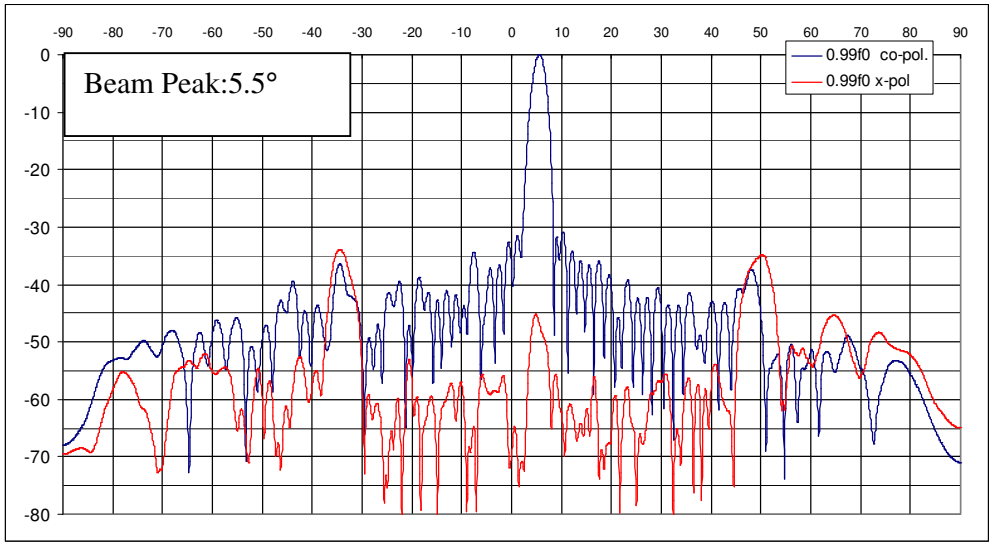

Figure 3.16 Measured azimuth (θ= 90°) co and cross - polarized patterns of the linear SR-SWGA antenna at $0.99f_0$.

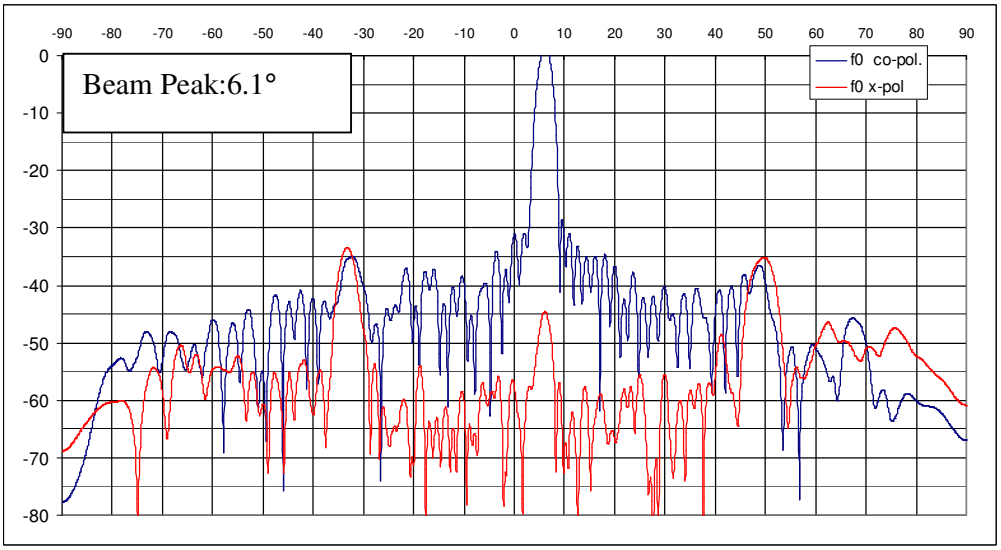

Figure 3.17 Measured azimuth (θ= 90°) co and cross - polarized patterns of the linear SR-SWGA antenna at f_0.

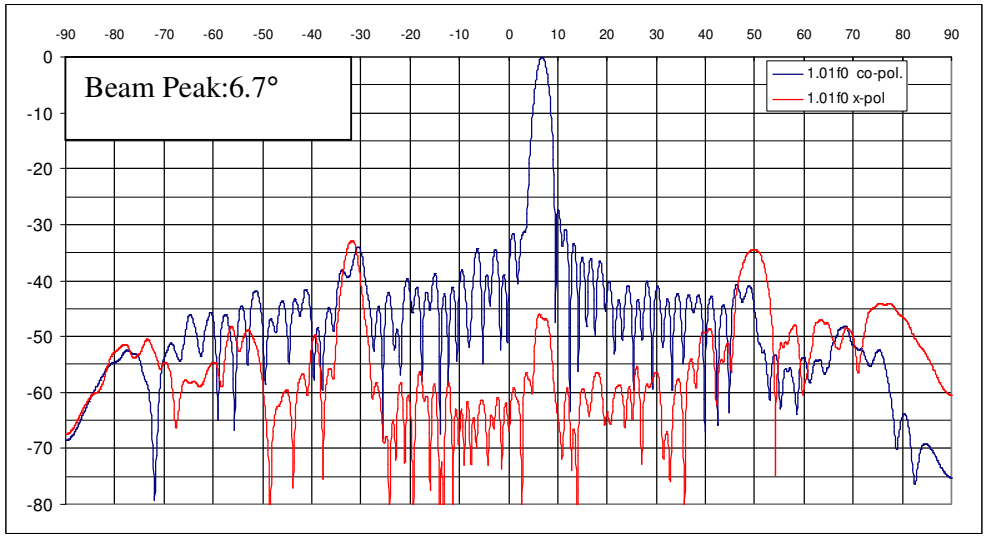

Figure 3.18 Measured azimuth (θ= 90°) co and cross - polarized patterns of the linear SR-SWGA antenna at $1.01f_0$.

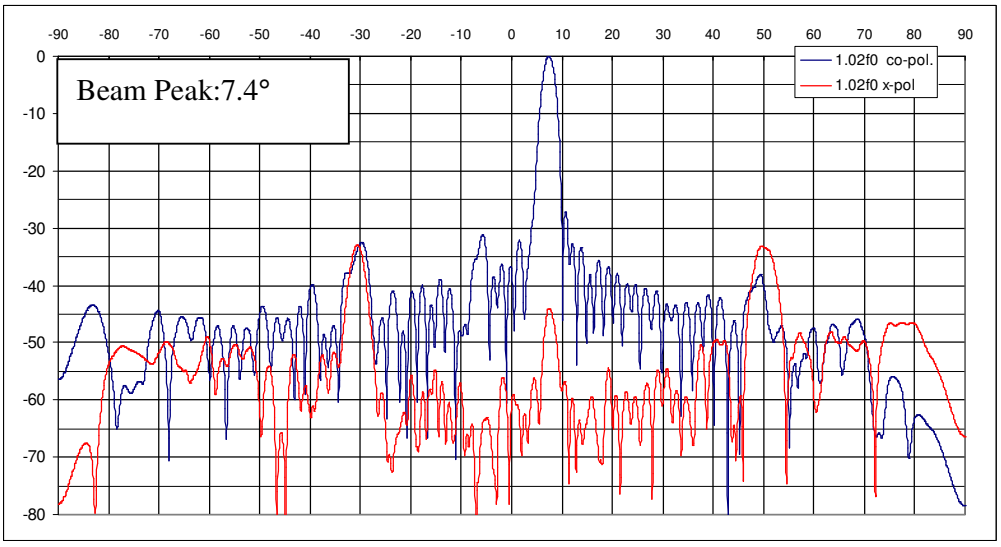

Figure 3.19 Measured azimuth (θ= 90°) co and cross - polarized patterns of the linear SR-SWGA antenna at 1.02 f_0.

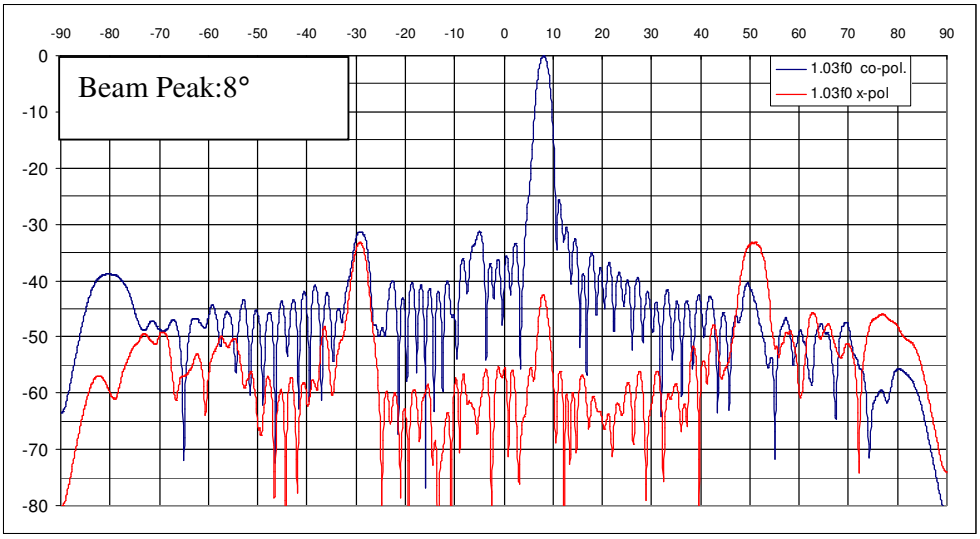

Figure 3.20 Measured azimuth (θ= 90°) co and cross - polarized patterns of the linear SR-SWGA antenna at 1.03 f_0.

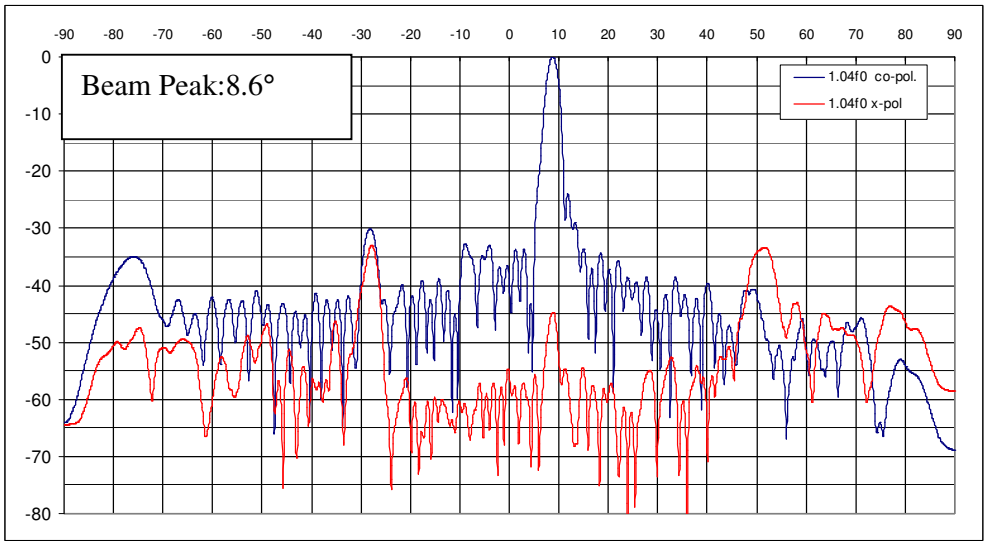

Figure 3.21 Measured azimuth (θ= 90°) co and cross - polarized patterns of the linear SR-SWGA antenna at 1.04f_0.

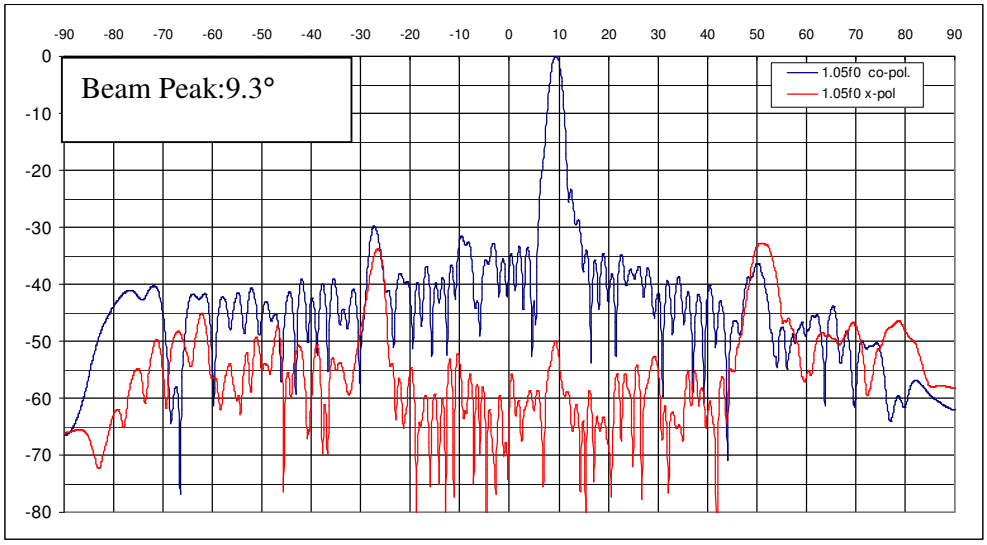

Figure 3.22 Measured azimuth (θ= 90°) co and cross - polarized patterns of the linear SR-SWGA antenna at $1.05f_0$.

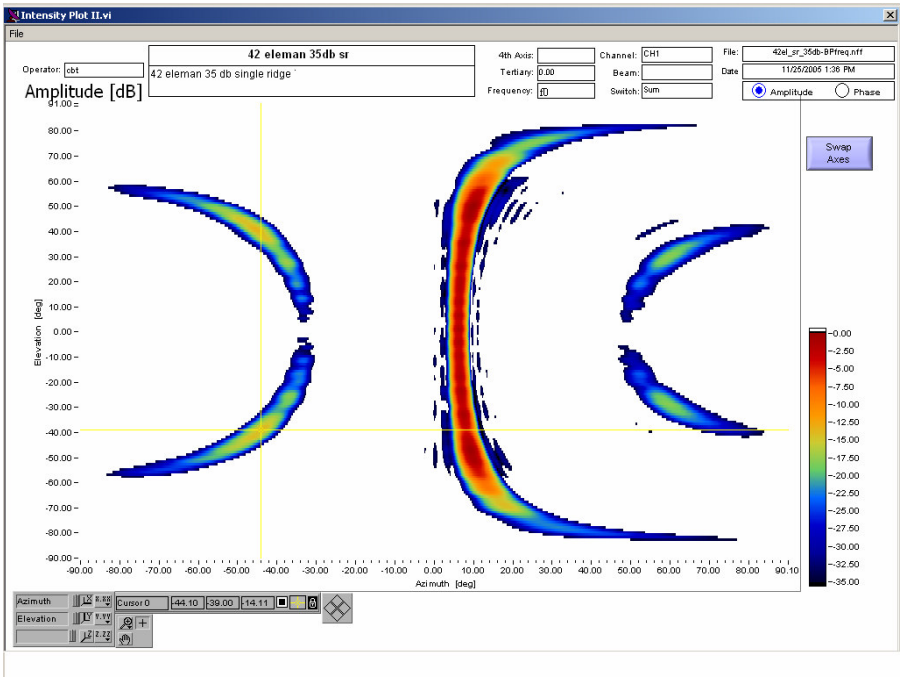

Figure 3.23 Measured color coded contour plot of radiation pattern for front hemisphere of linear SR-SWGA antenna at the center frequency.

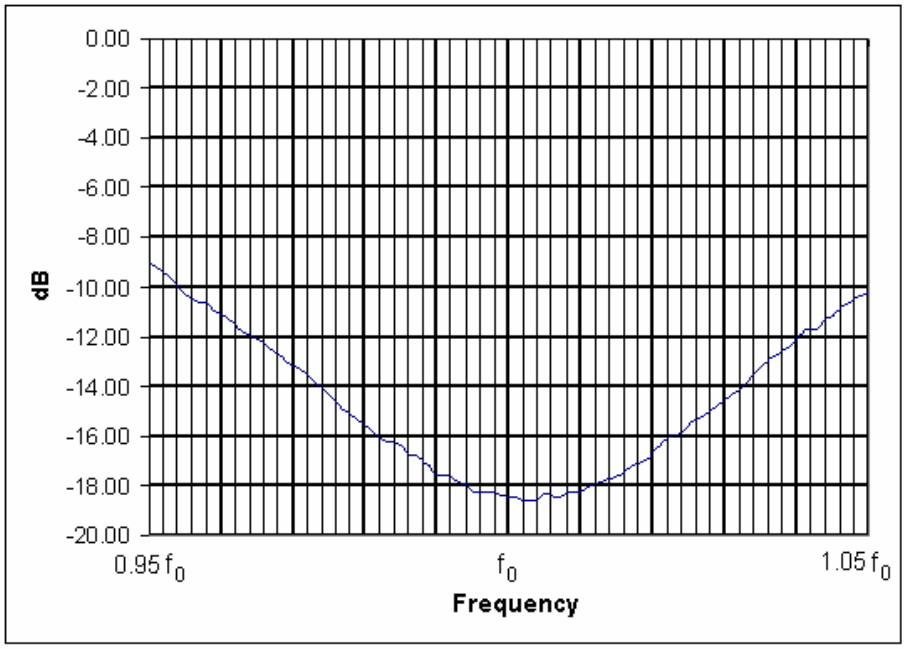

Figure 3.24 Measured transmission parameter of the linear SR-SWGA antenna (with HP8510C NA)

The fraction of the power delivered to the matched load (f_{load})can be calculated from the transmission parameter (S_{21}) of the antenna ($f_{load} = 10^{S21_{db}/10} \times 100$). It should be minimum at the center frequency since all the slot are resonant at that frequency, so the radiated power is maximum. Observing Figure 3.24, we can say that power dissipation is minimum near the design frequency (1.5 %). This fact also verifies that resonance condition for the slots are met at the design frequency. In 6% frequency band, power dissipation is less than 5%.

The first side lobes of the array increase as the operation frequency goes away from the center frequency, as expected. The design is done at only center frequency and the slots are no longer resonant for frequencies other than center. Thus, the amplitude distribution over the array is deviated from the designed amplitude distribution. Furthermore, the first side lobe levels are in the order of -30dB, which

is not sufficient for the design criteria. So, the amplitude distirbution is changed to Taylor 40dB for the next designed array in chapter 5.

At the center frequency, beampeak is at 6.1°, and half-power beamwidth is 2.2°. This value for beamwidth is large as compared to design criteria. Thus, the number of elements should be increased. Calculated and measured values of beam peak position is given in Table 3.2**.** There is a maximum 0.4° difference in beam peak position over the band. This may be due to the mutual coupling between slots. Half power beam width is 2.4° at the lowest frequency ($0.95f_0$) and 2° at the highest frequency ($1.05f_0$).

Table 3.2 Calculated and Measured Beam Peak Values for Different Frequencies

Frequency(f0)	Calculated Beam Peak Position (degrees)	Measured Beam Peak Position(degrees)
0.95	2.3	2.6
0.96	3.2	3.4
0.97	4.0	4.2
0.98	4.8	4.8
0.99	5.5	5.5
1	6.3	6.1
1.01	7.0	6.7
1.02	7.7	7.4
1.03	8.4	8
1.04	9.0	8.6
1.05	9.7	9.3

CHAPTER 4

SECOND ORDER BEAMS IN SWGA'S

4.1. Introduction

Because of the non-linear placements of the slots on the waveguide, at some specific angles, grating lobes which are called butterfly lobes, rise above the sidelobe level. Kurtz and Yee [12] and investigated this effect with a four-element array and derived the levels of the butterfly lobes for different kind of slotted waveguide arrays. Forooraghi and Kildal [13] used a linear longitudinal slotted waveguide array having all the slots have the same offset δ as in Figure 4.1.

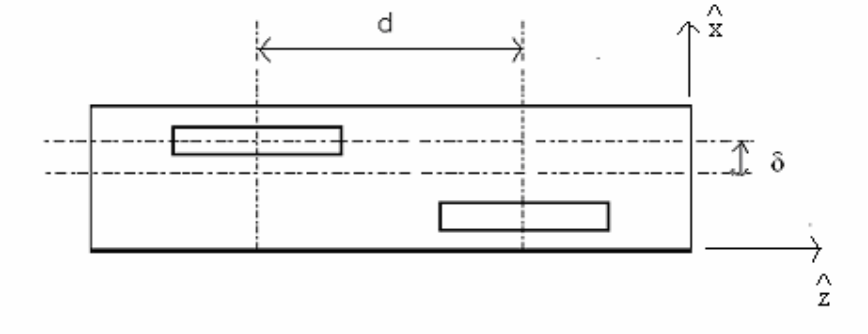

Figure 4.1 Two element array

For a planar array, radiation pattern is:

$$E(\theta,\phi) = \frac{e^{-jkr}}{r} G(\theta,\phi) A(\theta,\phi) \qquad (4.1)$$

where

$G(\theta,\phi)$ is the pattern of the two element as shown in Figure 4.1**.**

$$G(\theta,\phi) = G_{slot}(\theta,\phi)e^{-jk_0\delta\sin\theta\sin\phi} + G_{slot}(\theta,\phi)e^{+jk_0\delta\sin\theta\sin\phi}e^{+j(kd\cos\theta-\alpha)} \quad (4.2)$$

$G_{slot}(\theta,\phi)$ is the radiation pattern of a single slot.

$A(\theta,\phi)$ is the array factor of N pairs.

$$A(\theta,\phi) = \sum_{n=0}^{N-1} a_n e^{j2n(kd\cos\theta-\alpha)} \quad (4.3)$$

Array maximum occurs at $\cos\theta_0 = \frac{\alpha}{k_0 d}$ and first grating lobe occurs at $\cos\theta b = \frac{\alpha \mp \pi}{k_0 d}$.

The relative level of the grating lobe can be written as [12]:

$$B(\theta,\phi) = \left|\frac{G(\theta_b,\phi)}{G(\theta_0,0)}\right| \quad (4.4)$$

Isolated slot pattern can be approximated with a sinusoidal $G_{slot}(\theta,\phi) \cong Sin\theta$.

Therefore, $B(\theta,\phi)$ can be written as,

$$B(\theta,\phi) = \left|k_0\delta Sin\theta_b Sin\phi\right| \quad (4.5)$$

It is obvious from eqn.(4.5) that as the slot offset increases, level of the second order beams increase. Also, second order beams vanish at $\phi = 0°$.

The secondary beams are investigated with MATLAB. A linear array with ideal Taylor 40dB distribution is assumed for the array amplitude distribution, but slot positions are taken from the designed array in the previous chapter. Array factor with and without slot offsets are shown in Figure 4.2.

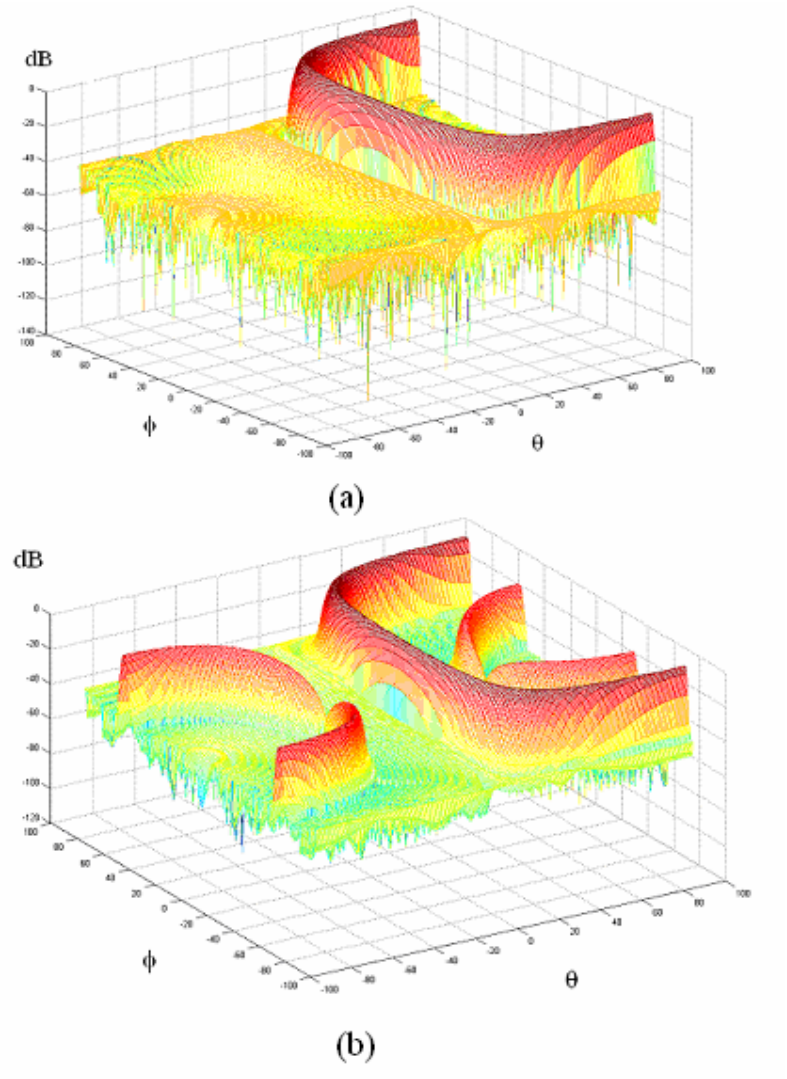

Figure 4.2 Calculated array factor of linear SR-SWGA (a) without offsets, (b) with calculated offsets.

Butterfly lobes diminish at the principal plane. Thus, if an array is formed in elevation, there will be no butterfly lobes if there is no beam steering in elevation plane. However, if beam is formed at angles different than 0 degree in elevation, the array factor cancellation will not be present. Using a MATLAB code, 2 –D array is formed with the design offset and length values (42 elements are used with the same spacing). Azimuth element amplitude distribution is ideal Taylor 40 dB ñ=6 and

elevation amplitude distribution is Taylor 30 dB ñ=4. 18 elements are chosen for elevation array. Figure 4.3 shows the 2-D array factor for scan angles 0, 5, 10 and 20 degrees, and also the principal azimuth plane cut. The situation gets worse as the scan angle increase. The level of the secondary beam is as high as -29dB relative to the main beam for 5 degrees; -22dB and -17 dB for 10 and 20 degrees steering angles respectively.

There are a number of ways in order to avoid these extra beams, which are discussed in the next section.

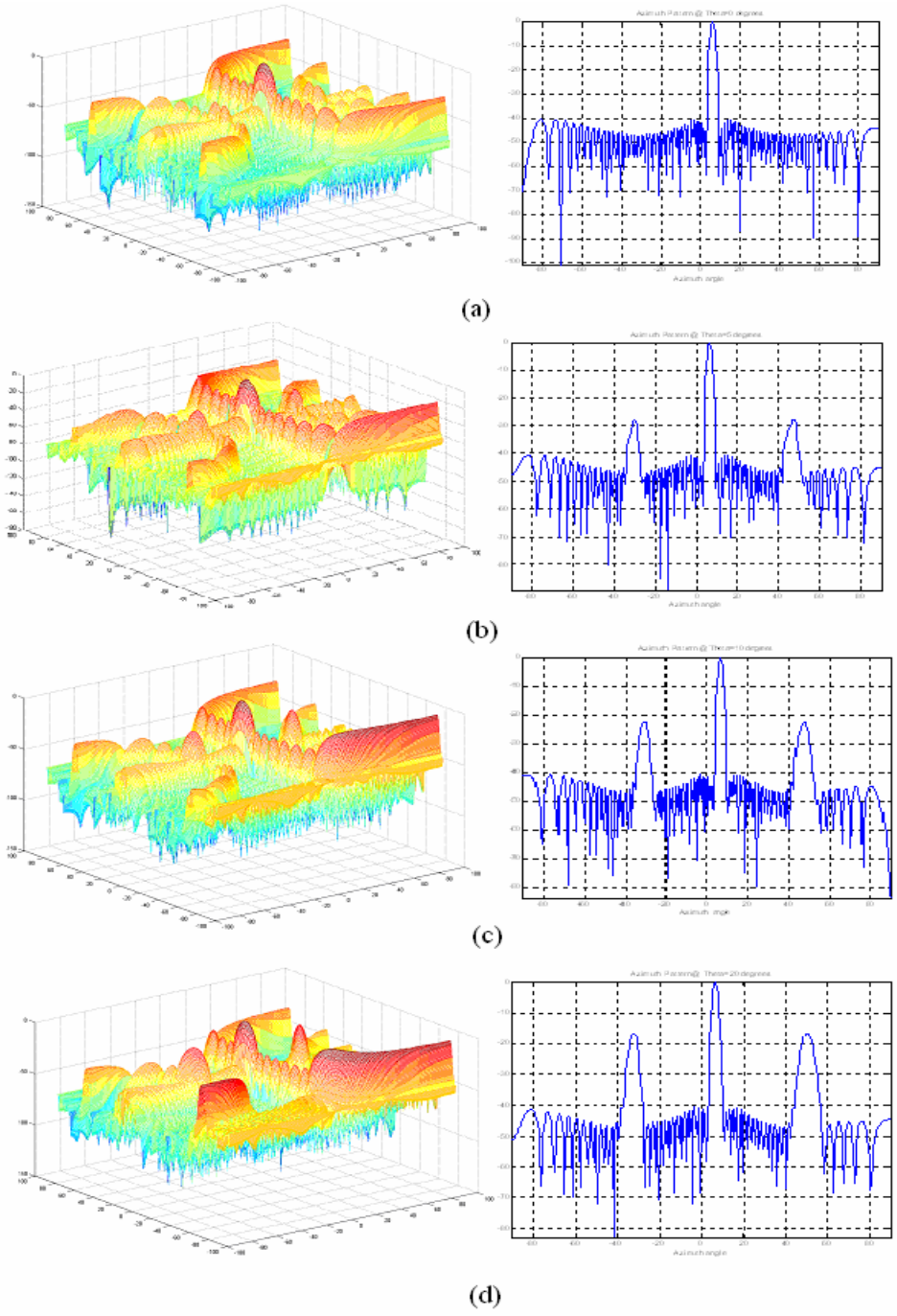

Figure 4.3 3-D patterns and azimuth cuts of the calculated array factor for planar SR-SWGA (18 x 42 elements) for beam steering in elevation to (a) 0°, (b) 5°, (c)10°, (d)20° .

4.2. Second Order Beam Suppression in Slotted Waveguide Phased Arrays

There are a number of ways for suppressing unwanted off-axis lobes [12]. Each of them tries to have a uniform E-field (a collinear array) on the aperture. Some of the methods can be listed as follows:

1) Placing all the slots on the center of the waveguide and excite the slots by having different waveguide heights on the sides of the ridge.

2) Placing all the slots on the center of the waveguide and excite the slots by irises or posts placed in the waveguide.

3) Placing baffles along the waveguide. The slots will radiate into a parallel plate region and the non-linear placement effect of the slots will be eliminated.

Second order beams can be also suppressed by changing the slot element spacing. This solution gives restrictions to the array size.

In this thesis the third option is chosen because of its design and manufacturing advantage over the first two. The next chapter is about designing a SR-SWGA with baffles.

CHAPTER 5

DESIGN OF A LINEAR SINGLE RIDGED WAVEGUIDE SLOTTED ANTENNA ARRAY WITH BAFFLES

5.1. Introduction

In order to avoid secondary beams, an effective method is to place baffles on top of the waveguide and make the slots radiate between the baffles. By this way, slots radiate into baffle region and at the aperture E-field distribution is continuous as opposed to discrete case for individual radiating slots. If the baffle geometry is chosen well, second order lobes can be kept below ordinary sidelobe level.

Baffles are also used for decreasing cross polarized component, decreasing mutual coupling between rows. In addition, gain can be increased by flaring out the baffle like a horn antenna.

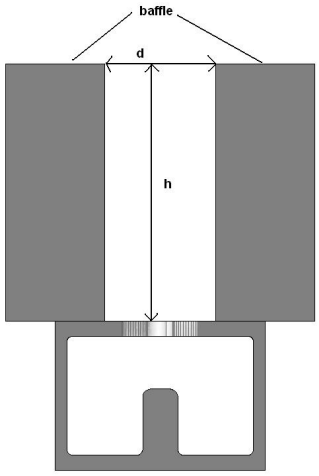

Figure 5.1 Baffle geometry on a SR-SWGA

For the design, isolated slot characterization polynomials should be formed in presence of the baffle, since the baffles affect the admittance of the slots. But before characterization, proper baffle geometry should be chosen. Distance between baffles (d) should be smaller than 0.5λ to avoid propagation of high order modes between the baffles [13]. The fundamental mode has uniform amplitude and phase between baffles. The element patterns of the successive alternating slots (i.e placed in different side of the waveguides) become same then, and second-order beams diminish. However, because of the evanescent higher order modes, field distribution at the mouth of the parallel plate (baffle) is effected and second-order beams do not vanish completely. To have evanescent modes diminish at the open end, baffle must be high enough. It is shown in [14] that as the baffle height increases, butterfly lobe level decreases. Two arrays with two different types of baffles, each having 0.3 λ distance (d), but one with 0.3 λ height, other with 0.7 λ height are simulated in HFSS. The slot offsets and lengths were taken from the design in chapter 3. Maximum second order levels are observed to be -22dB for the array having 0.3 λ height baffle and -33dB for the array having 0.7 λ-height baffle. Therefore, baffle height is chosen as 0.7 λ, and the distance between baffles is chosen as 0.3 λ at the center frequency.

5.2. Slot Characterization with Baffle

Characterization is repeated with the presence of baffles with Ansoft HFSS. For the synthesis of the array, mutual coupling between slots in the presence of baffle should be taken into account. However, in this thesis, mutual coupling is again taken as if the slots were embedded in an infinite ground plane.

In order to compare with the simulation results, a number of waveguides for characterization is manufactured and measured.

5.2.1. Isolated Slot Characterization with Measurements

To determine the admittance of a slot, firstly s-parameters of the waveguide part having a slot is measured, then slot is closed with a conductive tape and S_{21} is measured. This is the reference data. S_{21} of this reference is subtracted from the s-parameters of the measured parts. By this way the measurement plane is moved to the center of the waveguide, removing the empty waveguide (transmission line) sections. Measurements are done with HP8510 C Vector Network Analyzer. For feeding the waveguides, an adapter from SMA to single ridge waveguide part is developed. Before measurements, SMA calibration was performed in 7 – 12 GHz band. To minimize the reflections from the adapter, time domain gating is used.

The polynomials derived from the measured and simulated data are shown at the same figures (Figure 5.2, Figure 5.3, and Figure 5.4).

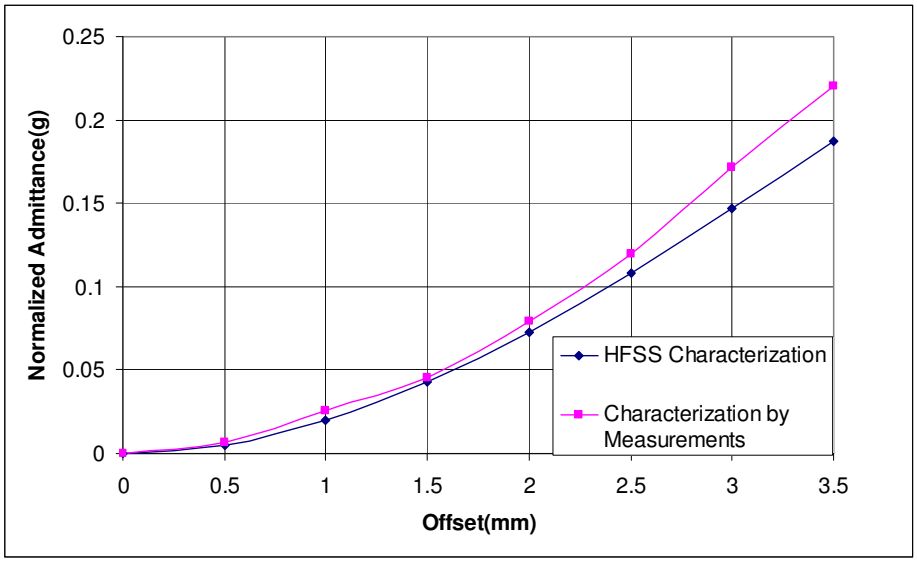

Figure 5.2 Admittance vs. slot offset for isolated slot radiating between baffles

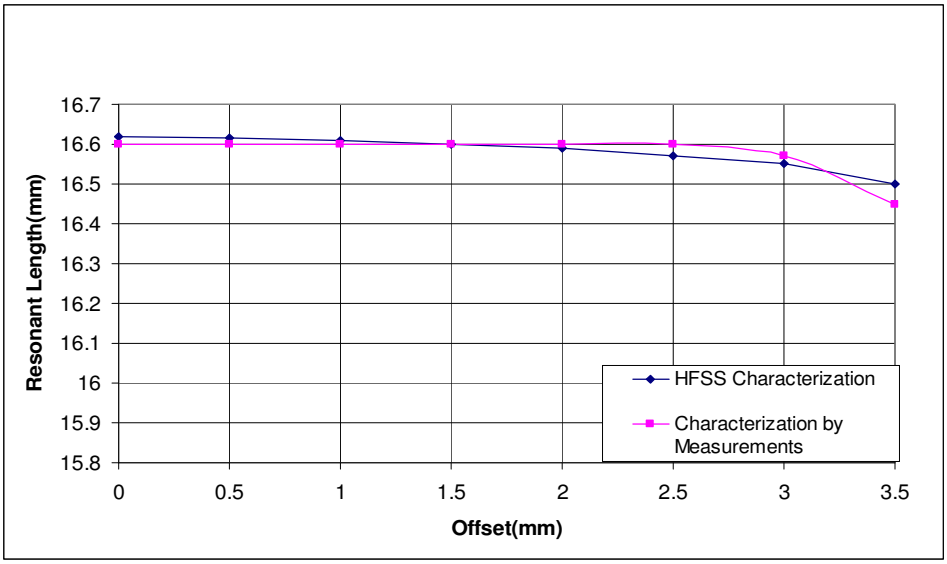

Figure 5.3 Resonant length vs. Slot offset for isolated slot radiating between baffles

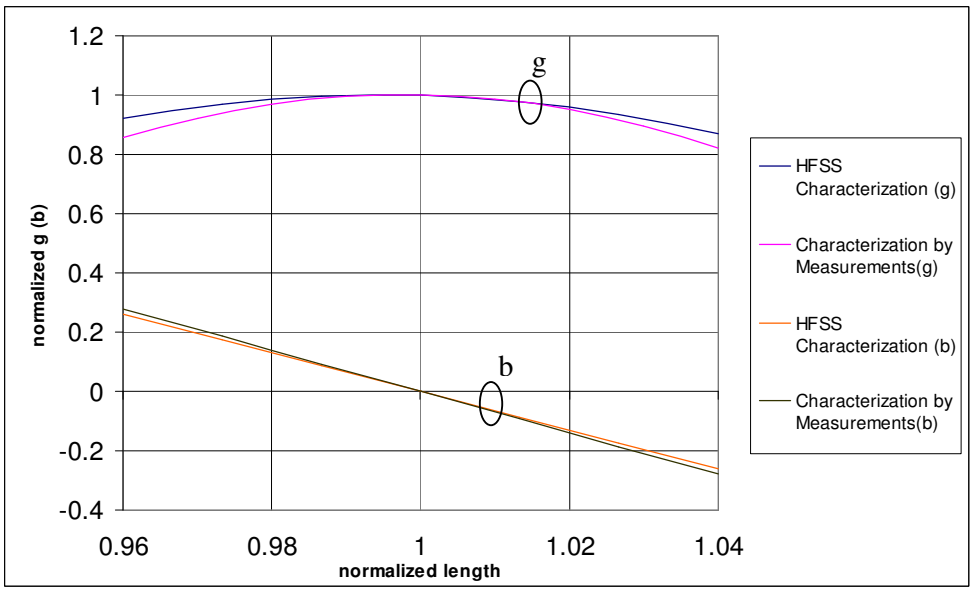

Figure 5.4 Normalized admittance vs. normalized length for isolated slot radiating between baffles

Results show that the simulated and measured values agree quite well despite some differences espeially for large offsets. It can be deduced from Figure 5.3 that resonant slot length became insensitive to slot offset as compared to the case without baffles. Also from Figure 5.4, bandwidth of the slots is wider. These two observations mean that the mechanical tolerances for the slot length can be much higher and the bandwidth of the designed array will be larger considering the radiation pattern bandwidth.

A linear array having 48 elements with Taylor 40dB ñ=6 amplitude distribution is synthesized with the new polynomials. The synthesis is again done with the MATLAB code that was used for designing the array without baffles, by only changing the characterization polynomial functions.

5.3. Simulation Results of the Linear SR-SWGA with Baffles

Analysis of the array is carried out with Ansoft HFSS with the geometry shown in Figure 5.5.

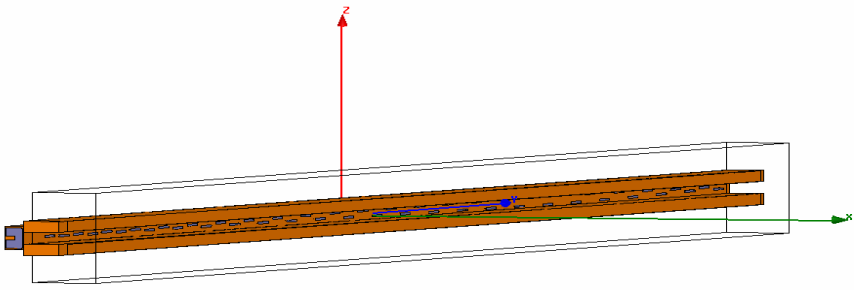

Figure 5.5 Geometry of the linear SR-SWGA with baffles

Figure 5.6 shows the simulated azimuth (θ= 90°) radiation pattern (normalized w.r.t main beam). Results show that secondary lobes are diminished (Figure 5.7, Figure 5.8). The first side lobe level is at -37dB.

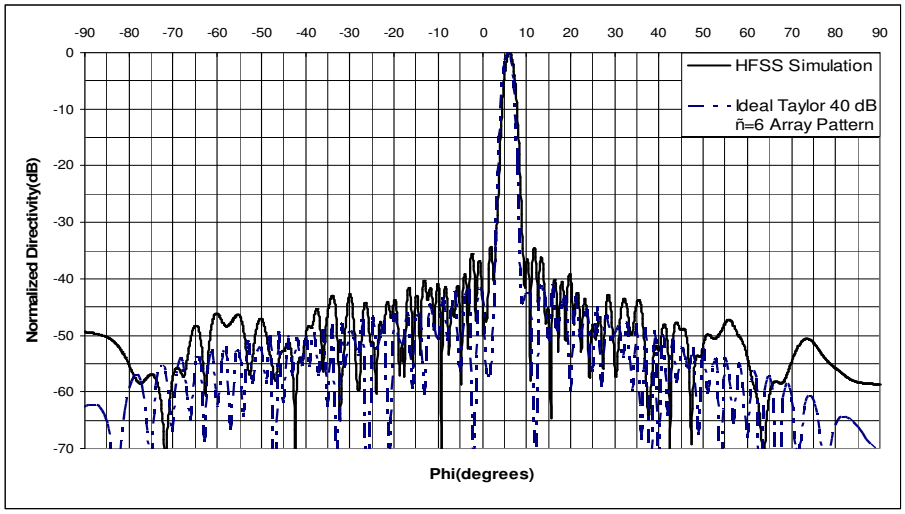

Figure 5.6 Simulated azimuth (θ= 90°) co-polarized pattern of the linear SR-SWGA antenna

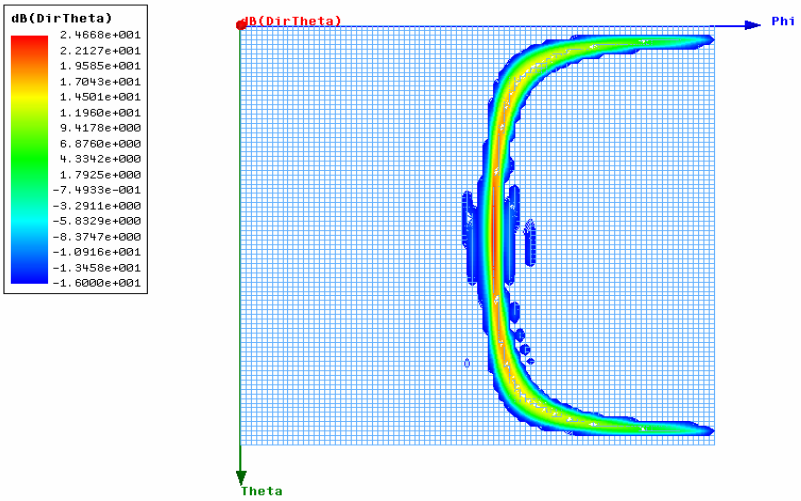

Figure 5.7 2-D simulated co-polarized radiation pattern of the linear SR-SWGA antenna with baffles

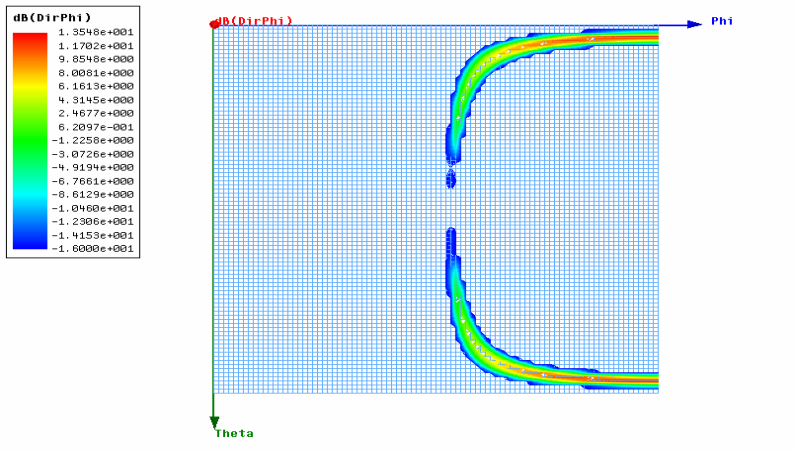

Figure 5.8 2-D simulated cross -polarized radiation pattern of the linear SR-SWGA antenna with baffles

We should also investigate return loss and insertion loss of the array. Figure 5.9 show that the array has maximum insertion loss of 15dB, and return loss of 36 dB. Thus the power dissipated in the matched load is maximum 4% at the band edges and 2.5% at the center frequency.

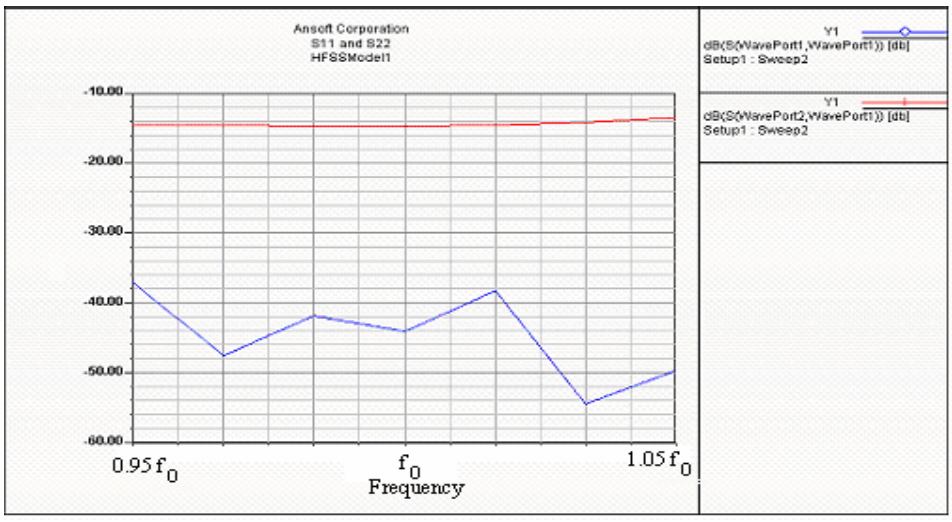

Figure 5.9 Simulated reflection and transmission results of the linear SR-SWGA with baffles

When we examine the frequency charateristics of the power delivered to load from S_{21} parameter, we see that the center frequency is shifted to a lower frequency (the power deliver to load should be minimum at the center frequency since all the slot are resonant at that frequency, so the radiated power is maximum). This may be due to the fact that in designing the array, mutual coupling is not calculated in the presence of the baffles, and the resonance condition for all the slots formed in a lower center frequency.

The half power beamwidth is 1.95 degrees in the azimuth cut at the center frequency. Since this array's properties complies with the design criteria, it is manufactured in ASELSAN.

5.4. Measurements of the Linear SR-SWGA with Baffles

The radiation pattern of the array is measured in a planar near – field antenna measurement system. The azimuth plane cut is shown in Figure 5.10 with solid lines.

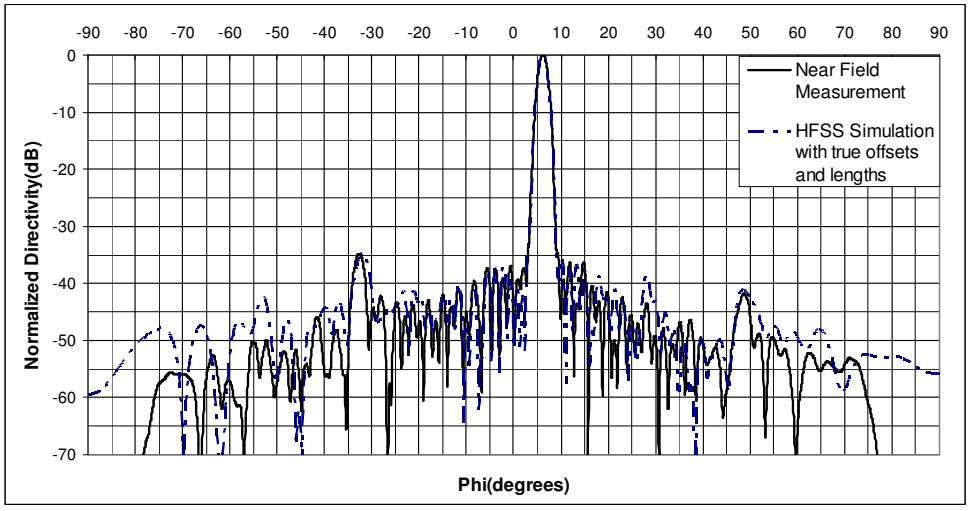

Figure 5.10 Measured azimuth (θ= 0°) co-polarized pattern of the linear SR-SWGA antenna with baffles

First side lobes are at -36dB relative to the main beam. Nevertheless, there are far side lobes that go up to -34 dB. Cause of this rise is the manufacturing errors in slot offsets. Every slots offset and length in the array is mechanically measured by a coordinate measuring machine (CMM). Measurement results (Figure 5.11) show that there is a maximum of 80 micrometer deviation on the slot offsets in the entire array. Some of the slot offsets could not be measured due to the closeness of the slot to the baffle making the measurement impossible. The array is simulated in HFSS with offsets and lengths changed according to CMM measurement results (Figure 5.10).

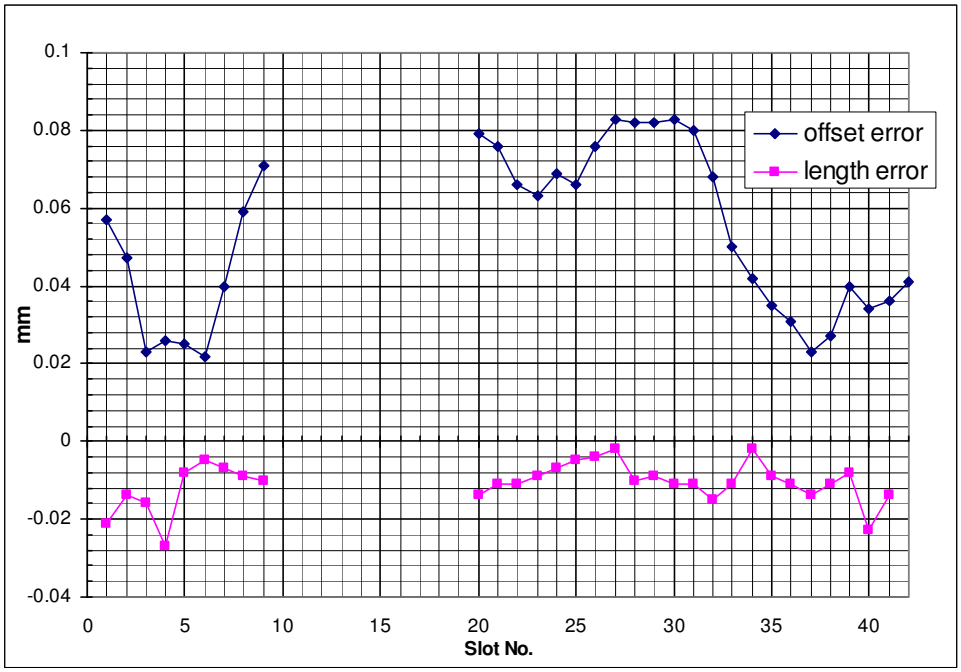

Figure 5.11 Slot offset and length errors measured with CMM.

The near field measurements and HFSS simulation results are quite similar. It is evident that for achieving the desired side lobe level, mechanical tolerances are very tight. Besides, we can say that the mechanical accuracy of the slot offsets are more

important than slot lengths by looking at the slope of design curves: Admittance vs. offset (Figure 5.2) and admittance vs. resonant length (Figure 5.3).

The azimuth cuts of the antenna radiation pattern for various frequencies are given in Figure 5.12 to Figure 5.22.

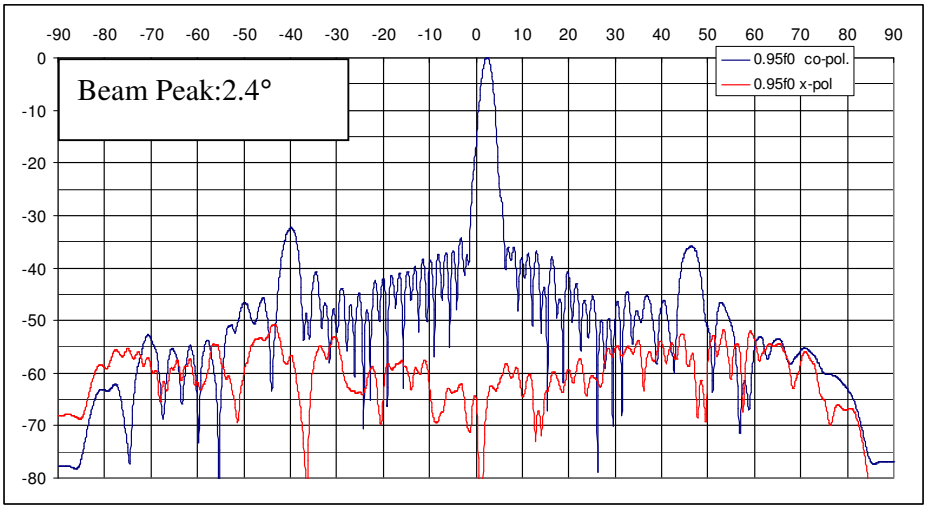

Figure 5.12 Measured azimuth (θ= 90°) co and cross - polarized patterns of the linear SR-SWGA antenna with baffles at $0.95f_0$.

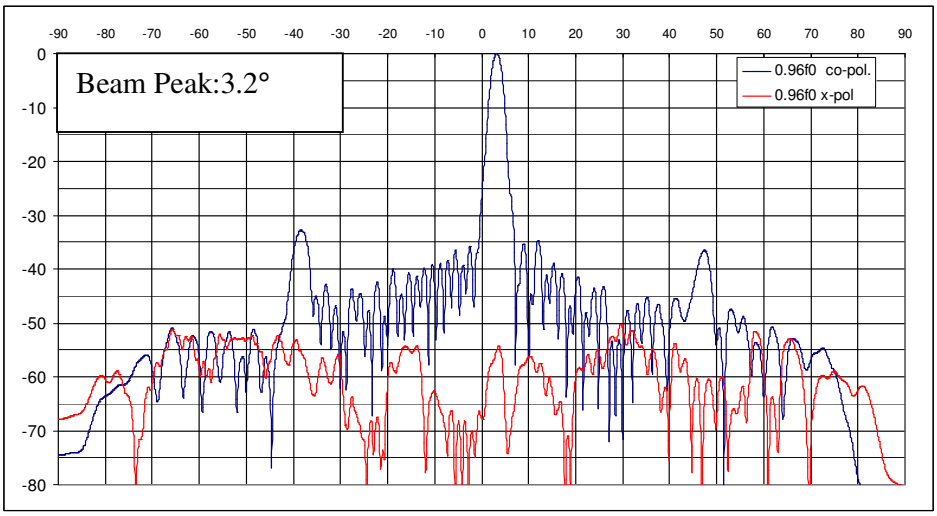

Figure 5.13 Measured azimuth (θ= 90°) co and cross - polarized patterns of the linear SR-SWGA antenna with baffles at $0.96f_0$.

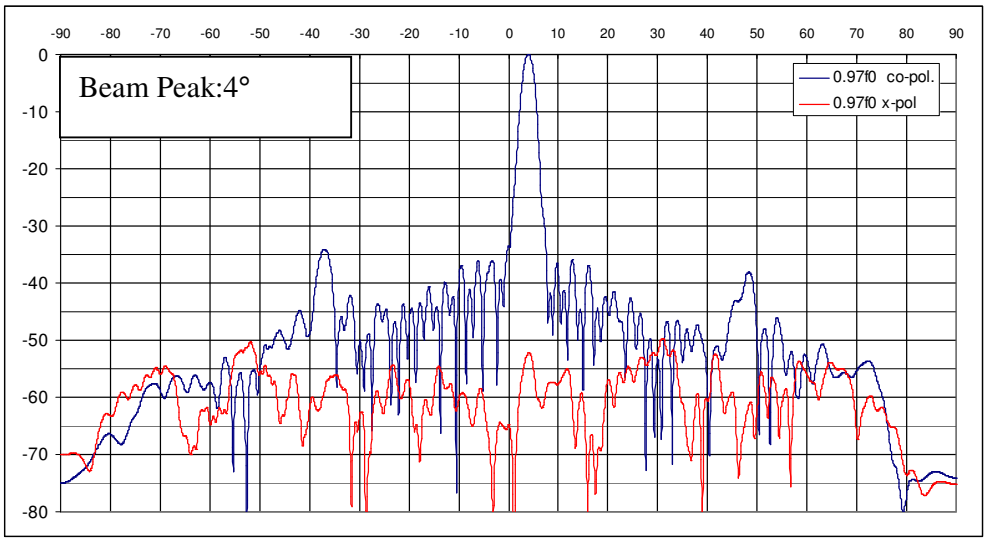

Figure 5.14 Measured azimuth (θ= 90°) co and cross - polarized patterns of the linear SR-SWGA antenna with baffles at $0.97f_0$.

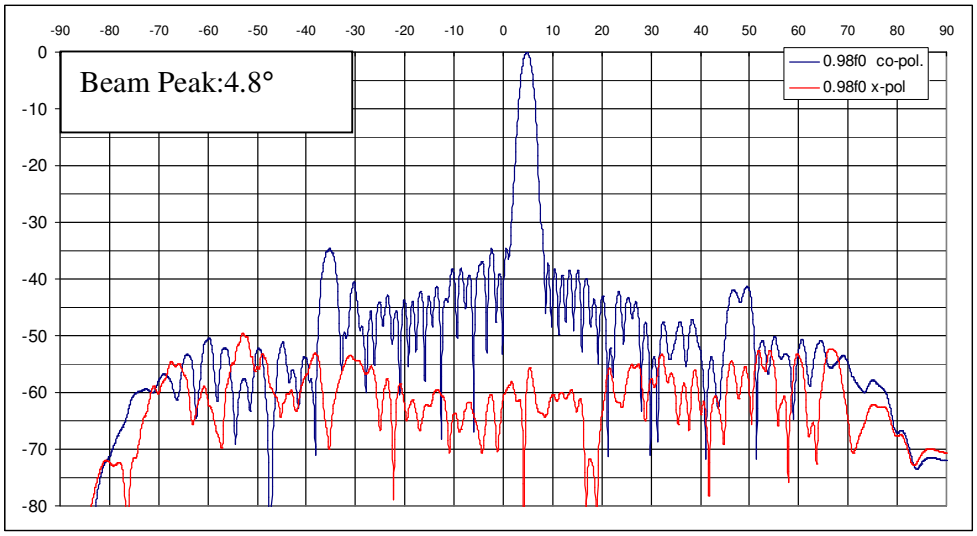

Figure 5.15 Measured azimuth (θ= 90°) co and cross - polarized patterns of the linear SR-SWGA antenna with baffles at $0.98f_0$.

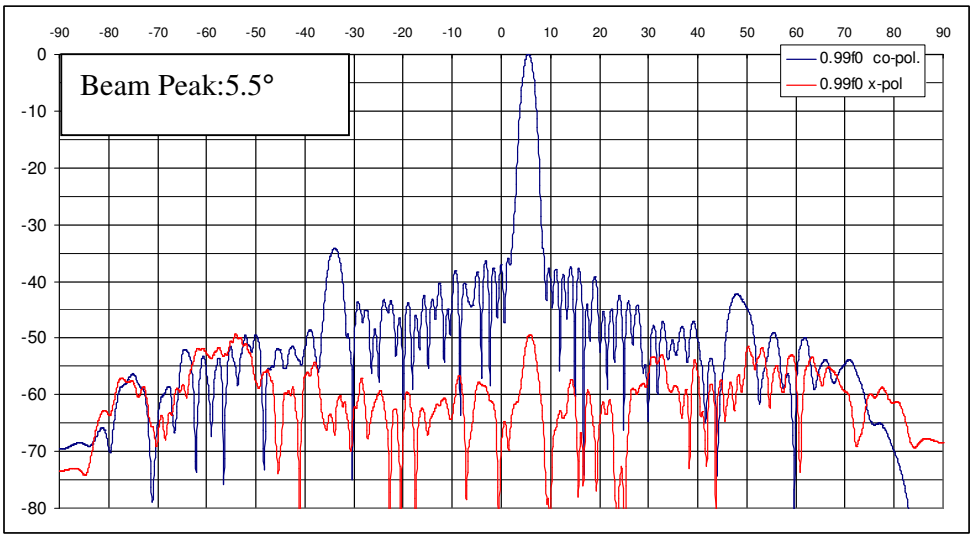

Figure 5.16 Measured azimuth (θ= 90°) co and cross - polarized patterns of the linear SR-SWGA antenna with baffles at $0.99f_0$.

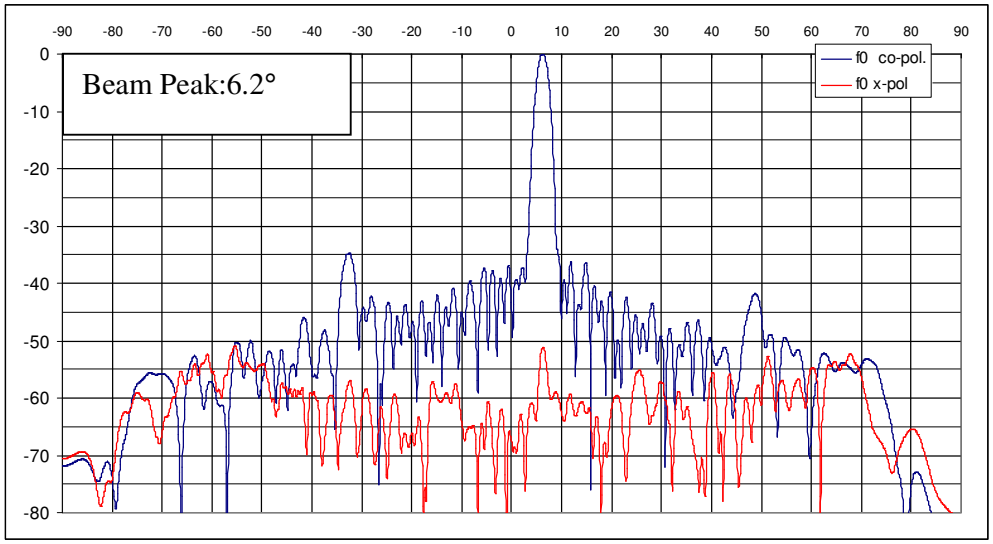

Figure 5.17 Measured azimuth (θ= 90°) co and cross - polarized patterns of the linear SR-SWGA antenna with baffles at f_0.

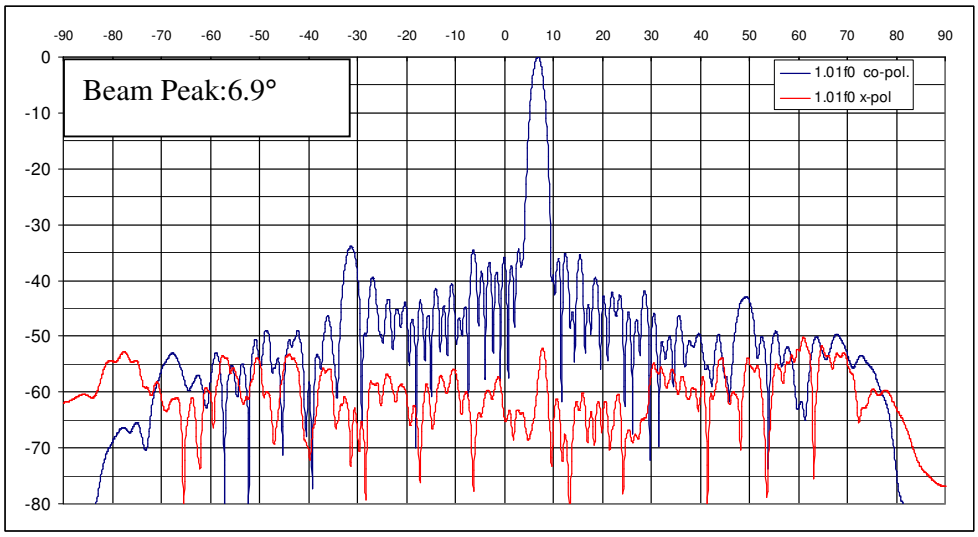

Figure 5.18 Measured azimuth (θ= 90°) co and cross - polarized patterns of the linear SR-SWGA antenna with baffles at $1.01f_0$.

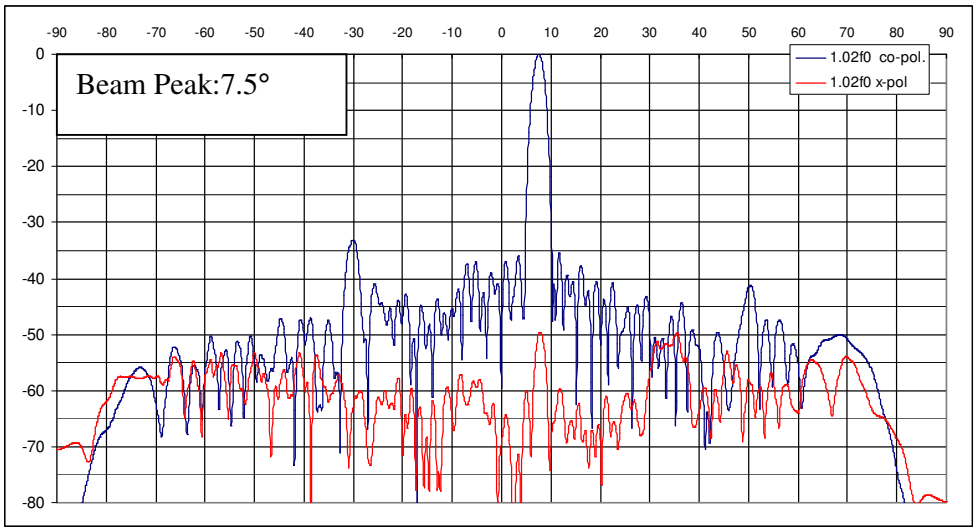

Figure 5.19 Measured azimuth (θ= 90°) co and cross - polarized patterns of the linear SR-SWGA antenna with baffles at $1.02f_0$.

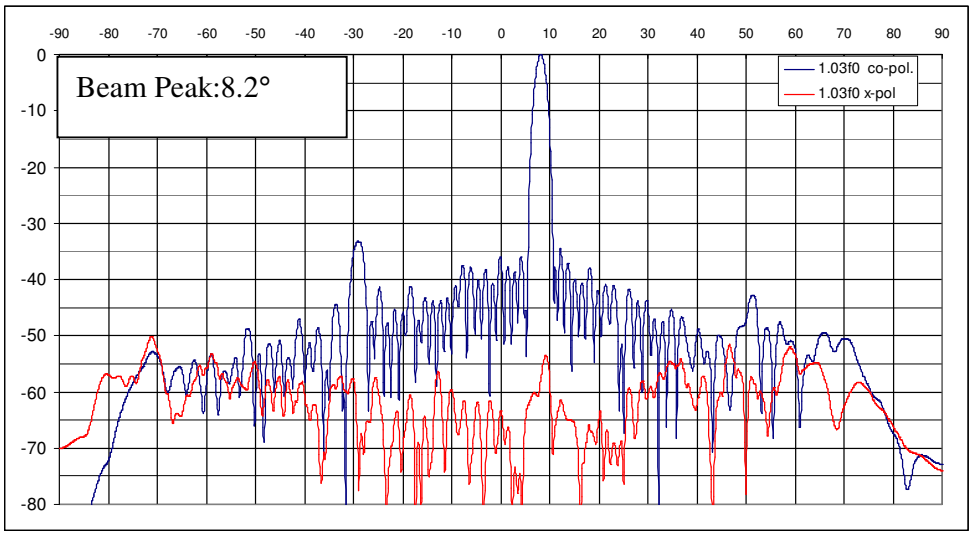

Figure 5.20 Measured azimuth (θ= 90°) co and cross - polarized patterns of the linear SR-SWGA antenna with baffles at 1.03 f_0.

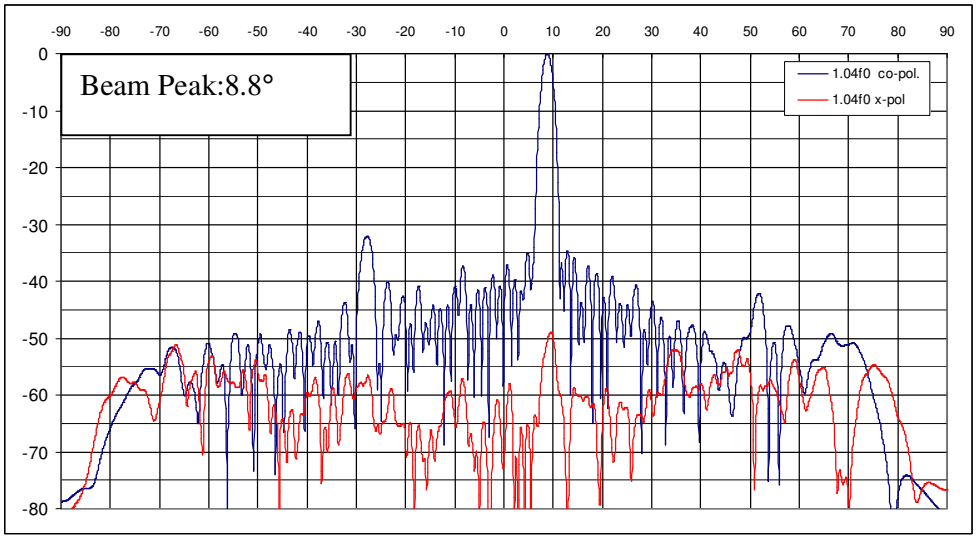

Figure 5.21 Measured azimuth (θ= 90°) co and cross - polarized patterns of the linear SR-SWGA antenna with baffles at 1.04f_0.

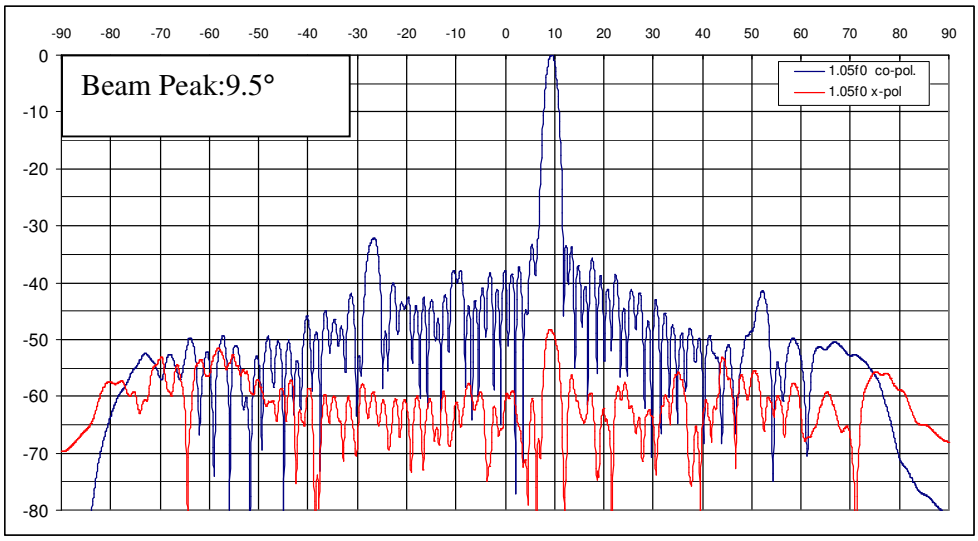

Figure 5.22 Measured azimuth (θ= 90°) co and cross - polarized patterns of the linear SR-SWGA antenna with baffles at $1.05f_0$.

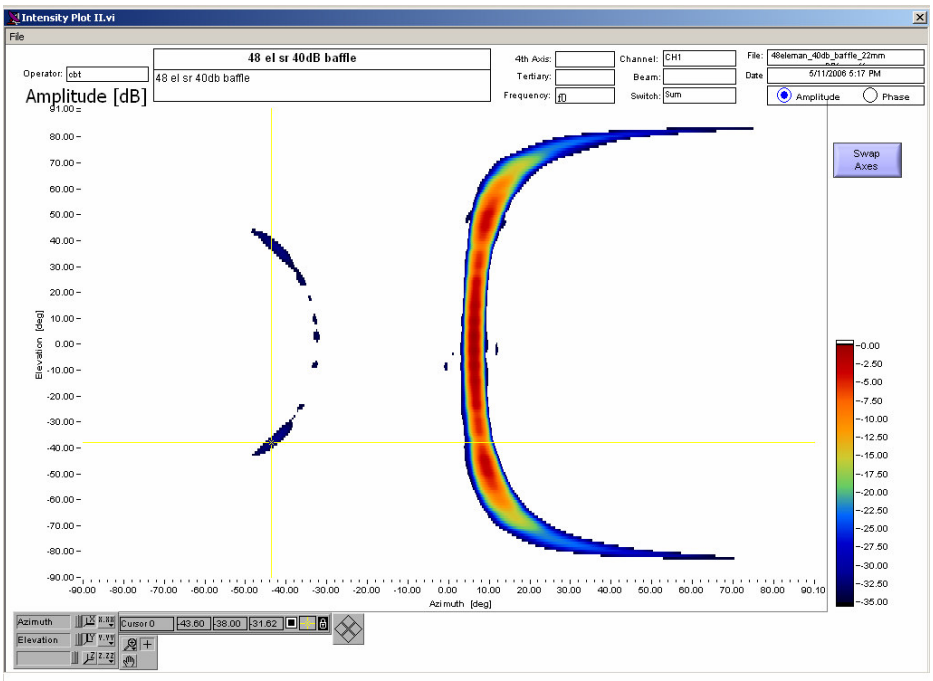

Figure 5.23 Measured color coded contour plot of radiation pattern for front hemisphere of linear SR-SWGA antenna at the center frequency.

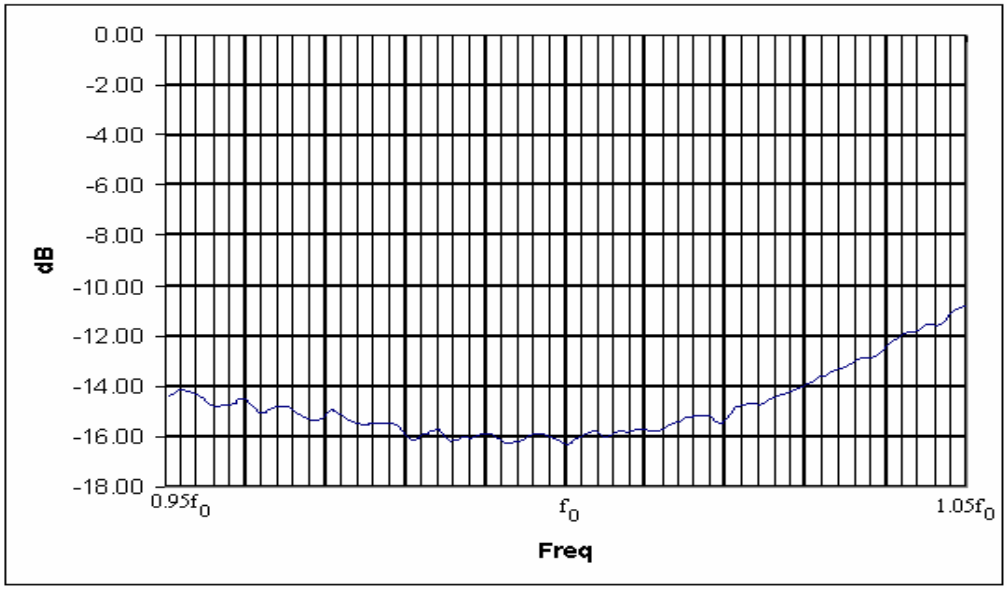

Figure 5.24 Measured transmission parameter of the linear SR-SWGA antenna with baffles (with HP8510C NA)

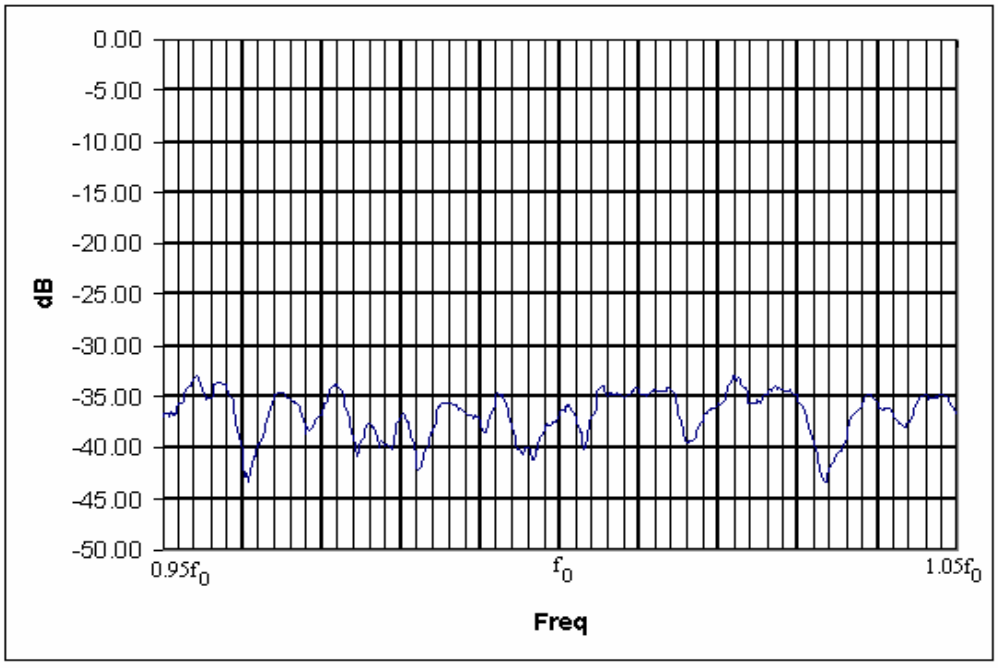

Figure 5.25 Measured reflection parameter of the linear SR-SWGA antenna with baffles (with HP8510C NA)

Table 5.1 Properties of linear SR-SWGA antenna with baffles at different frequencies.

Freq(normalized w.r.t center)	3dB Beamwidth(degrees)	First SLL	Beam Peak @(degrees)	S11(dB)	S21(dB)
0.95	2	-34.3 dB	2.4	<-30	-14.3
1	1.9	-37.5 dB	6.2	<-30	-16.25
1.05	1.8	-33.5 dB	9.5	<-30	-11

It is observable from Figure 5.23 that the second order beam is suppressed below -31dB relative to beam peak. The cross-pol.values are well below -40dB.

The radiation pattern bandwidth of the antenna can be said to be enlarged, observing the azimuth cuts for different frequencies (Figure 5.12 **-** Figure 5.22). This result can be deduced by looking at the slot characterisation curves (Figure 5.3, Figure 5.4). The slot resonant length became nearly independent from slot offset and normalized admittance has a broder bandwidth.

Basic properties of the array is listed in Table 5.1. The half power beamwidth is decreased to 1.9° at the center frequency by increasing element number from 42 to 48. Return loss is below 30dB over 10% frequency band (Figure 5.25). From the measured transmission parameter of the antenna, it can be observed that the power dissipated at the load is lower than 5% in 7% frequency band whereas 2.4% at the center frequency (Figure 5.24). However, there is a shift to lower band as observed in the HFSS simulation result.

Calculated and measured values of beam peak position is given in Table 5.2**.** There is a maximum 0.2° difference in beam peak position over the band. This may be due to coupling between slots.

Table 5.2 Calculated and Measured Beam Peak Values for Different Frequencies

Frequency(f0)	Calculated Beam Peak Position (degrees)	Measured Beam Peak Position(degrees)
0.95	2.3	2.4
0.96	3.2	3.2
0.97	4.0	4
0.98	4.8	4.8
0.99	5.5	5.5
1	6.3	6.2
1.01	7.0	6.9
1.02	7.7	7.5
1.03	8.4	8.2
1.04	9.0	8.8
1.05	9.7	9.5

In the next chapter this linear element is used and a planar SR-SWGA with baffles is formed.

CHAPTER 6

SINGLE RIDGED WAVEGUIDE PLANAR ARRAY

6.1. Introduction

The designed single ridged slotted waveguide arrays with baffles are stacked in elevation plane forming the planar array.

Design criteria for elevation:

- Elevation 3dB Beamwidth : 7°
- Max. Sidelobe Level : -30 dB
- Operation Band : X - Band
- Scanning :+/- 35°

In order to meet 7 degree beam width in elevation, element number is chosen as 18. The array is simulated with CST Microwave Studio EM simulation software which uses finite integration method in time domain. It can handle bigger structures as compared to HFSS and is used to get an idea about the 3D pattern of the entire array; the level of secondary lobes with respect to the main beam, the beamwidths of the array in two planes. The side lobe levels are not very accurate for the azimuth plane because of the fact that meshing could not be done sufficiently small. The cause of this is the computer's memory constraints.

It is observed by measurements that row to row coupling is negligible especially for SWGA antennas with baffles. Therefore, identical linear arrays are used to construt the array. The array is fed from one end with a Taylor 35dB ñ=5 amplitude distribution. 18 Ports are simultaneously excited for 0 and 35 degrees beam steering

positions because the secondary lobes are mostly effective at higher scan angles. Simulation results are given in Section 6.2. in Figure 6.1 to Figure 6.4.

6.2. Simulation Results

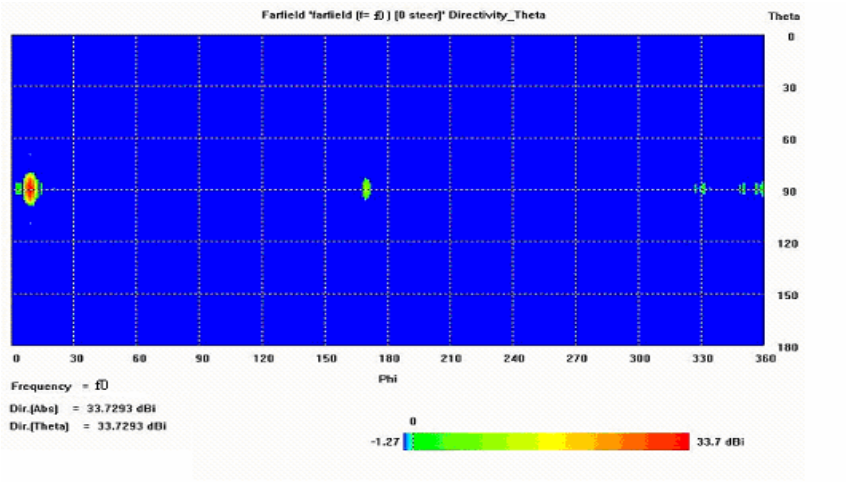

Figure 6.1 Simulated co-polarized 2D farfield of the planar SR-SWGA antenna with baffles at the center frequency (with no beam steering in elevation).

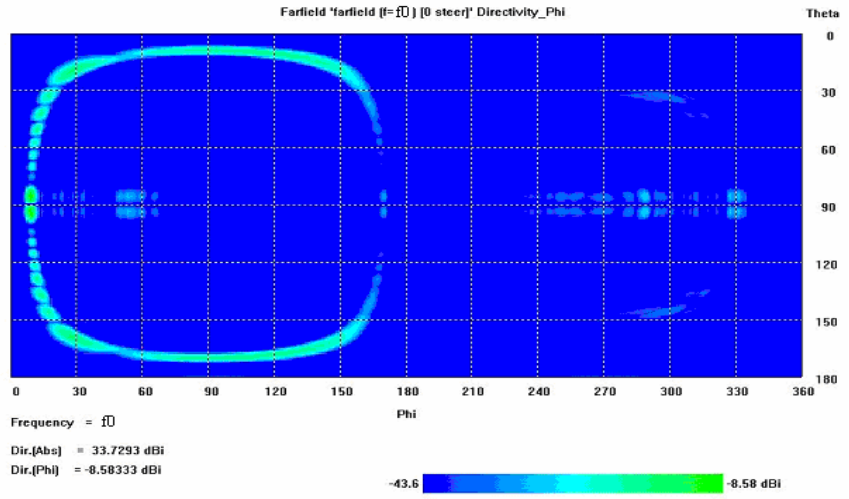

Figure 6.2 Simulated cross-polarized 2D farfield of the planar SR-SWGA antenna with baffles at the center frequency (with no beam steering in elevation).

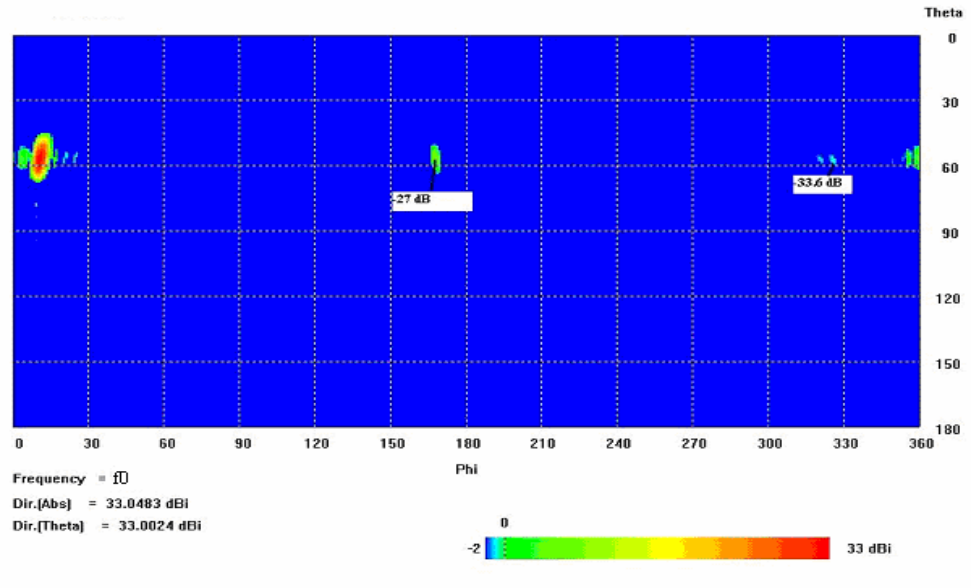

Figure 6.3 Simulated co-polarized 2D farfield of the planar SR-SWGA antenna with baffles at the center frequency (with +35° beam steering in elevation).

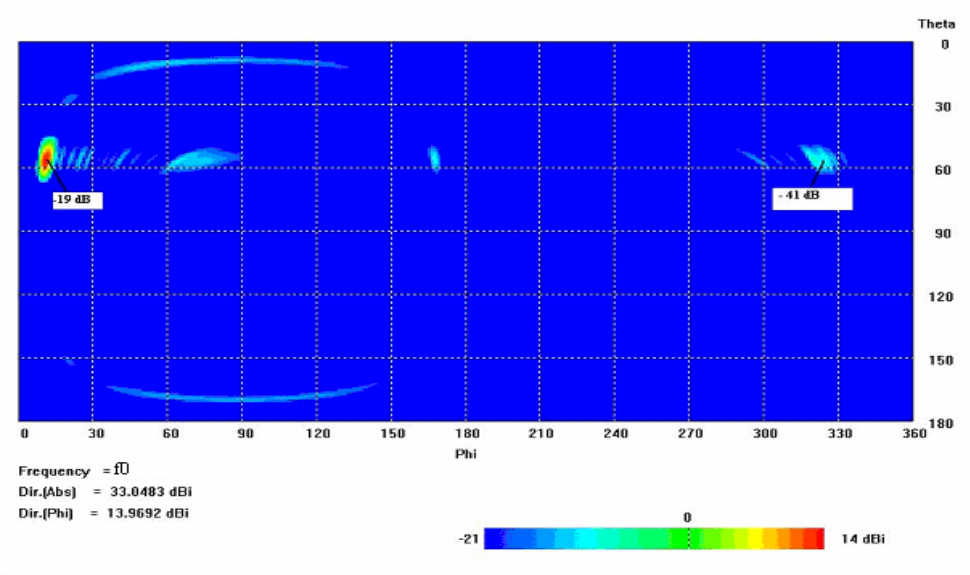

Figure 6.4 Simulated cross-polarized 2D farfield of the planar SR-SWGA antenna with baffles at the center frequency (with +35° beam steering in elevation).

Simulation results show that the secondary beams are suppressed efficiently proving the usefullness of baffles. In Figure 6.1 and Figure 6.2 co and cross-polarized 2-D

patterns of the planar array with no beam steering are given respectively. The threshold level is clipped to -35dB relative to the beam peak in order to clearly show the second order lobe levels are lower than the side lobe levels. Note that due to the travelling wave design, main beam has an 6.2 degrees squint in azimuth axis. In Figure 6.3 and Figure 6.4 co and cross-polarized 2-D patterns of the planar array with +35 degrees beam steering in elevation axis are given respectively. The threshold level is clipped to -35dB level indicating second order lobe levels are below -35dB.

We have a cross-pol. level of 19dB at the main lobe for +35degrees beamsteering in elevation axis. It is also worth mentioning that cross-polarized pattern makes a peak at the position of the main lobe with an inreasing value with increasing steering elevation angle.

6.3. Measurement Results

The planar array is manufactured in Communications Division of ASELSAN.

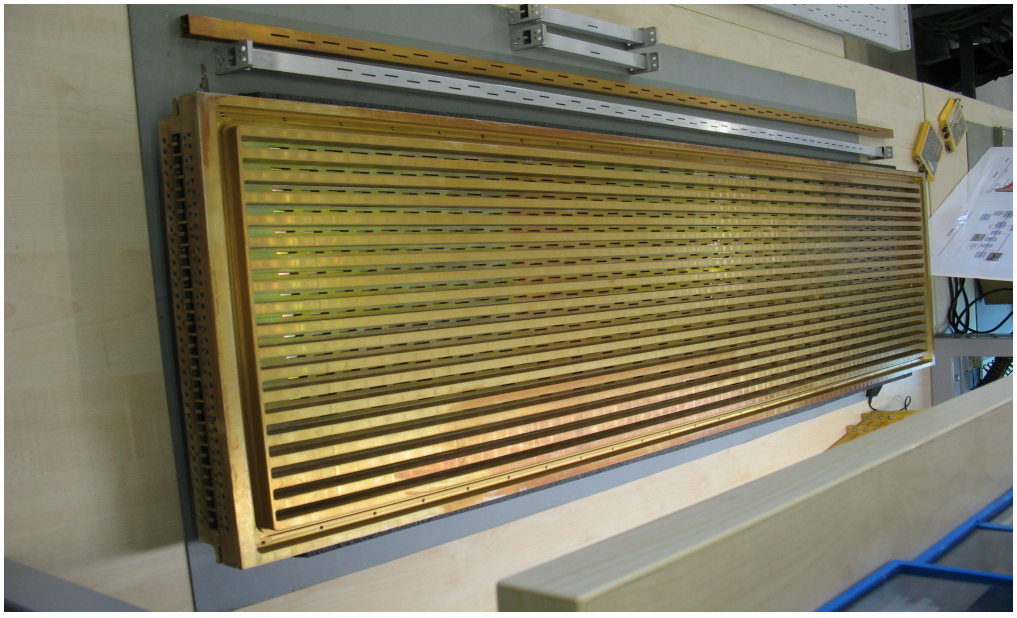

Figure 6.5 Manufactured Planar SR-SWGA antenna with baffles.

The beam forming unit is formed with commercial 6-bit phase shifters and 6-bit attenuators (Figure 6.6). The input power is divided into two by a two-way power divider, than each arm is again divided by 10-way dividers. One end of each 10-way divider is finished with a matched load, while other ends are connected to computer controlled phase shifters followed by attenuators for each channel (SWGA) which are connected to the related power divider via semi-rigid SMA cables. SMA to Single ridged waveguide adapter is used to feed each SWGA antenna.

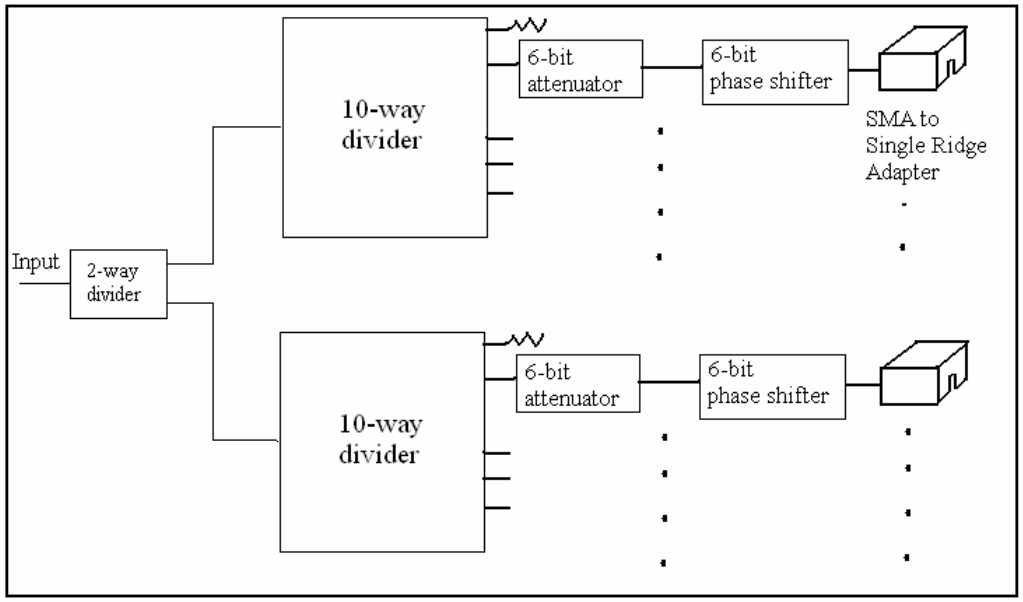

Figure 6.6 Beam forming Network for the planar Array

Taylor 35dB ñ=5 amplitude distribution is employed in the elevation array by adjusting the attenuators. The beam is scanned in 0° - 40° degrees sector in elevation with 5-degree steps in the planar near field antenna measurement system (Figure 6.7 to Figure 6.16).

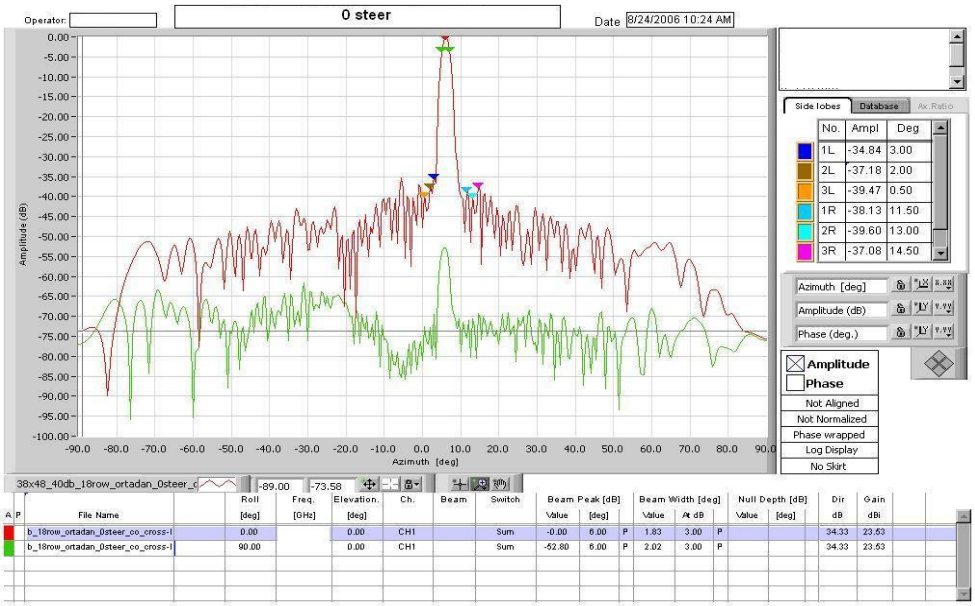

Figure 6.7 Measured azimuth (θ= 90°) co and cross - polarized patterns of the planar SR-SWGA antenna with baffles at 0 degrees beam steering.

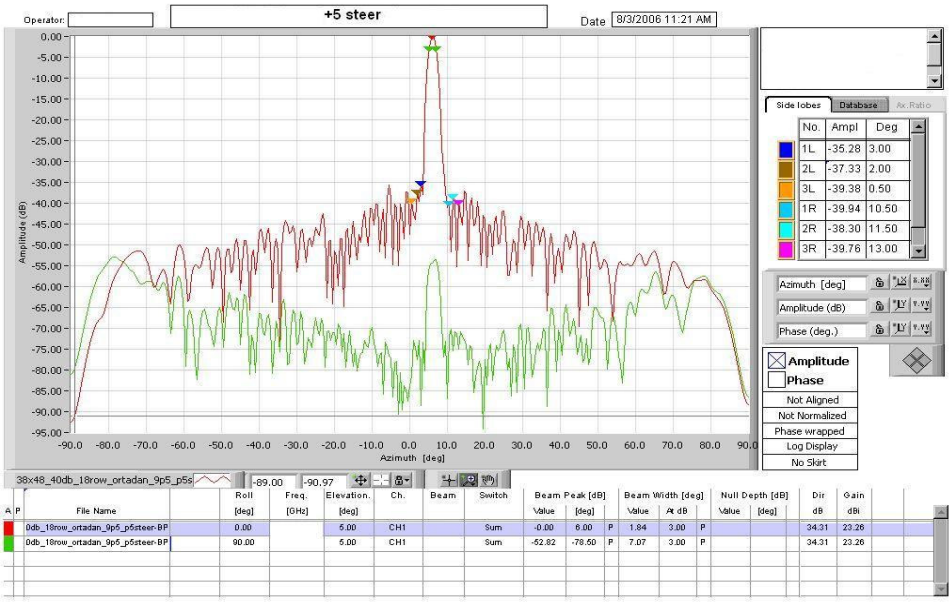

Figure 6.8 Measured azimuth (θ= 90°) co and cross - polarized patterns of the planar SR-SWGA antenna with baffles at +5 degrees beam steering.

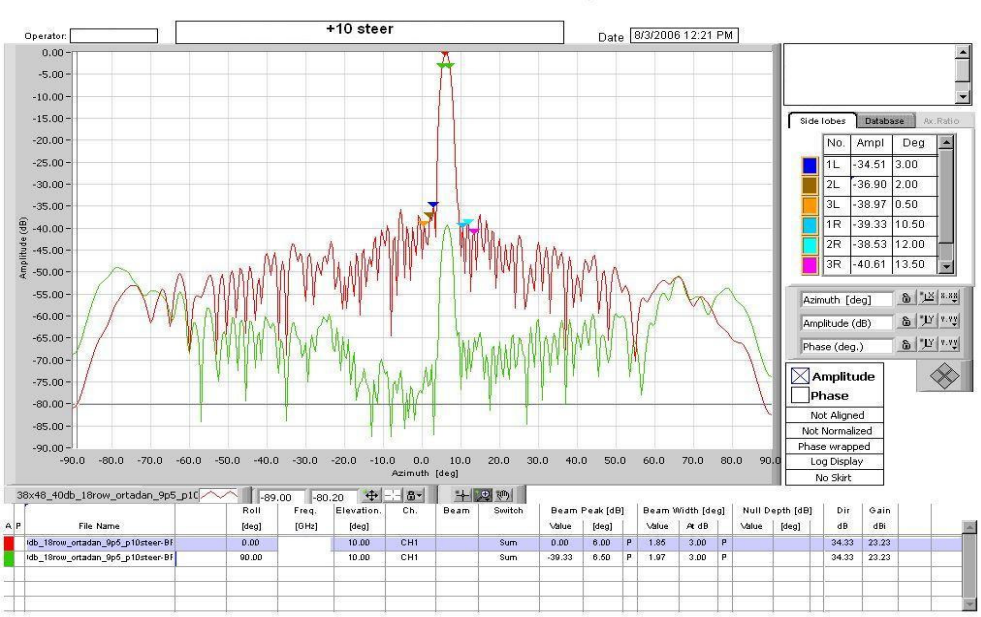

Figure 6.9 Measured azimuth (θ= 90°) co and cross - polarized patterns of the planar SR-SWGA antenna with baffles at +10 degrees beam steering.

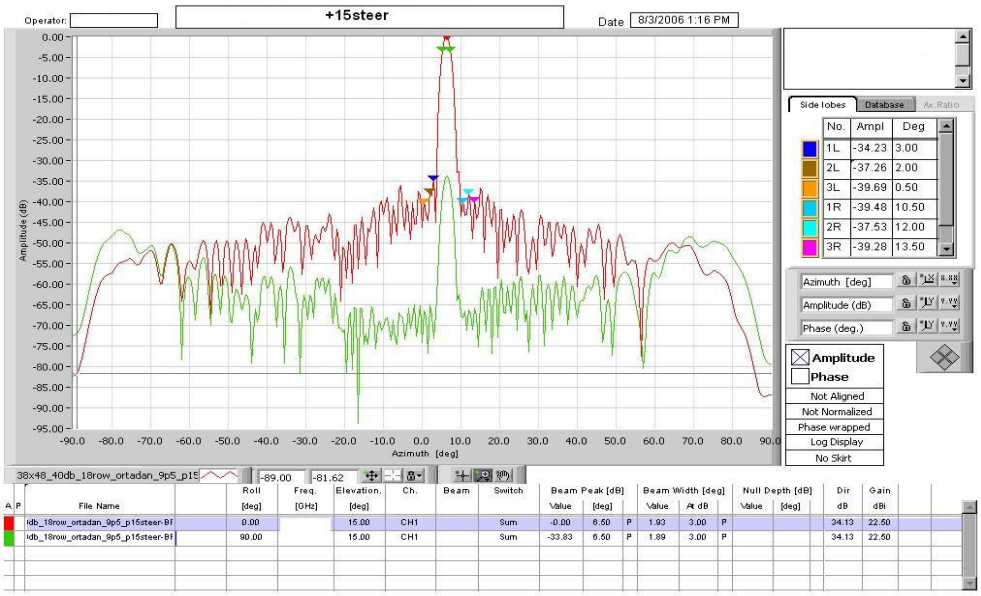

Figure 6.10 Measured azimuth (θ= 90°) co and cross - polarized patterns of the planar SR-SWGA antenna with baffles at +15 degrees beam steering.

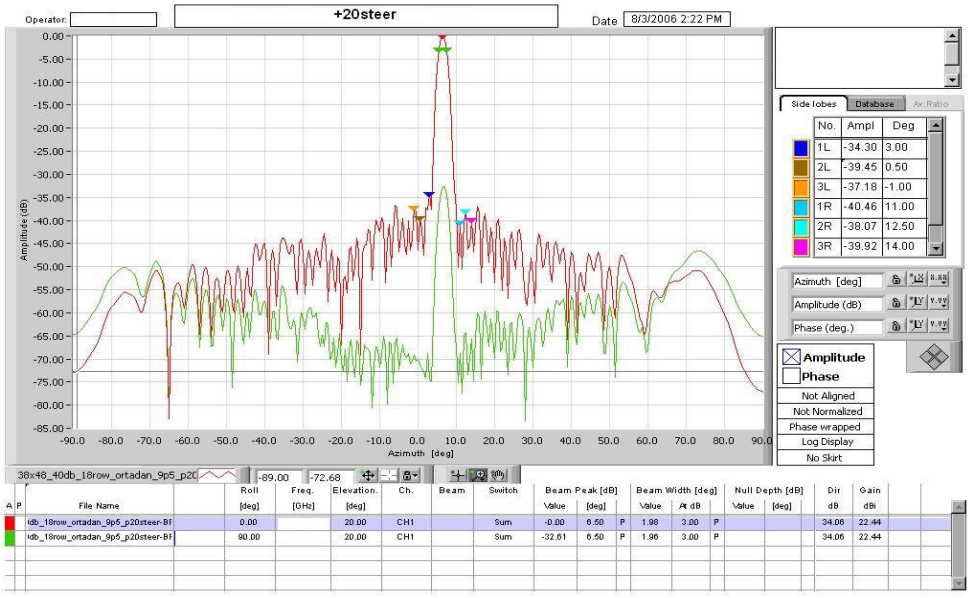

Figure 6.11 Measured azimuth (θ= 90°) co and cross - polarized patterns of the planar SR-SWGA antenna with baffles at +20 degrees beam steering.

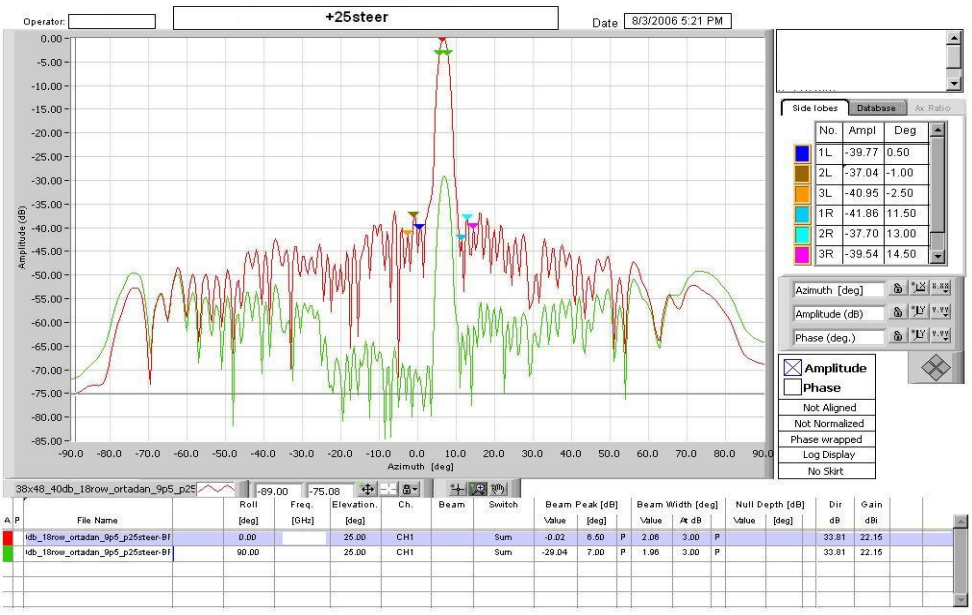

Figure 6.12 Measured azimuth (θ= 90°) co and cross - polarized patterns of the planar SR-SWGA antenna with baffles at +25 degrees beam steering.

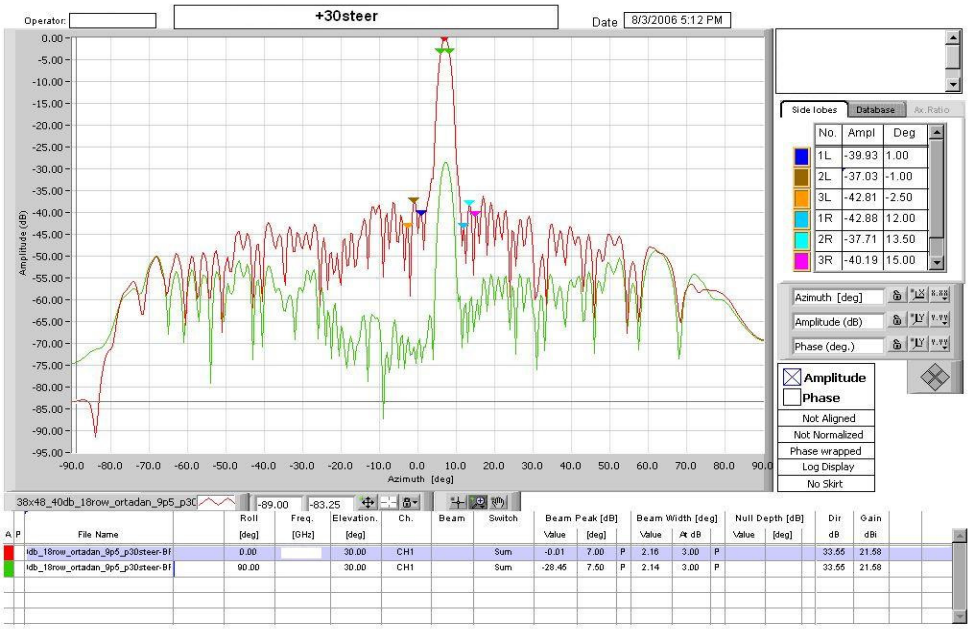

Figure 6.13 Measured azimuth (θ= 90°) co and cross - polarized patterns of the planar SR-SWGA antenna with baffles at +30 degrees beam steering.

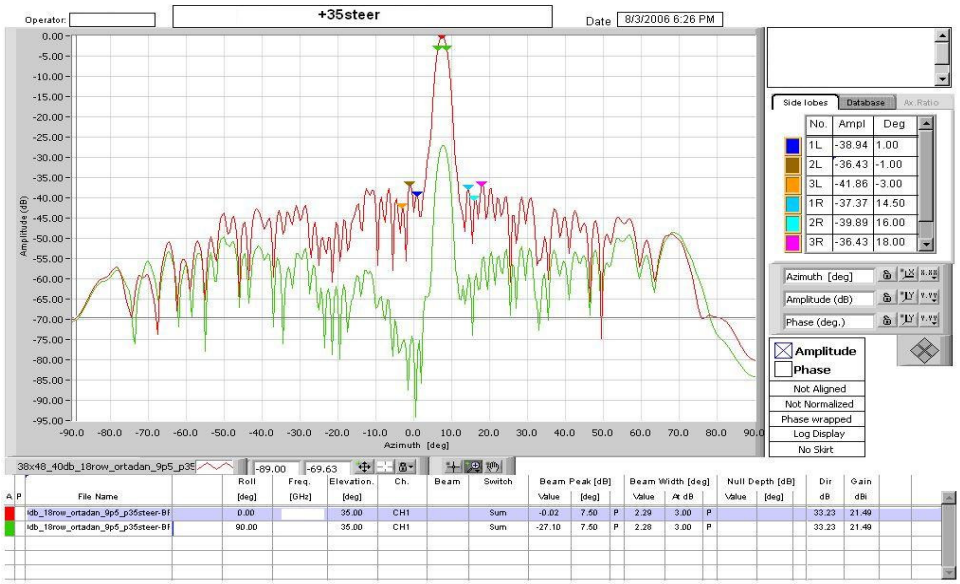

Figure 6.14 Measured azimuth (θ= 90°) co and cross - polarized patterns of the planar SR-SWGA antenna with baffles at +35 degrees beam steering.

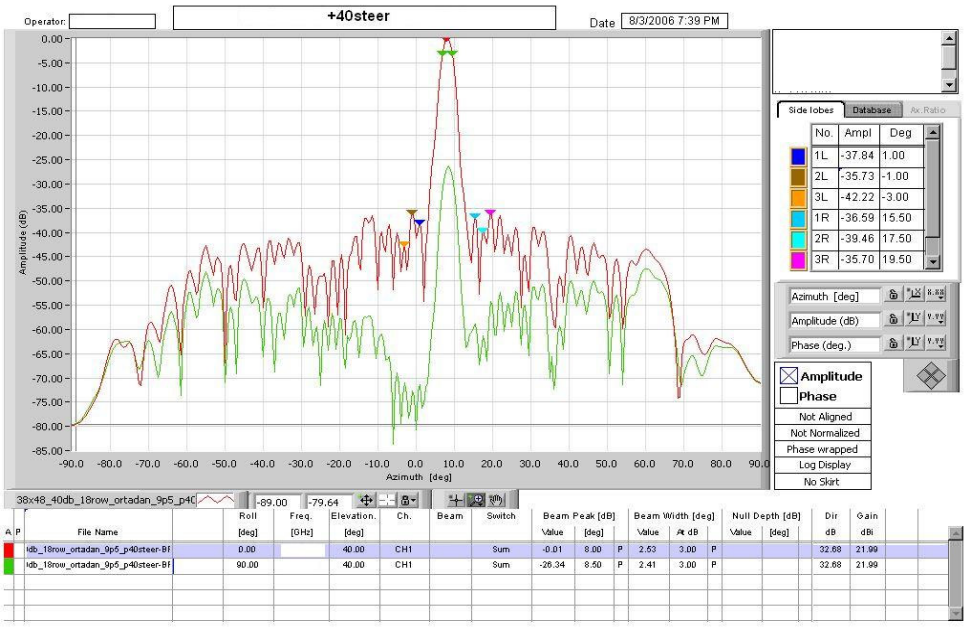

Figure 6.15 Measured azimuth (θ= 90°) co and cross - polarized patterns of the planar SR-SWGA antenna with baffles at +40 degrees beam steering.

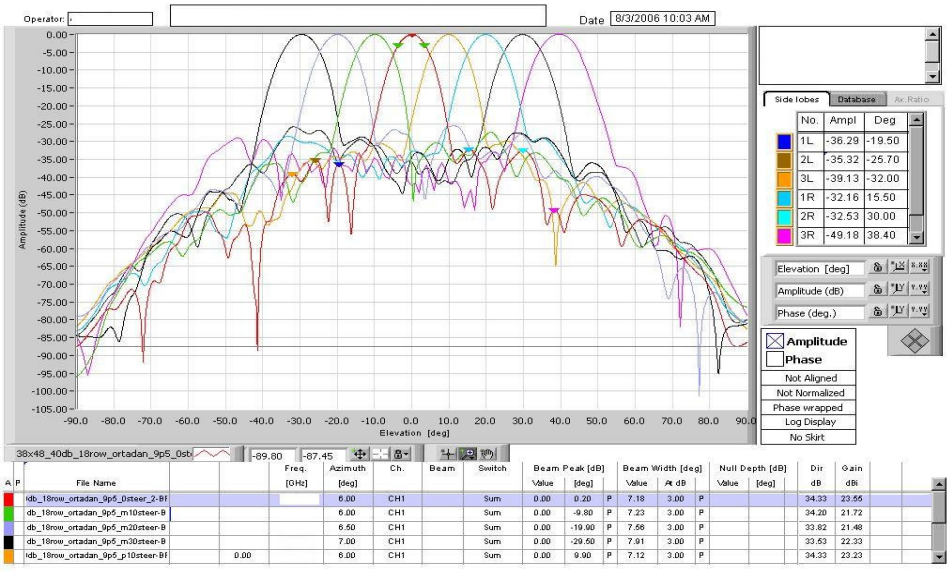

Figure 6.16 Measured elevation co - polarized patterns of the planar SR-SWGA antenna with baffles for -30, -20, -10, 0, 10, 20, 30, 40 degrees beam steering.

In the measured characteristics, cross-polarization level goes up to -27dB for +35 degrees beam steering (Figure 6.14). The difference of the simulated and measured value for the cross-polarization level at +35 degrees steering may be due to the coarse meshing of the large structure in the simulation software.

The high cross-polarization level of the antenna at high scan angles is due to the cross-polarized component at the end of the slots, which was discussed in chapter 3.

The secondary beams are suppressed efficiently for all steering angles (Figure 6.7 to Figure 6.14). The half power beam width of the array broadens with increasing steer angle. It is 1.83° when there is no beam steering whereas this value increases to 2.29° when the beam is steered to +35 degrees scan angle.

In the elevation – cut (Figure 6.16), side lobes are higher than the desired value. The calibration of the beamforming system for the desired amplitude distribution does not include the SMA-Single Ridge adapter section. Therefore, some error is introduced in amplitude and phase of the channels, in the adapters. Also there exist quantization errors of the attenuators and phase shifters. These errors are thought to be the reasons for increased side lobes.

CHAPTER 7

A SECTORAL CORRUGATED HORN POWER DIVIDER

7.1. Introduction

The planar slotted waveguide array designed in this thesis will transmit high power. Thus, the feed section must be able to handle the delivered high power from the input. At the same time, the amplitude tapering should be done in the power divider. Required phases for phase steering can be provided by using high power ferrite phase shifters. The block diagram of the system is simply shown in Figure 7.1.

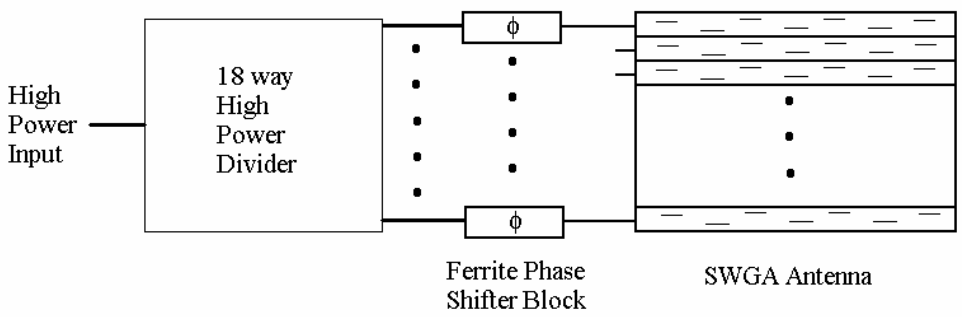

Figure 7.1 Transmitter Antenna Block

For high power power division, waveguide power dividers are generally used. These include dividers employing branch line couplers, tee junction dividers, endfed slotted waveguide power dividers, etc. In this thesis a different power divider is proposed. The aperture of an E-plane sectoral corrugated horn is segmented to give the desired amplitude distribution. A different type (with a non-corrugated sectoral horn) of this power division was done [15] to give a uniform amplitude distribution to open ended waveguide.

7.2. Corrugated Sectoral Horns

Sectoral horns are used for obtaining fan beams in the plane of the flare. The flare can either be E-plane or H-plane. Corrugations in the E-plane provide tapering of the E-plane across the horn. Since the horn will be used for power division with amplitude tapering, the corrugated E-plane sectoral horn, which inherently has a tapering, is a good candidate for this kind of application.

In order to have the Taylor 35dB amplitude distribution, the heights of the coupling waveguides are chosen according to the field distribution on the aperture (Figure 7.2).

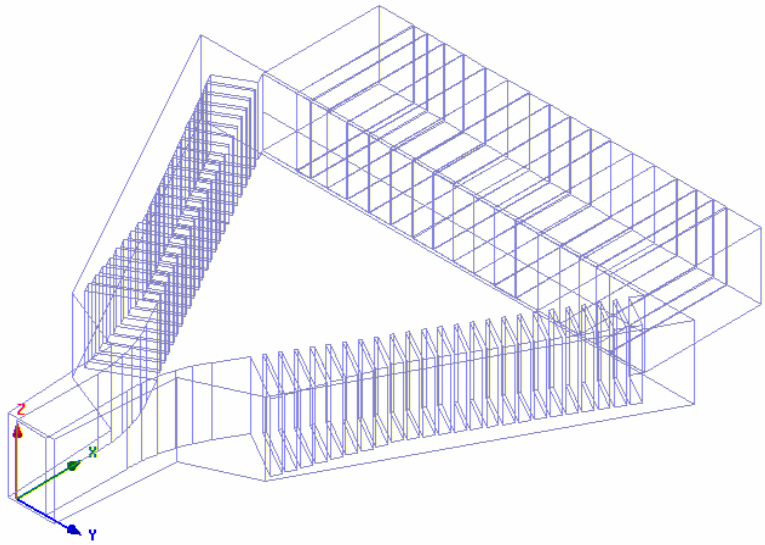

Figure 7.2 HFSS model of the corrugated e-plane sectoral horn.

The design of this divider can be divided into two parts: design of the horn itself and the design of the coupling section.

7.3. Design of the Horn Itself

The corrugated horn should be designed so that the return loss is low. The VSWR properties of the E-plane corrugated sectoral horns are investigated by Terzuoli *et al*. [16]. It was shown that length of the flare doesn't affect VSWR of the horn and it is possible to have a low VSWR by smoothing the waveguide – horn junction and including a matching section for corrugations.

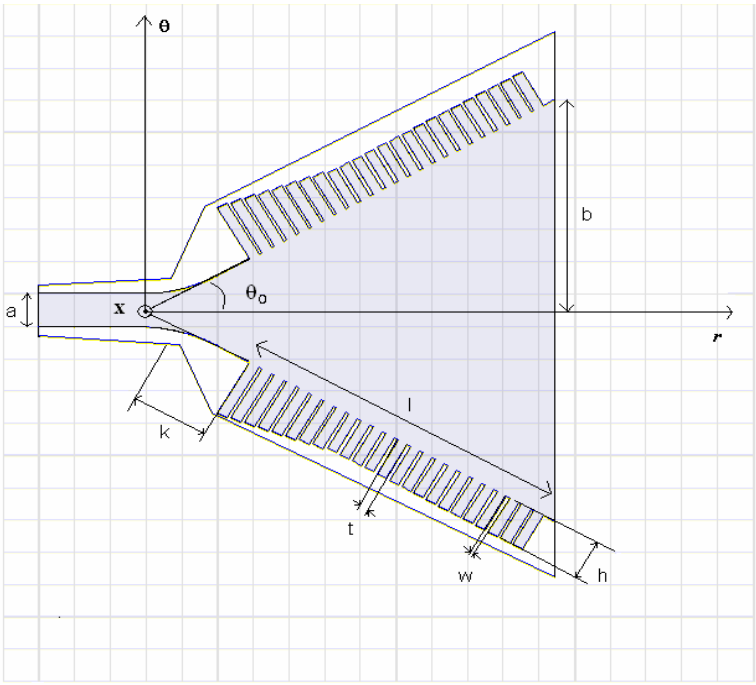

Figure 7.3 Corrugated E-plane Sectoral Horn Geometry

In the design, corrugations are 3/8 λ deep at center frequency. And there is a linear taper with 8 corrugations in corrugations starting from λ/2 at center frequency in order to have a good matching.

Θ_0 is chosen to be 30°, b = 130 mm , l = 101.45 mm. t and w are chosen such that t =3w and (t + w) = λ /8 at center frequency.
Flare length (k+l) is 4 λ and smoothed junction length is 0.8 λ.

EM simulation of this horn is done with HFSS. Return loss over the 10% frequency band is less than 20dB (Figure 7.5).

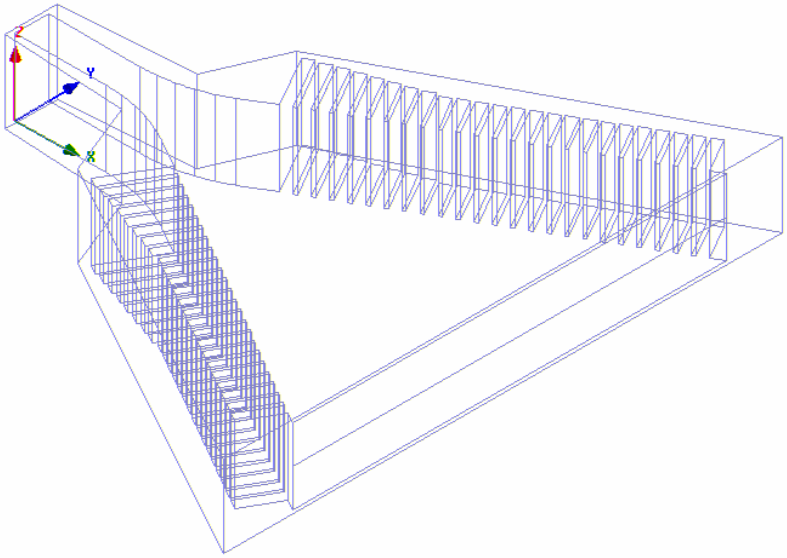

Figure 7.4 HFSS model of the corrugated e-plane sectoral horn

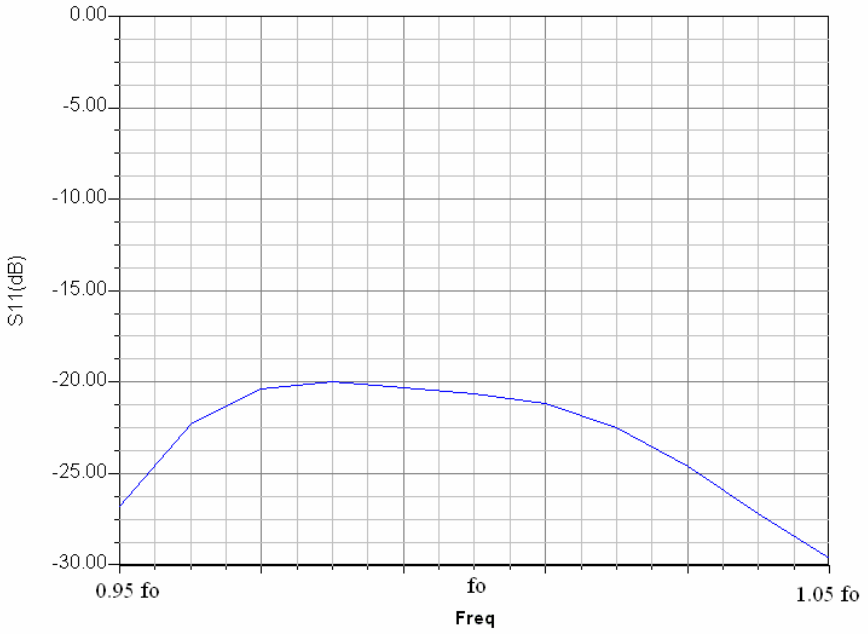

Figure 7.5 Simulated S11 of the corrugated e-plane sectoral horn

7.4. Design of the Coupling Waveguides

The heights of the coupling waveguides should be chosen such that the coupled power is the fraction determined by the Taylor amplitude distribution. The required height of each waveguide can be calculated using the e-field on the aperture which is given by [17]:

$$E_r = \frac{E_1}{r} q \cos\left(\frac{\pi x}{a}\right) \sin(q\theta) H_q^{(2)}(k_r r) \qquad (7.1)$$

$$E_\theta = E_1 k_r \cos\left(\frac{\pi x}{a}\right) \cos(q\theta) H_q^{(2)'}(k_r r) \qquad (7.2)$$

$$E_x = 0 \qquad (7.3)$$

Only one half of the horn will be considered, since the other half will be symmetrical.

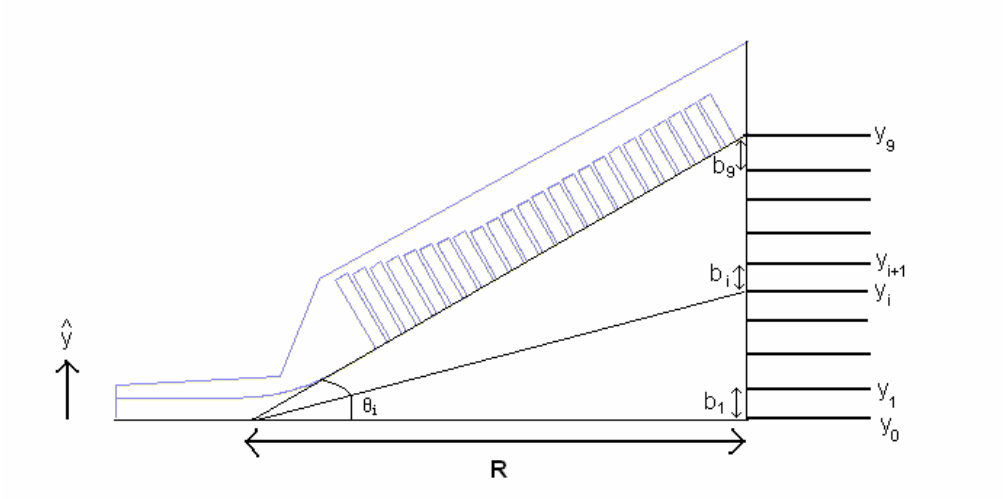

Figure 7.6 Corrugated e-plane sectoral horn with coupling waveguides.

The fraction of power coupled to i'th waveguide is the integration of the y-component of the square of E – field along i'th waveguide.

$$P_i = \frac{\int_{y_i}^{y_{i+1}} (E_y)^2 .dy}{2x\int_{y0}^{y9} (E_y)^2 .dy} \qquad (7.4)$$

E_y at some point y is:

$$E_y = E_r .Sin(\theta) + E_\theta Cos(\theta) \qquad (7.5)$$

where

$$\theta = \arctan(y/R) \qquad (7.6)$$

Since it is hard to find the integrals in E-field equation directly, E_y is plotted taking 100 points and polynomial fitted using MATLAB.

A cubic polynomial function fits well to the curve with a 0.02 error in residuals.

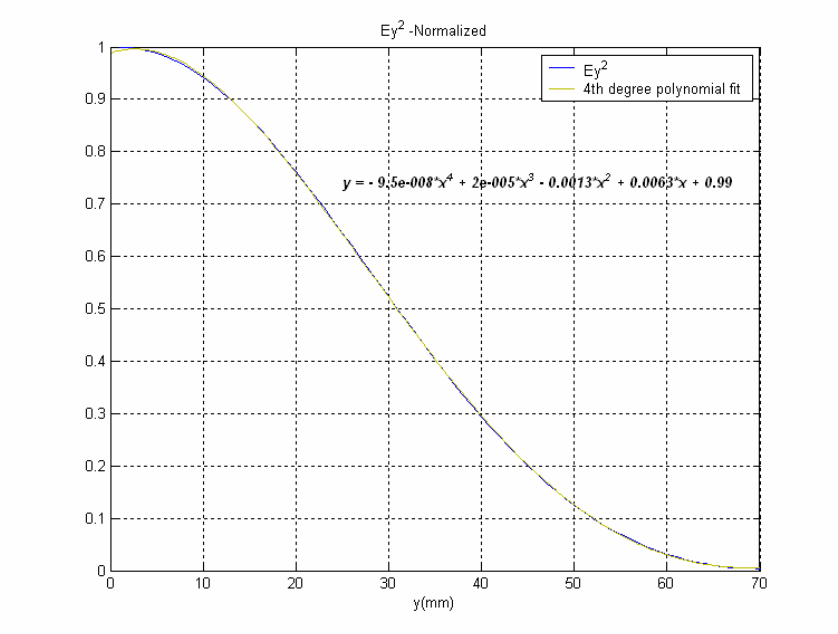

Figure 7.7 Calculated y component of the e-field on the aperture of the corrugated sectoral horn and its polynomial fiting.

Now,

$$Ey^2(y) = -9.542x10^{-8}\,y^4 + 2.0476x10^{-5}\,y^3 - 0.001256y^2 + 0.006294y + 0.98786$$

(7.7)

$$\int Ey^2(y)dy = -1.9084x10^{-8}\,y^5 + 0.5119x10^{-5}\,y^4 - 4.187x10^{-4}\,y^3 + 0.003148\,y^2 + 0.98786\,y + C$$

(7.8)

Total power :

$$\text{Pt} = 2x\int_{y0}^{y9}(E_y)^2.dy =$$

$$2.(-1.9084x10^{-8}\,y^5 + 0.5119x10^{-5}\,y^4 - 4.187x10^{-4}\,y^3 + 0.003148y^2 + 0.98786y + C\Big|_{y0=0}^{y9=65.5})$$

$$=63.52 \qquad (7.9)$$

The Taylor 35dB amplitude distribution is shown in Table 7.1. Heights of the coupling wave guides are calculated for this distribution using the above method.

Table 7.1 Taylor 35dB ñ=5 amplitude distribution coefficients for 18 elements.

Output Port No	Power Coefficient	Normalized (w.r.t total power) Power Coefficient	Normalized Output Power Coefficients (S21_ dB)
9	0.027	0.003	-24.60
8	0.040	0.005	-22.84
7	0.089	0.012	-19.36
6	0.189	0.025	-16.10
5	0.342	0.044	-13.53
4	0.532	0.069	-11.61
3	0.733	0.095	-10.22
2	0.903	0.117	-9.32
1	1.000	0.130	-8.87

$$P1 = 0.13 = \frac{\int_{y0}^{y1} (E_y)^2 .dy}{2x\int_{y0}^{y9} (E_y)^2 .dy} \qquad (7.10)$$

$$-1.9084x10^{-8}\, y_1^{\,5} + 0.5119x10^{-5}\, y_1^{\,4} - 4.187x10^{-4}\, y_1^{\,3} + 0.003148\, y_1^{\,2} + 0.98786\, y_1 - 8.26 = 0$$

Solving for the above equation, y1 can be found as 8.34mm.

Thus, b1 = y1 = 8.34mm.

For y2,

$$\text{P2} = 0.117 = \frac{\int_{y1}^{y2} (E_y)^2 .dy}{Pt} = \frac{\int_{y0}^{y2} (E_y)^2 .dy - \int_{y0}^{y1} (E_y)^2 .dy}{Pt} = \frac{\int_{y0}^{y2} (E_y)^2 .dy}{Pt} - P1 \quad (7.11)$$

$$\int_{y0}^{y2} (E_y)^2 .dy = (\text{P2}+\text{P1}).\text{Pt} = (0.117+0.13).63.52 = 15.69$$

y2 can be found as 16.55

b2 = y2 - y1 = 8.21 mm

Generalizing,

$$\text{Pi} = \frac{\int_{y0}^{y_i} (E_y)^2 .dy}{Pt} - \sum_{k}^{i-1} P_k \quad (7.12)$$

Coupling waveguides' narrow wall dimensions (b1-b9) are found with this method (Table 7.2).

Table 7.2 Calculated heights of the coupling waveguides for corrugated e-plane sectoral horn divider.

B1	8.34 mm	B4	7.89 mm	B7	5.54 mm
B2	8.21 mm	B5	7.47 mm	B8	4.75 mm
B3	8.11 mm	B6	6.75 mm	B9	8.32 mm

The wall thickness between the waveguides is chosen as 0.2 mm. Using these dimensions, a power divider is formed in HFSS. Simulated return loss and power distribution in 10% frequency band are shown in Figure 7.8 and Figure 7.9 respectively. The whole divider is well matched in the 10% frequency band of operation.

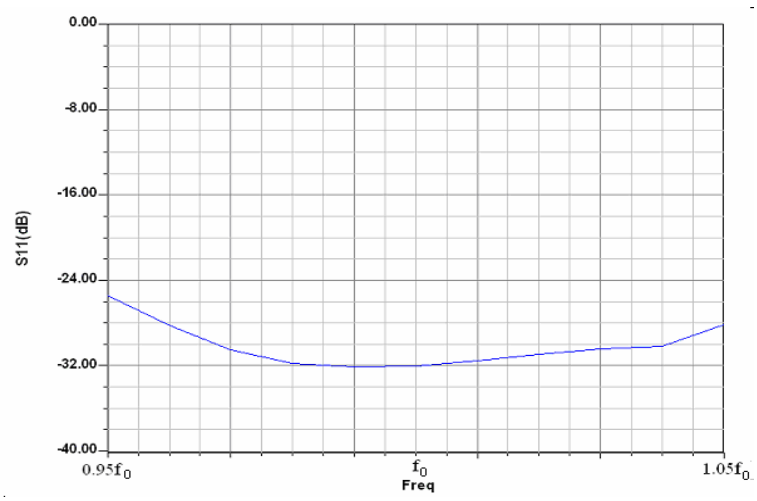

Figure 7.8 Simulated S11 of the corrugated e-plane sectoral horn divider.

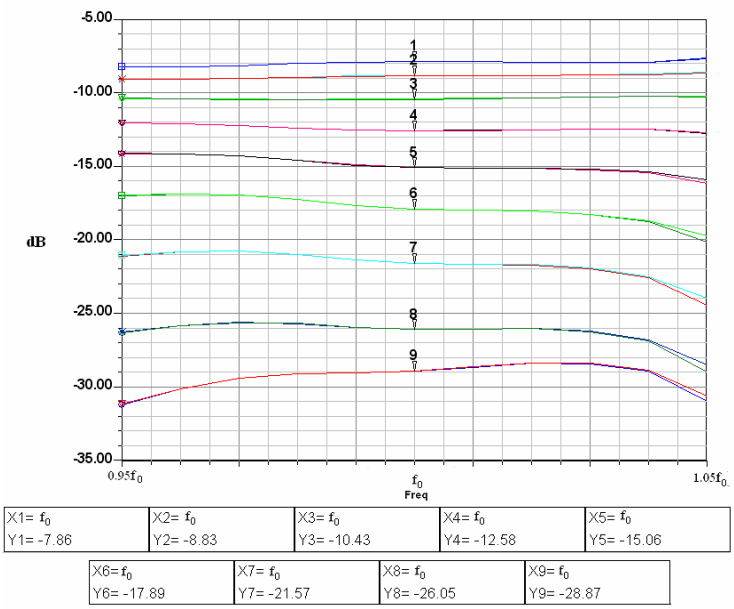

Figure 7.9 Simulated power distribution of the corrugated e-plane sectoral horn divider.

Nevertheless, the power distribution is not well suited to the desired amplitude tapering. Therefore, the heights of the coupling waveguides are optimized in order to acquire the correct amplitudes. Figure 7.10 and Figure 7.11 show the power distribution and return loss of the optimized junctions respectively. There is a

maximum 2 dB variation of the power along the band for low power channels. Using this power distribution result, array factor is calculated at the band edges and in the midband (Figure 7.12). At the center frequency -35dB first sidelobe level can be met. There appears a side lobe inrease due to the taper deviation in some channels for frequencies off that from f_0. The side lobe levels are below -30 dB over the 10% frequency band.

Table 7.3 Optimized heights of the coupling waveguides for corrugated e-plane sectoral horn divider.

B1	6.8 mm	B4	7.4 mm	B7	5.6 mm
B2	6.8 mm	B5	7.3 mm	B8	4.4 mm
B3	7.2 mm	B6	6.5 mm	B9	11.8 mm

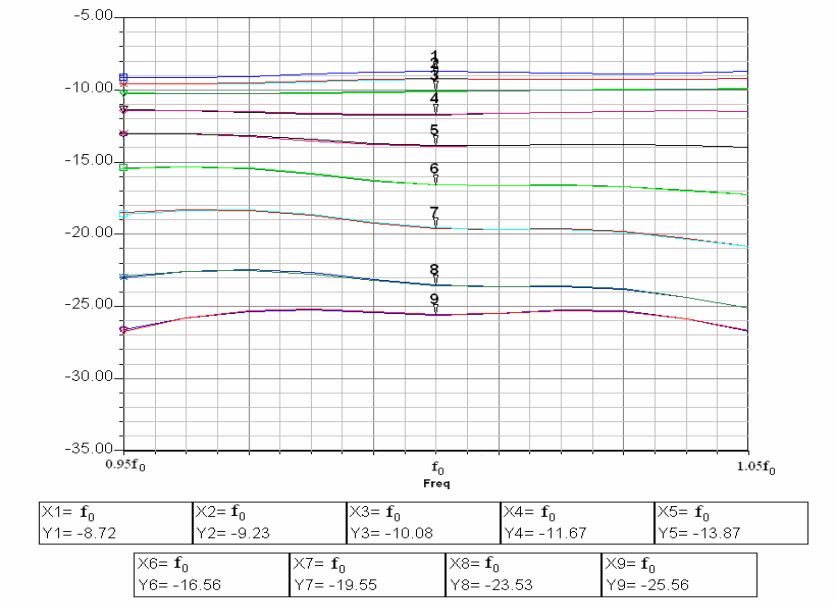

Figure 7.10 Simulated power distribution of the corrugated e-plane sectoral horn divider after optimization.

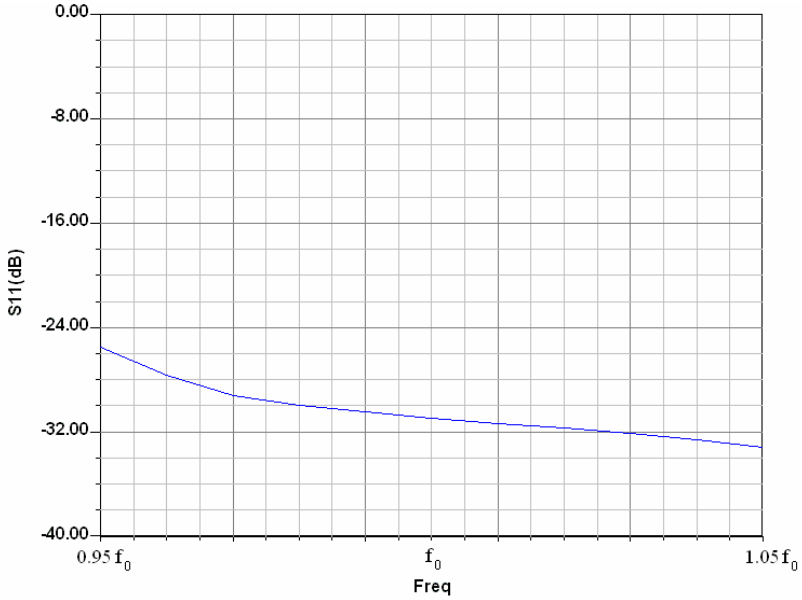

Figure 7.11 Simulated S11 of the corrugated e-plane sectoral horn divider after optimization.

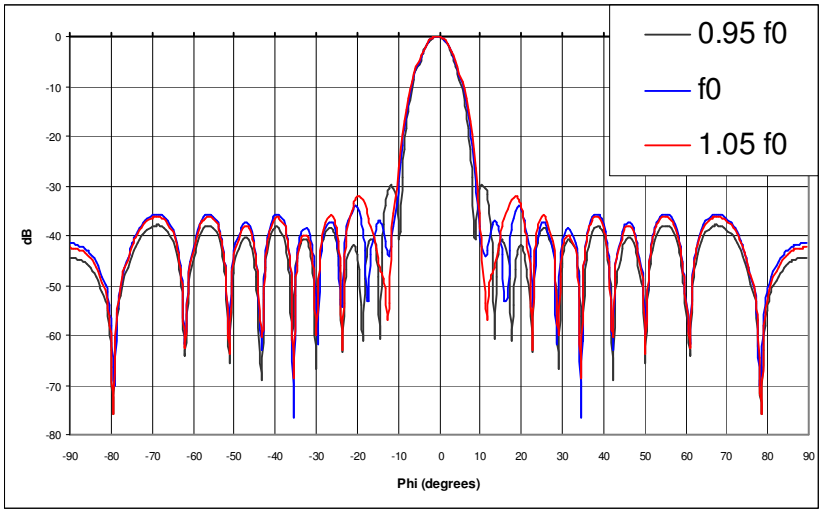

Figure 7.12 Calculated array factor (from simulation results) of the corrugated e-plane sectoral horn divider after optimization.

The various height waveguides should be transformed mechanically to the antenna waveguide dimensions. An adapter section must also be designed for this purpose. This adapter section is not the subject of this thesis.

CHAPTER 8

CONCLUSIONS

Longitudinal broad wall slotted waveguide array antennas are investigated in this thesis. Their power handling capability and planarity makes them very useful in applications such as radars which do not have the electronically scanning property in any plane or have electronically scanning in only in one plane. For two plane scanning operations, each element should have its own T/R modules which can not be applied to this type of antennas.

In the design of SWGA antennas, there are two important parameters; the admittance model of isolated slot and mutual coupling between slots. If these data are accurate, the linear array can be synthesized with the use of design equations of Elliott. Otherwise, the radiation pattern of the antenna will be degraded. The modeling of an isolated slot can be done numerically or empirically. In this thesis, it is done not only with Ansoft HFSS, but with measurements as well. There were slight differences between the two. The mutual coupling between slots is analytically calculated. The analogy of slots to dipoles is used in the calculation of mutual coupling, even tough the slots were radiating into a baffle region. The results were satisfactory in this case, however if the first sidelobe levels of the antenna are to be ultra low (<-45dB), the effect of baffles in mutual coupling should be taken into account.

The type of the designed array was traveling-wave. The waveguide is fed from one end and it is terminated with a matched load in the other end. The advantage of this type to the resonant type is the increased bandwidth of the array. The beam is squinted in this case and the degree of squint changes as the frequency changes. A small portion of the power is dissipated in the load decreasing the gain of the

antenna by 0.2dB at most, however the input matching and the pattern bandwidth are superior compared to resonant case.

Since the slots are offsetted from the center line of the waveguide, there are inherently unwanted grating lobes in the antenna pattern. As the maximum offset in the array increases, the levels of these grating lobes increase. In order to avoid this second order lobe effect for all frequencies and steer angles, baffles are introduced to the structure. The usage of baffles not only suppress the second order lobes, but increase the bandwidth of the antenna, by increasing the bandwidth of an isolated slot, as well.

The mechanical accuracy in carving the slots on the waveguide is very important, since the admittance of the slot depends on its mechanical position with respect to the center line of the waveguide. The sensitivity increases as the dimensions of the waveguide decreases, since a slight change in offset bring more admittance change for a smaller size of broadwall dimension.

The planar array is formed stacking identical linear SWGA antennas. The radiation pattern is not affected if there is no beam steering. However, the beamwidth increases for increased scanning angles. Experimental works show that stacking identical linear SWGA's have little influence on the pattern of the planar array.

In order to feed the planar array, a high power divider is required. There can be various ways for the feed section. An E-plane corrugated sectoral horn is devised for this purpose. The input power for each waveguide is adjusted by the height of the coupling waveguides. The heights were calculated analytically from the field on the aperture of the horn. Although the results were good but not sufficient and an optimization was necessary in order to get better results.

APPENDIX

ASELSAN Near Field Antenna Measurement System

In ASELSAN, there exists a Planar Near Field Antenna measurement System, capable of making measurements in 0.8 - 40 GHz frequency band. The scanner area is 4m. x 4m. The chamber has dimensions 6m x 8m x 4m, and its walls are fully covered with pyramidal microwave absorbers of 18" length at the back of AUT and at the back of the scanner and 12" length elsewhere. The figure shows the funtional block diagram of the system.

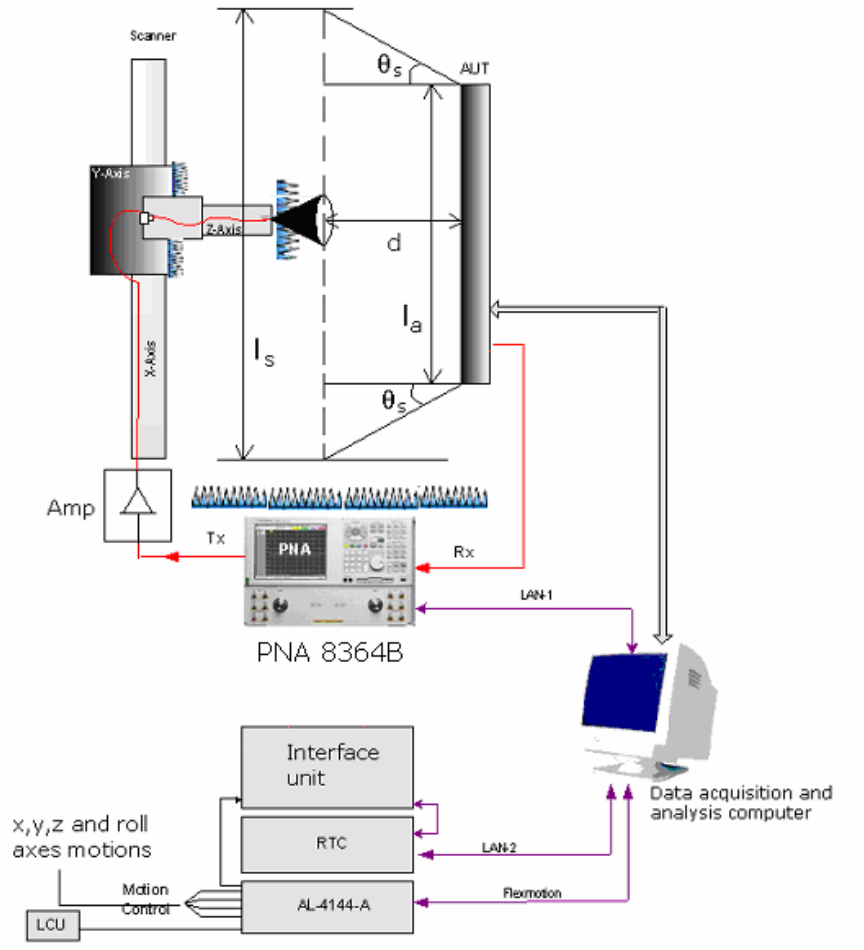

Figure 1. FunctionalBlock Diagram of the Planar Near-Field Antenna Measurement System

The manufatured antennas are measured in this facility. In the measurement setup, AUT – probe distance (d) is 6λ and θs is 60° in both X and Y axes. Antenna is probed with 0.4 λ spacings .

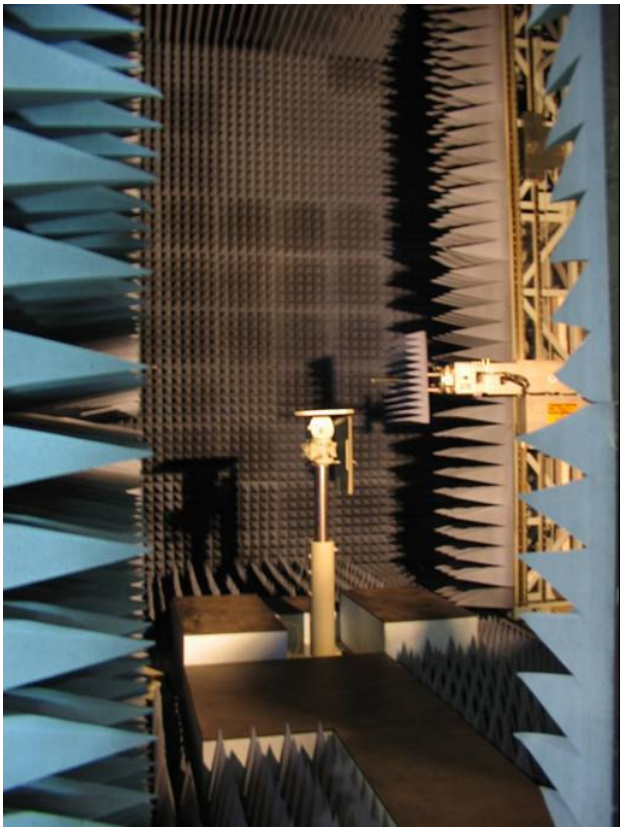

Figure 2. Photograph of the Planar Near-Field Antenna Measurement System

REFERENCES

[1] H. G. Brooker, “Slot aerials and their relations to complementary wire aerials (Babinet’s Principle),” JIEE(London), 93, pt.III A:pp. 620-626, 1946.

[2] W. H. Watson,The Physical Principles of Waveguide Transmission Antenna Systems, Clarendon Press, Oxford, 1947.

[3] A. F. Stevenson, “ Theory of slots in rectangular waveguides,” Journal of Applied Physics, vol. 19, pp.24-38,1948.

[4] R. J. Stegen, ”Longitudinal shunt slot characteristics,” Technical Report 261, Hughes Technical Memorandum, Nov. 1971.(Stegen’s data are reproduced in R. C. Johnsson and H. Jasik, Antenna Engineering Handbook, McGraw Hill, New York, 1984).

[5] R. S. Elliott and L.A.Kurtz, “The design of small slot arrays,” IEEE Trans. Antennas Propagation, vol. AP-26, no. 2, pp. 214-219, Mar. 1978.

[6] R. S. Elliott, “On the design of traveling-wave-fed longitudinal shunt slot arrays,” IEEE Trans. Antennas Propagation, vol. AP-27, no. 5, pp. 717-720, Sept. 1979.

[7] R. S. Elliott, “The Design of waveguide-fed slot arrays”, Lo and Lee Antenna Handbook, Chapter 12.

[8] S. W. Hopfer, “The Design of Ridged Waveguides”, Trans. PGMTT, pp.20-29, Oct. 1955.

[9] T.-S. Chen, “Calculation of the Parameters of the Ridged Waveguides”, IRE Trans. Microwave Theory and Techniques, pp. 12-17, Jan. 1957.

[10] D. A. McNamara, J. Joubert, “Experimentally Determined Equivalent Network Sattering Parameters for Edge Slots in Rectangular Waveguide for Use as Reference Data,” IEEE Microwave and Guided Wave Letters, vol.3, no.11, Nov. 1993.

[11] H. Gruenberg, “Second order beams of slotted waveguide arrays,” Canadian Journal of Physics, vol. 31, pp. 55-69, 1953.

[12] L. A. Kurtz and J. S. Yee, “ Secondorder beams of two dimensional slot arrays,” IRE Trans. Antennas Propagat., vol. 5, no. 4, pp. 356 – 362, Oct. 1957.

[13] K. Forooraghi and P. S. Kildal, “Transverse radiation pattern a slotted waveguide array radiating between finite height baffles in terms of a spectrum of two-dimensional solutions,” IEE Proceedings-H, Vol. 140, No. I , Feb. 1993.

[14] K. Forooraghi and P. S. Kildal, “Reduction of Second-Order Beams in Slotted Waveguide Arrays Using Baffles,” IEE Seventh International Conf. on Antennas & Propag.(ICAP’91), Vol.2, pp.725-728, Apr. 1991.

[15] T. C. Cheston and H. M. Grady, “A Phased Array using Sub-array techniques,” AP-S International Symposium 1965, Vol.3, pp.98-101, Aug 1965.

[16] A. J. Terzuoli, JR, and L.Peters, JR., “VSWR Properties of E-Plane Dihedral Corrugated Horns”, IEEE Trans. Antennas Propagation, vol. AP-26, no. 2, pp. 239-243, Mar. 1978.

[17] N. S. Narasimham and B.V. Rao, “Radiation Characteristiques of Corrugated E-Plane Sectoral Horns,” IEEE Trans. Antennas Propagation, pp. 320-327, May. 1973.